5-24-2012

Probing the phases of cold ultra-dense matter using neutron star physics

Simin Mahmoodifar
Washington University in St. Louis

WASHINGTON UNIVERSITY

Department of Physics

Dissertation Examination Committee:
Mark Alford (Chair)
Claude Bernard
Gregory Comer
Willem Dickhoff
Michael Ogilvie
Lee Sobotka

PROBING THE PHASES OF COLD ULTRA-DENSE MATTER USING NEUTRON STAR PHYSICS

by

Simin Mahmoodifar

A dissertation presented to the
Graduate School of Arts and Sciences
of Washington University in
partial fulfillment of the
requirements for the degree
of Doctor of Philosophy

May 2012

Saint Louis, Missouri

Abstract

Matter at very high densities and low temperatures is predicted to be in a "color superconducting" phase. At high enough densities, quark matter is in the Color-Flavor-Locked (CFL) phase, but the possible phases of matter at intermediate densities are unknown. Since the density at the core of a neutron star can be as high as a few times the nuclear saturation density, it is the most likely place to find these exotic forms of matter in the real world. The main goal of this thesis is to probe the phases of cold dense matter using neutron star physics.

Studying the transport properties of different phases of dense matter that may occur in a compact star is particularly important because transport properties such as viscosity, in addition to depending on the equation of state of matter, also depend on the low-energy degrees of freedom and therefore can discriminate between different phases of dense matter more efficiently.

In the first part of this thesis we calculate the mean free path and kaonic contribution to the shear viscosity of kaon-condensed color-flavor-locked (CFL-K^0) phase of quark matter. In the second part we calculate the large-amplitude enhancement of the bulk viscosity of dense matter. We obtain general analytic solutions as well as numerical solutions for the amplitude-dependent bulk viscosity of dense matter which are valid for any equations of state where equilibration occurs via fermions. In the third and fourth parts, we use our general results for the bulk viscosity to calculate the damping timescales of r-mode oscillations of neutron stars due to small-amplitude and large-amplitude bulk viscosity, the instability window of the r-modes and the saturation amplitude due to "supra-thermal" enhancement of the bulk viscosity for different cases of strange quark stars, hadronic stars and hybrid stars.

Acknowledgements

I would like to express my sincere gratitude and heartfelt thanks to my Ph.D. advisor Prof. Mark Alford for his continuous support, guidance and encouragement throughout the last four years of my work in his group. His logical way of thinking and his insightful questions have been always of great value for me. Prof. Alford is an amazing teacher and mentor, and I have always felt very lucky and fortunate for having him as my advisor.

My special thanks also go to Kai Schwenzer who closely collaborated with me in the last three years and had a substantial contribution to this thesis. I have benefitted a lot from his knowledge and experience and I am very grateful to him because of his generosity with his time. I would also like to thank Matt Braby who has collaborated with me in my first project.

I wish to thank the members of my dissertation committee, Prof. Bernard, Prof. Comer, Prof. Dickhoff, Prof. Ogilvie and Prof. Sobotka for their time, guidance and helpful comments and suggestions.

I am also very grateful to all the faculty, staff and graduate students in the Department of Physics at Washington University for providing a very calm and friendly atmosphere which made my last five years in this department an enjoyable experience.

I wish to thank all of my dear friends in St. Louis who have always been like family to me, specially my long-time officemates Dandan Hu and Nilushi Dasanayake and also my dear friend Sara Gharahbeigi with whom I spent the majority of the past five years.

I would also like to thank Nils Andersson, Jingyi Chao, Brynmor Haskell, Prashanth Jaikumar, Andrei Kryjevski, Cristina Manuel, Sanjay Reddy, Andreas Reisenegger, Gautam Rupak, Thomas Schafer, Andreas Schmitt, Igor Shovkovy, Andrew Steiner and Ira Wasserman for their helpful comments and discussions during this work.

Lastly, and most importantly, I wish to thank my parents, my sisters and my grandma for all their love, support, encouragement and patience. Thank you!

Contents

List of Figures

List of Tables

Chapter 1

Introduction

Matter at very high densities and low temperatures is predicted to be in a "color superconducting" phase [16, 17, 18], in which quarks near the Fermi surface pair and form a Bose-Einstein condensate. At high enough densities, quark matter is in the Color-Flavor-Locked (CFL) phase [19, 20], but the possible phases of matter at intermediate densities are not known. Compact stars are the only known objects that contain equilibrated matter that is compressed beyond nuclear saturation density, making them a valuable laboratory for the study of the structure of matter under extreme conditions. In addition to hadronic matter they may also contain exotic forms of matter that involve deconfined quarks [21, 22, 23, 2]. To probe the phases of cold ultra-dense matter we can compute transport and thermodynamic properties of different phases, and predict the behavior of a star that is made of matter in a given phase. Then by comparing our predictions with actual astrophysical observations we might confirm or rule out the existence of a particular phase in neutron stars. Studying the transport properties is particularly important because transport properties such as viscosity, in addition to depending on the equation of state of matter, also depend on the low-energy degrees of freedom and therefore can discriminate between different phases of dense matter more efficiently. One of these astrophysical

observables is the rotation frequency of the pulsars. After a supernova explosion a newborn neutron star has only a tiny fraction of its parent's radius and is formed with a very high rotation speed. Therefore we expect to observe fast rotating young neutron stars, but as can be seen in Fig. 1.1, no young, fast rotating neutron stars are observed (see the upper left hand side of the diagram)[1]. One possible explanation for this phenomenon is the existence of r-modes in neutron stars. R-modes are large scale currents in a rotating neutron star that couple to gravitational radiation and radiate away energy and angular momentum of the star in the form of gravitational waves. R-modes grow unstable by the back-reaction of the gravitational radiation [24] and if their growth is not stopped, they can spin the star down to very low frequencies very fast. However older fast rotating stars are still observed, so there must be some damping mechanisms that prevent the r-modes in older stars from growing to very large amplitudes. Bulk and shear viscosities are two of these damping mechanisms.

In the following sections of this chapter we first give an introduction to the phases of matter at high densities and low temperatures, we then discuss the internal structure and properties of neutron stars and at the end we explain the r-mode oscillations of neutron stars.

In the second chapter of this thesis, we calculate the mean free path and kaonic contribution to the shear viscosity of the kaon-condensed color-flavor-locked (CFL-K^0) phase of quark matter [25] using the kinetic theory and an effective Lagrangian for the CFL-K^0 phase. This contribution comes from a light Pseudo-Goldstone boson which arises from the spontaneous breaking of the flavor symmetry by the kaon

[1]The spin-down age in Fig. 1.1 is determined by the assumption that magnetic dipole breaking, which features a qualitatively similar behavior as gravitational wave emission, dominates the spin-down. It can thereby only give a rough order of magnitude estimate for the age. Age estimates are, in particular, not available for stars that currently spin up and which are correspondingly not included in the plot. However, for the youngest stars there are independent age determinations from the observation of the corresponding supernova remnant that qualitatively agree with these estimates.

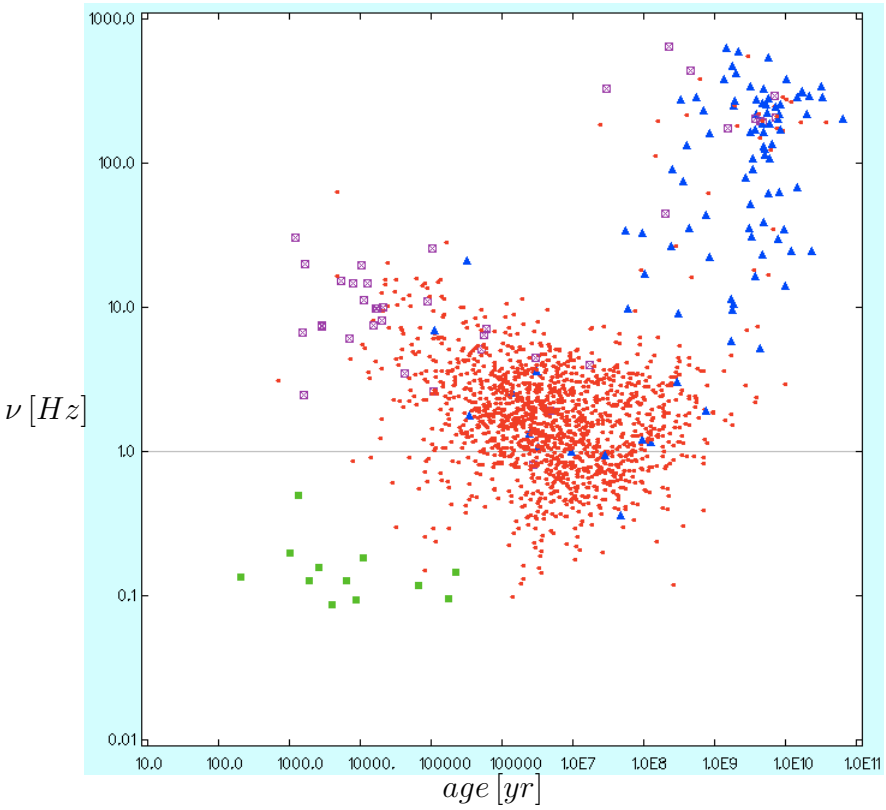

Figure 1.1: Rotation frequencies of observed pulsars versus their approximate spin-down age from the ATNF pulsar catalogue [1]. Binary pulsars are indicated in blue, AXP/SGRs are green, high energy pulsars are purple and the remainder in red.

condensate. We show that since the mean free path of kaons in the range of temperatures relevant to neutron stars is much shorter than that of superfluid phonons, they could easily provide the dominant contribution to the shear viscosity of CFL-K^0 quark matter in the temperature range of 10^8 to 10^{10} K.

In the third chapter we calculate the large-amplitude enhancement of the bulk viscosity of dense matter. We obtain general analytic solutions as well as numerical solutions for the amplitude-dependent bulk viscosity of dense matter which are valid for any equations of state where equilibration occurs via fermions (e.g. color superconducting quarks). We find that there is a huge enhancement of the bulk viscosity in this large amplitude "supra-thermal" regime, where the deviation of the chemical

potential μ_Δ from chemical equilibrium becomes larger than the temperature. The most obvious application of this work is in the analysis of the damping of the r-mode oscillations of neutron stars.

In the fourth and fifth chapters, we use our general results for the bulk viscosity from chapter 3 to calculate the damping timescales of the r-mode oscillations due to sub-thermal and supra-thermal bulk viscosity, the instability window of the r-modes and the saturation amplitude due to supra-thermal enhancement of the bulk viscosity for different cases of strange quark stars, hadronic stars and hybrid stars. We show that the boundary of the instability region and in particular its minimum, which determines the lowest frequency to which r-modes could spindown the star, is very insensitive to the microscopic details of the interactions that give rise to the viscosities, but is very different for a quark star (or a hybrid star with a large quark matter core) compared to a hadronic star (or a hybrid star with a small quark matter core).

1.1 Phases of dense matter

Quarks are the fundamental constituents of matter. The Standard Model of particle physics contains six types (flavors) of quarks: up, down, strange, charm, bottom, and top. Quarks also carry color charge which can be red, green or blue, and the strong interaction between them is described by the theory of quantum chromodynamics (QCD). The strong interaction between quarks is mediated by gluons. Two main properties of QCD are confinement and asymptotic freedom. Confinement states that color charged particles can not be isolated and quarks are confined inside baryons and mesons at physical densities. Asymptotic freedom [26, 27] states that the strong interaction becomes weak at small distances (large energy scales), which means that

the coupling constant of the strong interaction decreases with increasing the momentum ($\alpha_s \ll 1$ at very high densities). This allows weak-coupling calculations for QCD at ultra-high densities.

Fig. 1.2 shows the conjectured QCD phase diagram, where different phases of quark matter are shown at different temperatures T, and quark chemical potentials μ. Since baryon number density n increases monotonically by increasing the chemical potential, $n \sim \mu^3$, we sometimes use the terms "density" and "chemical potential" interchangeably. At low temperatures and low densities, quarks are confined inside the mesons and baryons described by nuclear matter. Increasing the temperature to very high values ($T \gg \mu$) we approach the quark-gluon plasma (QGP) phase, which is a soup of deconfined quarks and gluons. Heavy ion colliders at CERN and Brookhaven are probing the high temperature region of the QCD phase diagram by colliding heavy nuclei at ultra-relativistic energies. In these experiments one expect to create a quark-gluon plasma at least for a short period of time.

In certain regions of the QCD phase diagram, when thermodynamics is dominated by short-distance QCD dynamics, i.e. at very high densities or very high temperatures, asymptotic freedom of the QCD makes it possible to study the theory analytically. At zero chemical potential and non-zero temperatures Lattice gauge theory is a powerful tool for studying the QCD, but the so-called sign problem makes it very difficult to do lattice calculations at non-zero chemical potentials. Although in recent years there has been some progress in performing lattice computations at not too high chemical potentials $\mu < T$, but still the very high density region of the phase diagram $\mu \gg T$ can not be probed by Lattice QCD. The focus of this thesis is on this region of the QCD phase diagram which is also the relevant phase for the neutron stars. Quark matter at very high densities and low temperatures is believed to be in the color superconducting phase which will be explained in the following.

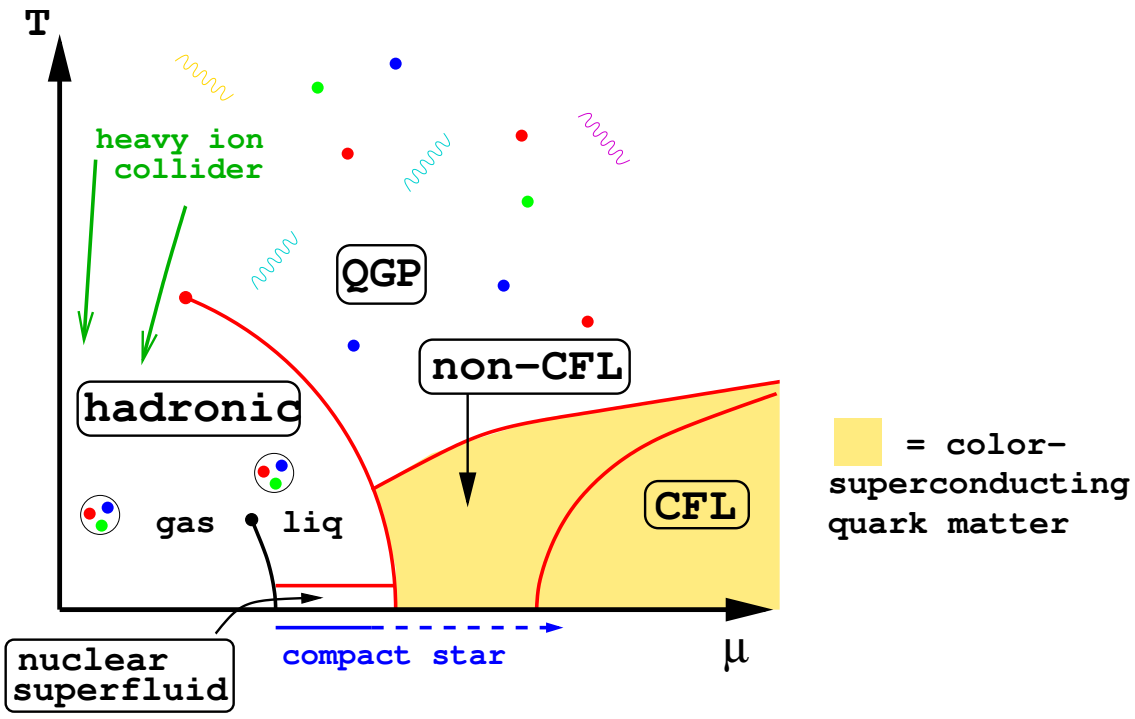

Figure 1.2: Schematic QCD phase diagram shows different phases of dense matter as a function of temperature and chemical potential [2].

Stellar compact objects are the only place in nature that this phase of quark matter may exist.

An ordinary superconductor (in QED) consists of a sea of electrons and a lattice of ions and can be described theoretically by Bardeen-Cooper-Schrieffer (BCS) theory of superconductivity. Electrons in an ordinary superconductor are fermions and obey the Pauli exclusion principle and therefore at zero temperature all of their quantum states are filled up to the Fermi energy $E_F = \mu$ where μ is the electron chemical potential, and all the states above E_F are empty. The grand thermodynamic potential (Landau free energy) at zero temperature for this system is given by $\Omega = E - \mu N$ where E is the total energy of the system and N is the number of electrons. When there are no interactions, adding or subtracting a particle (or hole) near the Fermi surface would cost zero free energy. According to the BCS theory if there is an arbitrarily weak

attractive force between the fermions, a new ground state will be formed, in which electrons in the vicinity of the Fermi surface form pairs (Cooper pairs) and the total energy of the system is reduced by the sum of the binding energies of the electron pairs. These pairs are bosons, and will condense and form a Bose-Einstein condensate near the Fermi surface. The single-particle excitation energies will be also modified and will acquire a gap.

As we mentioned earlier one of the features of QCD is asymptotic freedom which says the force between quarks goes to zero at asymptotically short distances (very large energy scales). Therefore at very large densities and low temperatures (similar to the condition in the interior of neutron stars) quarks act similar to the electrons in a metal. In QCD there is an attractive interaction between quarks whose color wave function is antisymmetric. Therefore at sufficiently high densities and low temperatures quarks will form Cooper pairs and we will have the same mechanism as electron superconductivity for quarks. This is called "color superconductivity" because quark-pairs can not be color-singlet and therefore the condensate breaks the local $SU(3)$ color symmetry. In the unpaired phase of quark matter the splitting between the Fermi momenta of different quark species is given by $\frac{M_s^2}{4\mu}$. At very high densities, $\mu \gg M_s$, one can neglect the mass of the strange quark and treat all the quarks equally. At asymptotically large densities and low temperatures, QCD with 3 quark flavors (u, d and s quarks) is in color-flavor locked (CFL) state [19, 20], where all quarks with all colors and flavors have the same Fermi momentum and they all take part in the Cooper pairing (see Fig. 1.3). This is only possible when the energy that is released by the formation of Cooper pairs, which is $\mu^2\Delta_{CFL}^2$, is larger than the energy cost for making all quarks to have the same Fermi momentum, which is given by $\mu^2\delta p_F^2 \sim M_s^4$. Here μ is the quark chemical potential, Δ_{CFL} is the CFL gap parameter, $\delta p_F \simeq \frac{M_s^2}{4\mu}$ is the splitting between the Fermi momentum of the different

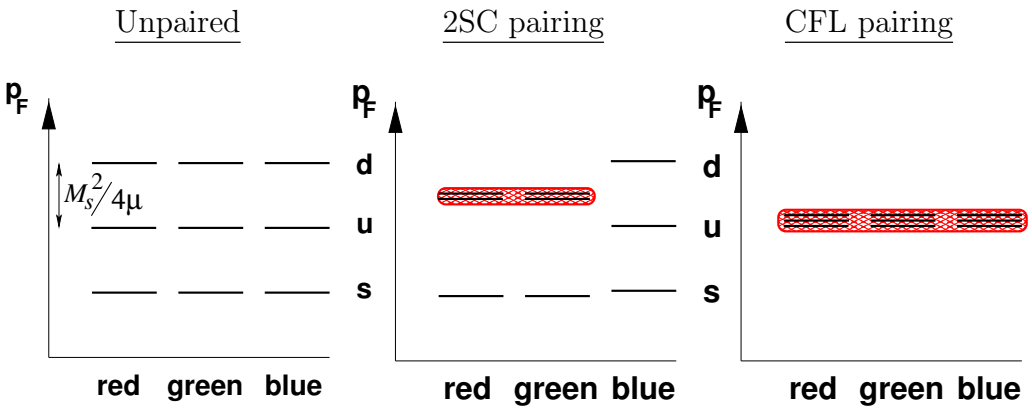

Figure 1.3: Fermi momenta of various colors and flavors of quarks in the unpaired, 2SC and CFL phases are shown. The splitting of the Fermi momenta increases with decreasing density, as μ decreases and as $M_s(\mu)$ increases [2].

quark species, and M_s is the constituent strange quark mass. In the CFL phase, the symmetry $SU(3)_{color} \times SU(3)_L \times SU(3)_R \times U(1)_B$ of QCD is broken down to the global diagonal $SU(3)_{color+L+R}$ symmetry due to the Cooper pairing between quarks near the Fermi surface. The low energy excitations about the $SU(3)$ symmetric CFL ground state consist of a nonet of massless Goldstone bosons transforming under the unbroken $SU(3)$ as an octet plus a singlet. A tenth pseudo-Goldstone boson is also expected arising from spontaneously broken approximate axial $U(1)_A$ symmetry.

When we go to lower densities, non-zero strange quark mass along with charge neutrality and beta equilibrium will put stress on the Cooper pairing by shifting the Fermi momenta of quarks, and the CFL phase will not be favored anymore and there must be a phase transition in quark matter. If the stress is small enough, there will be no effect. If it is larger than a certain threshold there will be K^0 condensation. Since K^0 mesons carry negative strangeness, this condensation will reduce the stress on the CFL phase by reducing its strangeness content. This is called the kaon-condensed color-flavor locked (CFL-K^0) phase [28, 25] which will be explained in more detail in chapter 2. But if the stress is too large the CFL pairing will go away.

Going to lower densities where the separation of Fermi momenta are large enough

that the strange quarks can not take part in the Cooper pairing with light quarks, quark matter may be in the 2SC phase where only up and down quarks with only two colors (say, red and green) pair. The color gauge group is broken down to $SU(2)$, so five of the gluons will become massive and only three gluons that are associated to the unbroken $SU(2)$ red-green gauge symmetry remain massless. In the 2SC phase no global symmetries are broken, so there are no light scalars and therefore the 2SC phase is not a superfluid. There are other possible phases for color superconducting quark matter at intermediate densities, such as Crystalline (FFLO or LOFF) phase [29], where quarks with different Fermi momenta form pairs with a net momentum (this is beyond BCS pairing pattern in which only quarks with momenta that add to zero pair). This may be favorable because it gives rise to a region of phase space where both of the quarks in a pair are close to their respective Fermi surface, and such pairs can be created at low cost in Fermi energy. Other possible phases are gapless isotropic phases (g-2SC, g-CFL, etc) [30], spin-1 color superconducting phase [31, 32], p-wave kaon condensate [33], etc (for a review on color superconductivity see Ref. [2]).

1.2 Physics of neutron stars

Neutron stars are one of the densest objects in the universe which are born in the gravitational collapse of the core of a massive star ($M > 8M_{\odot}$) at the end of its life, which triggers a type II supernovae explosion. The mass of a neutron star M is about $1.5M_{\odot}$, its radius R is about 10 km, its initial temperature is about 10^{11} K and its central density can be as high as 5 to 10 times the nuclear saturation density $\rho_0 \simeq 0.16$ fm^{-3}. The core of a neutron star consists mainly of neutrons with some protons and enough electrons and muons for charge neutrality. At very high densities in the core of

neutron stars exotic forms of matter such as hyperons [34], condensed mesons (pion or kaon) [35], or even deconfined quarks [36] may appear. Neutron stars are composed of five major regions [37]. The outermost region is the atmosphere, then the outer crust (or the envelope), the inner crust, the outer core and the inner core. The atmosphere is a thin plasma layer, where the spectrum of thermal electromagnetic neutron star radiation is formed. The depth of the atmosphere varies from tens of centimeters in a hot neutron star to millimeters in a cold one. The outer crust (outer envelope) extends from the atmosphere bottom to a layer of density about the neutron drip density $\rho_d \approx 4.3 \times 10^{11}$ gcm^{-3} $\approx 1.5 \times 10^{-3}\rho_0$, and has a depth of some hundred meters. The outer crust consists of ions and electrons. At the boundary of outer crust and inner crust neutrons start to drip out of nuclei and form a free neutron gas. the next layer is the inner crust which extends from ρ_d to densities about $0.5\rho_0$. The inner crust consists of free neutrons, electrons and neutron-rich atomic nuclei. For temperatures less than ~ 0.1 MeV, the neutron fluid in the crust probably forms a $^1S_0$ superfluid. The next region is the outer core which extends to densities about $2\rho_0$ and can be several kilometers in depth. It consists of neutrons with some admixture of protons, electrons and muons. The neutrons could form a $^3P_2$ superfluid and the protons a $^1S_0$ superconductor within the outer core. More massive neutron stars also have an inner core where the central density can get as high as $10\rho_0$ and exotic particles such as hyperons and/or Bose condensates (pions and kaons) may become abundant, also it is possible to have an inner core of deconfined quark matter or color-superconducting quarks.

The global structure of neutron stars, such as the mass-radius (M-R) relation is described by Tolman-Oppenheimer-Volkoff (TOV) equations [38, 39], which are a set of ordinary differential equations that determine the structure of general relativistic static perfect fluid spheres:

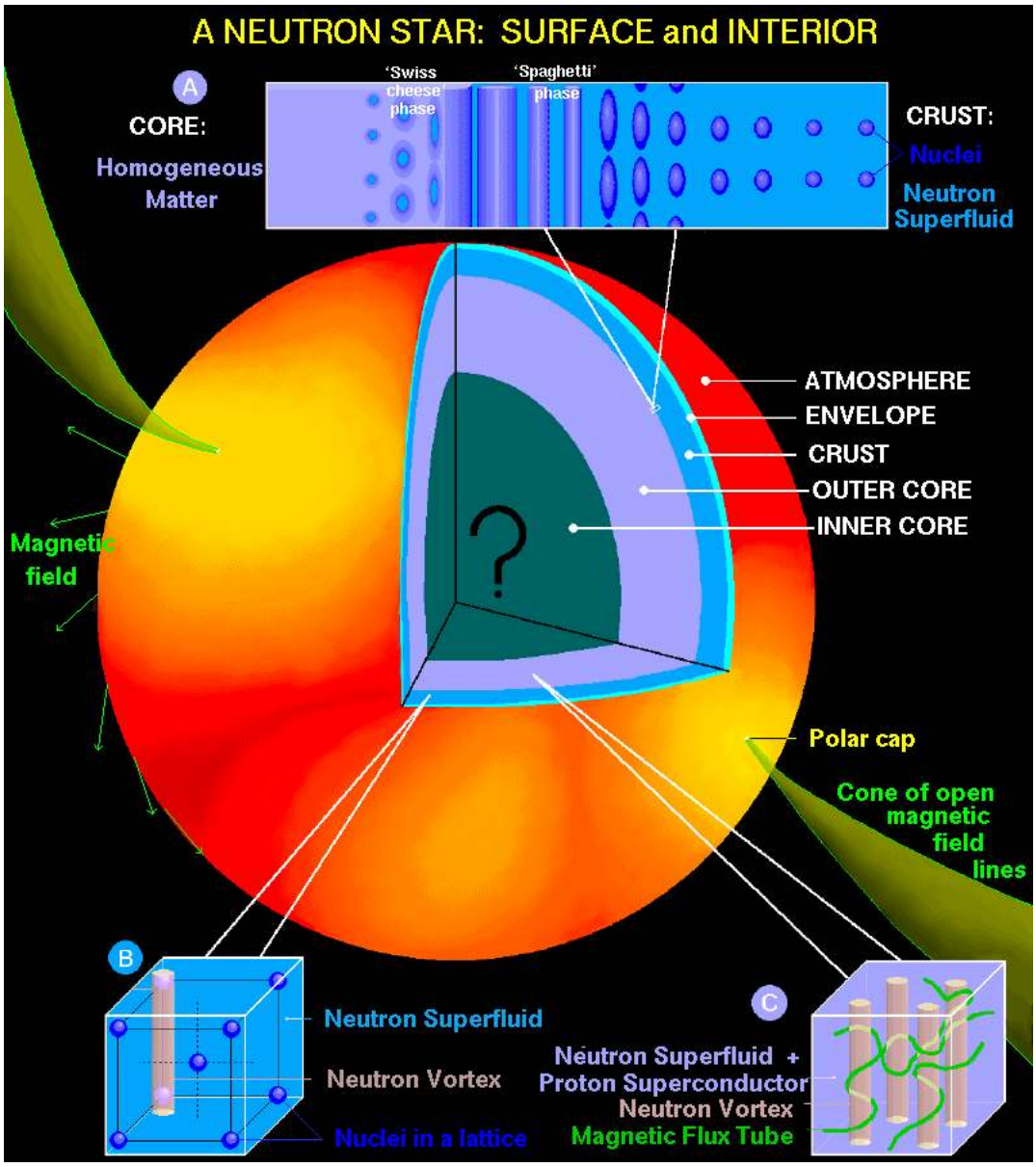

Figure 1.4: Internal structure of a neutron star [3].

$$\begin{aligned} \frac{dP(r)}{dr} &= -\frac{G(M(r)+\frac{4\pi r^3 P(r)}{c^2})(\rho(r)+\frac{P(r)}{c^2})}{r(r-\frac{2GM(r)}{c^2})} \\ \frac{dM(r)}{dr} &= 4\pi\rho(r)r^2 \end{aligned} \tag{1.1}$$

where P and ρ are the pressure and energy density at the radius r, and $M(r)$ is the gravitational mass enclosed in a sphere of radius r. For a given equation of state (i.e. $P-\rho$ relation), the TOV equations can easily be integrated from the origin with the initial conditions $M(0)=0$ and an arbitrary value for the central density $\rho_c = \rho(0)$, until the pressure $P(r)$ vanishes at some radius R. For each possible equation of state(EOS), there is a unique family of stars parametrized by the central density, $M = M(\rho_c)$. Mass-radius (M-R) curves of neutron stars can be used to constrain the EOS of dense matter in two ways. One way is to generate the physically reasonable M-R curves and the EOS that they satisfy, and the other way is to generate arbitrary EOS and compute M-R curves from them, then select those curves that pass within the error box of the astrophysical observations. For example existence of massive neutron stars ($M > 1.7M_\odot$) constraints the EOS of exotic matter, because the appearance of new degrees of freedom at and above the nuclear saturation density, such as quarks, hyperons, or bosons, softens the equation of state and lowers the maximum mass of the star. The highest neutron star mass by far is $1.97 \pm 0.04M_\odot$ which has been measured with a high precision by Demorest et. al [4], using the Shapiro delay (an increase in light travel time through the curved space-time near a massive body). Fig. 1.5, which is the mass-radius (M-R) diagram of neutron stars, shows how this precise mass measurement can constrain the EOS of neutron star matter. In that diagram the M-R curves for typical neutron star matter equations of state have been shown. Any EOS curve that doesn't intersect with the $\sim 2M_\odot$ band is ruled out by this measurement. Most EOS curves involving exotic matter tend to predict maximum masses well below $2M_\odot$, and therefore are ruled out. The

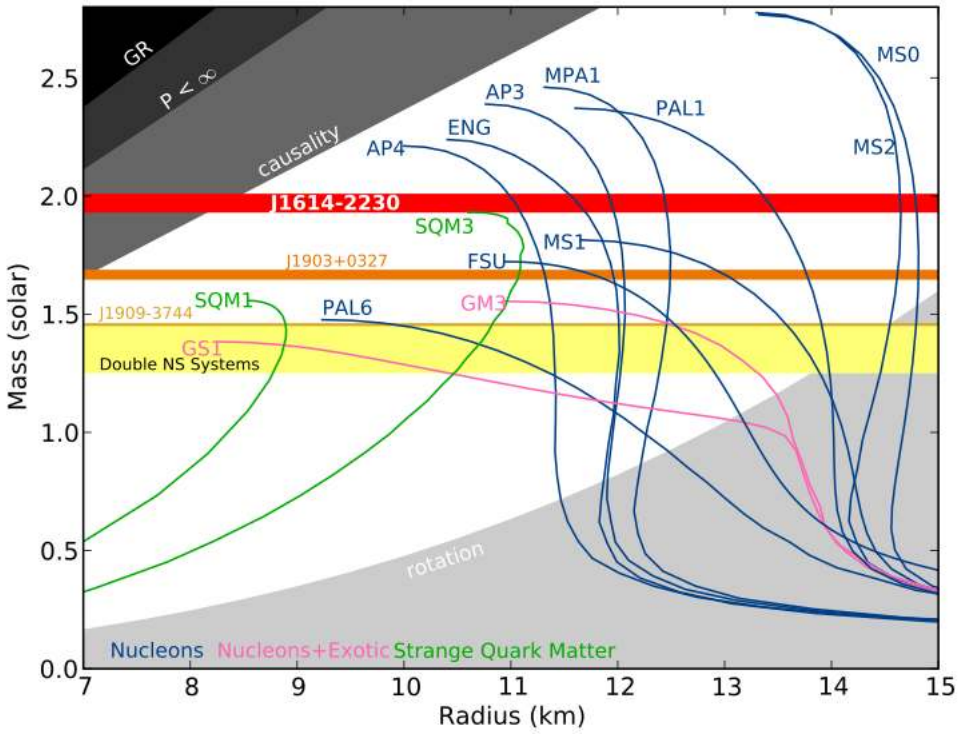

Figure 1.5: Neutron star mass-radius diagram for several typical neutron star equations of state [4]. The horizontal bands show the observational constraint from J1614-2230 mass measurement of $1.97 \pm 0.04 M_{\odot}$, similar measurements for two other millsecond pulsars [5], and the range of observed masses for double NS binaries [6].

region in Fig. 1.5 bounded by the Schwarzschild condition $R \leq \frac{2GM}{c^2}$ is excluded by general relativity, and that bounded by $R \lesssim \frac{3GM}{c^2}$ is excluded by causality ($c_s < c$). An accurate, simultaneous mass and radius measurement from even one neutron star would provide a significant constraint.

In contrast to the static properties of compact stars which only depend on the equation of state of matter [40], dynamic properties also depend on the low energy degrees of freedom and thereby might be able to discriminate more efficiently between different forms of strongly interacting matter. One of the dynamic properties of dense matter is viscosity, which determines the damping of mechanical perturbations, and a particularly important application is to the damping of r-mode oscillations of compact

stars [41, 24, 42, 43, 44], which will be explained in the next section.

1.3 R-modes of Neutron Stars

R-modes are non-radial pulsations of neutron stars that couple to gravitational radiation. They are primarily surface currents driven by Coriolis forces. R-modes are generally defined to be solutions of the perturbed fluid equations having (Eulerian) velocity perturbations of the form [45]

$$\vec{\delta v} = \frac{1}{\sqrt{l(l+1)}} \alpha R \Omega (\frac{r}{R})^l \vec{r} \times \vec{\nabla} Y_{lm} e^{i\omega t} + O(\Omega^3) \tag{1.2}$$

where α is a dimensionless amplitude, R and Ω are the radius and angular velocity of the unperturbed star, Y_{lm} are the spherical harmonics and ω is the frequency of the mode. R-modes exist if and only if $m = l$ [46]. The fluid motion has no radial component, and is the same inside the star as the outside although smaller. For example in the case of $l = m = 2$ it is smaller by a factor of the square of the distance from the center. The density perturbations associated with these modes vanish at lowest order in the angular velocity:

$$\delta\rho = O(\Omega^2) \tag{1.3}$$

The frequency of these modes in the inertial frame is given by [47]

$$\omega = -\frac{(m-1)(m+2)}{m+1}\Omega + O(\Omega^3) \tag{1.4}$$

From eq. (1.2) we have $\delta v \propto \exp(im(\phi - \frac{(m-1)(m+2)}{m(m+1)}\Omega t))$, where ϕ is the azimuthal angle. So the "flow pattern" of the r-modes moves with an angular speed $\frac{(m-1)(m+2)}{m(m+1)}\Omega > 0$ in the inertial frame and therefore all the modes are prograde in

this frame, i.e. they move in the same direction as the star's rotation as seen by an observer at infinity. However in the frame that co-rotates with the star, $\bar{\phi} = \phi - \Omega t$, $\delta v \propto \exp(im(\bar{\phi} - (\frac{(m-1)(m+2)}{m(m+1)} - 1)\Omega t))$ and therefore the modes are retrograde in the co-rotating frame, which means they move in the opposite direction as the star's rotation as seen by an observer at rest on the star.

R-modes couple to gravitational radiation, and the back reaction to the emission of gravitational radiation drives an instability in the r-modes of rotating neutron stars. Any mode that is retrograde in the co-rotating frame and pro-grade in the inertial frame grows as a result of its emitting gravitational waves. This is the Chandrasekhar-Friedman-Schutz (CFS) mechanism [48, 49]. The CFS instability can be understood in the following way: Modes that are retrograde in the co-rotating frame have negative angular momentum and modes that are prograde in the inertial frame have positive angular momentum. Gravitational radiation lives in the inertial frame and always removes positive angular momentum. So since the fluid (co-rotating frame) sees the mode as having negative angular momentum, radiation drives the mode rather than damps it.

The r-modes evolve with time dependence of $e^{(i\omega t - \frac{t}{\tau})}$, where the imaginary part of the frequency $\frac{1}{\tau}$ is determined by the effect of gravitational radiation, viscosity, etc. τ can be evaluated by computing the time derivative of the energy of the mode E (as measured in the co-rotating frame).

$$\frac{dE}{dt} = -\frac{2E}{\tau} \tag{1.5}$$

Gravitational radiation drives the r-mode, and bulk and shear viscosities damp it, so $\frac{1}{\tau}$ can be decomposed as

$$\frac{1}{\tau(\Omega)} = \frac{-1}{|\tau_{GR}(\Omega)|} + \frac{1}{|\tau_B(\Omega)|} + \frac{1}{|\tau_S(\Omega)|} \tag{1.6}$$

where τ_{GR}, τ_B and τ_S are gravitational radiation, bulk viscosity and shear viscosity timescales, respectively. R-modes are unstable when $\tau < 0$.

The rotation frequency of the star can change over time both by accretion of matter that transfers angular momentum from a companion star and by the emission of gravitational radiation. In the absence of viscous damping r-modes are unstable at all rotation frequencies [24]. Because of this instability, the rotational energy of the star will be transformed into gravitational wave energy and this leads to an exponential rise of the r-mode amplitude. When viscous damping is taken into account the star is stable at low frequencies but there remains an instability region at high frequencies [45, 9]. If this instability is stopped at a large amplitude, r-modes are a strong and continuous source of gravitational waves and could provide an efficient mechanism for the spin-down of a young compact star [50, 51]. Observational data for spin frequencies of pulsars, that spin down and allow the determination of an approximate age associated to their spin-down rate is shown in Fig. 1.1. Whereas observed old pulsars in binary systems can spin nearly as fast as the maximum Kepler frequency, above which the binding force cannot counteract the centrifugal pseudo-force anymore, and can feature rotation periods in the milli-second range, younger stars spin much more slowly. This is surprising since in their creation during a supernova a significant fraction of the angular momentum of the initial star should be taken over by the much smaller compact core which therefore should dramatically spin up. This naive assumption is backed up by explicit analyses where millisecond rotation frequencies at birth are indeed possible [52].

R-modes are also relevant for the case of older stars in binaries that are spun up by accretion since they generally limit the maximum possible rotation frequency of a star

to values substantially below the Kepler frequency. A challenging finding is that, in contrast to purely hadronic stars, more exotic possibilities like selfbound strange stars [44], hybrid stars [9] or stars where hyperons are present in the core [53] can feature so-called "stability windows" where over a range of intermediate temperatures the r-mode instability is absent up to rather high frequencies. The observation of stars rotating at such frequencies could therefore provide evidence for exotic phases in their interior. In this context the masses and radii of stars provide further important information. The recent precise measurement of a heavy compact star with $M \approx 2M_{\odot}$ [4, 54] puts constraints on the presence of exotic phases since such phases lead to a softening of the equation of state which in general leads to a smaller maximum mass that is achievable for such an equation of state. In combination with pulsar data this should lead to more restrictive bounds on the possible presence of certain forms of matter in compact stars.

A major problem for the extraction of information on the composition of compact stars from observational data is the huge theoretical uncertainty in the equation of state of dense matter and its transport properties. This holds both for the hadronic side, where nuclear data is only available at low densities and large proton fractions, and also for hypothetical phases of quark matter, since QCD as the fundamental theory of strong interactions cannot be solved so far in this non-perturbative regime. Unfortunately due to all this, even if two phases feature significant qualitative differences these are often overshadowed by the huge quantitative uncertainties in the detailed microscopic properties of either of them. However, it will be shown in chapter 4 that certain features, like the important case of the minimum of the instability region can be surprisingly insensitive to quantitative details of the considered models [45]. If such statements can be substantiated this could allow us to devise robust signatures of the qualitative features that can be tested with present and forthcoming

astrophysical data.

As we mentioned earlier r-modes can be a strong and continuous source of gravitational waves. They are an interesting possibility for gravitational wave emission in both newborn neutron stars and accreting neutron stars in low mass X-ray binaries. In the case of r-modes the gravitational radiation is dominated by the mass current quadrupole instead of the usual mass quadrupole. If the saturation amplitude of the r-modes gets to high values O(1) there will be more gravitational radiation because of the larger oscillations. However r-modes with a low saturation amplitude can be also a good source for the gravitational wave emission, since in this case r-modes will be active in neutron stars for a much longer time and therefore they can be a source for continuous gravitational wave emission. An estimated or upper-limit gravitational wave amplitude h_0 can be converted to an r-mode amplitude α by the following equation [55]

$$h_0 = \sqrt{\frac{8\pi}{5}} r^{-1} \omega^3 \alpha M R^3 \tilde{J} \tag{1.7}$$

where r is the distance between the GW detector and the neutron star, ω is the gravitational wave frequency which is identical to the mode frequency, given by eq. (1.4), M and R are mass and radius of the star and $\tilde{J}$ is a dimensionless constant defined by $\tilde{J} = \frac{1}{MR^4} \int_0^R \rho r^6 dr$ where ρ is the mass density. Using the numerical values for a typical $1.4 M_\odot$ neutron star with $n = 1$ polytropic equation of state that has a radius of 11.7 km and $\tilde{J} \simeq 0.0164$ the amplitude of the r-mode can be written in terms of the gravitational wave amplitude in the following form [55]

$$\alpha = 0.028 \left(\frac{h_0}{10^{-24}}\right) \left(\frac{r}{1\text{kpc}}\right) \left(\frac{1\text{Hz}}{f}\right) \tag{1.8}$$

where $f = \frac{\omega}{2\pi}$.

Using data from the Laser Interferometer Gravitational-Wave Observatory, the

LIGO and Virgo Collaborations have published searches for periodic gravitational waves from rapidly rotating neutron stars [56, 57, 58, 59] and have given upper limits for the intrinsic gravitational-wave strain h_0 which can be used for getting an upper limit on the r-mode amplitude α using the above equations [59, 55]. We will explain more about the r-mode oscillations of neutron stars in chapters 4 and 5.

Chapter 2

Shear viscosity due to kaon condensation in color-flavor locked quark matter

In the previous chapter we gave an introduction to the physics of the color superconductivity and introduced the kaon-condensed color-flavor-locked phase (CFL-K0) as one of the possible phases of quark matter at high densities and low temperatures. In this chapter which is based on Ref. [60] we study the kaonic contribution to the shear viscosity of quark matter in the CFL-K0 phase. As we discussed in the previous chapter transport properties of quark matter, such as the shear viscosity, are of interest because they are the basis for signatures by which we could infer or rule out the presence of exotic phases in the core of neutron stars. The shear viscosity is phenomenologically relevant in the damping of physically important excitation modes of the star, in particular the r-mode oscillations.

In the first section we explain the physics of the CFL-K0 phase in more details. In the second section, Sec. 2.2, we discuss the low-energy effective theory of the CFL-K0 phase and the interactions among the lowest-energy excitations of the theory.

In Sec. 2.3, we calculate the mean free path of the Goldstone kaons, because the concept of shear viscosity will only be applicable to the matter in the neutron star if there is local equilibration on distance scales much smaller than the size of the star. In Sec. 2.4, we discuss the derivation of the shear viscosity using the viscous hydrodynamic equations and solving the Boltzmann equation. In Sec. 2.5 we give the analytic and numerical results for the shear viscosity. Section 2.6 will present some conclusions and discuss future directions of this work. In appendix A we calculate the scattering mean free path of the kaons and in the appendices B and C we cover technical details of the treatment of the co-linear regime of the collision integral, and the approximate evaluation of the collision integral.

2.1 CFL-K0 phase of quark matter

As we discussed earlier in Sec. 1.1, in the color-flavor locked phase of quark matter all the quarks with different colors and flavors have the same Fermi momentum and all of them will take part in the formation of Cooper pairs. When we go to lower densities where the mass of the strange quark can not be ignored anymore, a splitting between the Fermi momentum of strange quark and the light quarks will happen and the BCS pairing will be suppressed [2]. When the shift between the Fermi momenta is larger than the gap, $\Delta P_F > \Delta$, pairing between s and u, d quarks is not possible anymore. But when the stress is not too large the CFL pairing pattern can be modified by forming a condensate of K^0 mesons. Since K^0 mesons carry negative strangeness the stress on the CFL phase will be relieved by forming a K^0 condensate. Bedaque and Schafer have explained the effect of kaon condensation in two different ways, [28, 25]. The first one is a chiral rotation of the CFL order parameter. The order parameter of a two-flavor superfluid quark matter is given by $< \epsilon^{abc} u^a C\gamma_5 d^c >$

which is a flavor singlet [18, 19, 20]. The superfluidity has to be destroyed in order to create a macroscopic occupation number of charged excitations. But the order parameter of CFL matter is a matrix in color and flavor space: $< q^a_{L,i} C q^b_{L,j} >= - < q^a_{R,i} C q^b_{R,j} >= \phi(\delta^a_i \delta^b_j - \delta^b_i \delta^a_j)$, where i, j label flavor and a, b label color indices. One can introduce a chiral field Σ that characterizes the relative flavor orientation of the left- and right-handed condensates [61]. In the vacuum $\Sigma = 1$, but under the influence of a perturbation Σ may rotate. Because Σ has the quantum numbers of pseudoscalar Goldstone bosons, such a rotation corresponds to a macroscopic occupation number of Goldstone bosons. The second approach in explaining the kaon condensation in the CFL-K0 phase which is simpler than the first one is as following: In normal quark matter a non-zero strange quark mass, which causes a splitting of the order of $\frac{M_s^2}{2P_F}$ between the Fermi surfaces of strange quarks and light quarks, leads to the decay $s \to u + e^- + \bar{\nu_e}$ or $s \to u + d + \bar{u}$. In superfluid quark matter the system can also gain energy $\frac{M_s^2}{2P_F}$ by introducing an extra up quark and a strange hole. But since all up quarks are gapped this process requires the breaking of a pair and therefore involves an energy cost of the order of the gap Δ. But this is not correct because an up-, down-particle/strange-hole pair has the quantum numbers of a kaon. This means that the energy cost is not Δ but $m_K \ll \Delta$. The CFL vacuum can decay into K^+ or K^0 collective modes via processes like $0 \to (\overline{ds})(du) + e^- + \bar{\nu_e}$ or $0 \to (\overline{us})(du)$.

The kaon condensate spontaneously breaks the flavor symmetry, producing a Goldstone boson[25, 62]. Since the flavor symmetry is also explicitly broken by the weak interaction, this Goldstone kaon acquires a small mass in the keV range [63]. Our analysis is relevant to temperatures above this value, where one can ignore this small mass. We use the effective theory of the Goldstone kaon, which was worked out in Ref. [64]. The full interaction lagrangian has three independent coupling constants, but we will specialize to a specific ratio of their values, which makes our results depen-

dent on one overall kaon interaction coupling. This enables us to make an estimate of the expected scale of the shear viscosity in this phase.

2.2 Low-Energy Effective Theory

2.2.1 Lowest-order lagrangian

The low-energy degrees of freedom in color-flavor-locked phases of quark matter are the massless superfluid Goldstone mode, arising from the spontaneous breaking of baryon number, and the light pseudo-Goldstone meson octet, arising from the spontaneous breaking of three-flavor chiral symmetry. The contribution of the superfluid mode to transport properties has been studied previously [65, 66]. We focus on the contribution from the meson octet, described by a meson field Σ whose effective lagrangian up to second order is [25, 62]

$$\mathcal{L} = \frac{f_\pi^2}{4}\mathrm{Tr}[D_0\Sigma\, D_0\Sigma^\dagger - v^2\nabla\Sigma\,\nabla\Sigma^\dagger] + a\frac{f_\pi^2}{2}\det M\,\mathrm{Tr}[M^{-1}(\Sigma+\Sigma^\dagger)] \qquad (2.1)$$

where $D_0\Sigma = \partial_0\Sigma - i[A,\Sigma]$. The Bedaque-Shäfer effective chemical potential [25] is $A = -\frac{M.M}{2\mu_q}$, μ_q is the quark chemical potential, and $M = \mathrm{diag}(m_u, m_d, m_s)$ is the quark mass matrix. At asymptotically high density the constants f_π, v, and a can be determined by matching the effective theory to perturbative QCD, [67, 68]

$$f_\pi^2 = \frac{21-8\ln 2}{18}\frac{\mu_q^2}{2\pi^2} \approx (0.21\mu_q)^2 \qquad v \equiv v_H = \frac{1}{\sqrt{3}} \qquad a = \frac{3\Delta^2}{\pi^2 f_\pi^2}\ , \quad (2.2)$$

where Δ is the fermionic energy gap at zero temperature. This dependence of a on Δ is also seen in NJL models [69], so from now on we will work in terms of f_π and Δ, assuming that a is given by eq. (2.2). The meson field Σ can be parameterized in

terms of fields θ_a,

$$\Sigma = \exp(i\theta/f_\pi) \ , \tag{2.3}$$

where $\theta = \theta_a T_a$, and T_a are the Gell-Mann matrices of SU(3) with normalization $\mathrm{tr}(T_a T_b) = 2\delta_{ab}$. The K^0 and K^+ are the lightest mesonic degrees of freedom [67, 68], and electric neutrality disfavors the presence of charged kaons (since they must be balanced by electrons), so we focus on the neutral kaons, K^0 and $\bar{K}^0$, corresponding to θ_6 and θ_7. The zero-temperature neutral kaon mass and chemical potential can be deduced from the Lagrangian

$$\begin{aligned} m_K^2 &= a m_u (m_d + m_s) \ , \\ \mu_K &= \frac{m_s^2 - m_d^2}{2\mu_q} \ . \end{aligned} \tag{2.4}$$

We will assume that $\mu_K > m_K$, so there is kaon condensation. We will also assume, following Ref. [64], that the condensate is small, so μ_K is only a little larger than m_K. It is then convenient to define, following Ref. [64], an energy gap

$$\delta m \equiv m_K - \mu_K \ , \qquad \frac{|\delta m|}{m_K} \ll 1 \ . \tag{2.5}$$

Note that δm is negative in the CFL-K0 phase. Because $|\delta m| \ll 1$ we can usually treat μ_K and m_K as being identical to leading order in δm (an exception is discussed in Sec. 2.5).

A self-consistent calculation [64] (see also Ref. [70]) then yields the excitation energies in the neutral kaon sector,

$$E_\pm^2 = E_p^2 + \mu_K^2 \mp \sqrt{4\mu_K^2 E_p^2 + \delta M^4} \ , \tag{2.6}$$

where

$$E_p^2 = v^2 p^2 + \bar{M}^2 \ . \tag{2.7}$$

In that self-consistent calculation, $\bar{M}$ and δM were thermal masses that depended on temperature and the underlying mass and chemical potential (see Eq. (81) in Ref. [64]). Here we are interested in the low-temperature range applicable for compact stars. In this case, the thermal masses become independent of temperature and are given by

$$\begin{aligned} \bar{M}^2 &= 2\mu_K^2 - m_K^2 \approx m_K^2 \ , \\ \delta M^2 &= \mu_K^2 - m_K^2 \approx 2 m_K |\delta m| \ . \end{aligned} \tag{2.8}$$

The mode with energy E_+ is massless: this is the Goldstone kaon. We can define a corresponding field ψ using the parameterization

$$\begin{aligned} \theta_6(x) &= \big(\phi + \rho(x)\big) \cos\vartheta(x) \ , \\ \theta_7(x) &= \big(\phi + \rho(x)\big) \sin\vartheta(x) \ , \\ \psi(x) &= f_\pi \sin(\phi/f_\pi)\, \vartheta(x) \ , \end{aligned} \tag{2.9}$$

so ϕ is the kaon condensate, ρ is the massive radial mode, and ϑ is the angular Goldstone mode which we have then rescaled to make a scalar field ψ with a canonically normalized quadratic derivative term and the conventional energy dimension of 1. The mass of the radial modes is given by the value of $E_-(p=0) = \sqrt{6\mu_K^2 - 2m_K^2} \approx 2m_K$, which is typically on the order of a few MeV, so at the 10 to 100 keV energy scale, which is relevant to neutron stars, it is heavily suppressed and can be ignored. The magnitude of the kaon condensate is [64]

$$\phi^2 = 2f_\pi^2\Big(1 - \frac{m_K^2}{\mu_K^2}\Big) \approx 4 f_\pi^2 \frac{|\delta m|}{m_K} \tag{2.10}$$

We can then linearize eq. (2.6) to obtain a linear dispersion relation for the Goldstone kaon,

$$\begin{aligned} E(p) &= \nu p \\ \nu &\equiv v\sqrt{\frac{\bar{M}^2-\mu_K^2}{\bar{M}^2+\mu_K^2}} \approx v\sqrt{\frac{|\delta m|}{m_K}} \ . \end{aligned} \tag{2.11}$$

The error involved in approximating eq. (2.6) by eq. (2.11) is less than 5% for $p < 0.6\sqrt{m_K|\delta m|}/v$.

We will obtain the contribution to the shear viscosity from the Goldstone kaon. For this we need its interaction lagrangian, but it is easy to see that eq. (2.1) does not contain any interaction terms for the field ψ. This follows from the fact that ψ, as a Goldstone boson, must couple via derivatives, and eq. (2.1) only goes to second order in derivatives. We therefore need to write down higher order derivative terms in the effective theory to obtain interactions among the Goldstone modes.

2.2.2 Interaction lagrangian for the Goldstone kaons

We obtain higher derivative terms in ψ by writing down the leading higher derivative terms in the lagrangian for Σ, and using eq. (2.9). We keep only terms with the symmetries of the system, namely rotational symmetry, parity, time-reversal, and the $SU(3)_L \otimes SU(3)_R$ chiral flavor symmetry. We also discard terms that, when we substitute eq. (2.9), will produce interactions that all involve the ρ field; an example is three-derivative terms where Σ enters four times. The allowed terms with no more than four derivatives of Σ are shown in Table 2.1 (left column). Since the effective theory breaks down at momenta of order Δ (for example, scattering of Goldstone bosons at that momentum will produce quasiquarks, which are not included in the effective theory) we expect that the momentum expansion will be in powers of $(1/\Delta)\vec{\nabla}$ [25]. We therefore expect the interactions in the left column of Table 2.1 to occur

1a.	$\left(\mathrm{Tr}[D_0\Sigma D_0\Sigma^\dagger]\right)^2$	$\frac{4}{f_\pi^4}(\partial_0\psi)^4 + \frac{16\mu_K \sin\varphi}{f_\pi^3}(\partial_0\psi)^3$
1b.	$2\mathrm{Tr}[(D_0\Sigma D_0\Sigma^\dagger)^2]$	
2a.	$\left(\mathrm{Tr}[\nabla\Sigma\nabla\Sigma^\dagger]\right)^2$	$\frac{4}{f_\pi^4}(\nabla\psi)^4$
2b.	$2\mathrm{Tr}[(\nabla\Sigma\nabla\Sigma^\dagger)^2]$	
3a.	$\mathrm{Tr}[D_0\Sigma D_0\Sigma^\dagger]\mathrm{Tr}[\nabla\Sigma\nabla\Sigma^\dagger]$	$\frac{4}{f_\pi^4}(\partial_0\psi)^2(\nabla\psi)^2 + \frac{8\mu_K \sin\varphi}{f_\pi^3}(\partial_0\psi)(\nabla\psi)^2$
3b.	$2\mathrm{Tr}[D_0\Sigma D_0\Sigma^\dagger\nabla\Sigma\nabla\Sigma^\dagger]$	

Table 2.1: The six interaction terms at fourth order in derivatives for the effective theory (first column), and the interaction terms for ψ that they transform to using eq. (2.9), when terms involving ρ are dropped. In the effective lagrangian they have coefficients of order f_π^2/Δ^2.

in the lagrangian with coefficients $C_i f_\pi^2/\Delta^2$, where the C_i are dimensionless coupling constants.

Using eq. (2.9) and dropping terms that involve the heavy field ρ, these six terms reduce to the three corresponding interaction terms for ψ shown in the right column. In each case, we find two different interaction terms for Σ reduce to the same interaction term for ψ. This means that the interaction lagrangian for ψ only depends on three linear combinations of couplings. Note that in Table 2.1 we have defined a scaled version of the kaon condensate expectation value eq. (2.9),

$$\varphi \equiv \phi/f_\pi \approx 2\sqrt{\frac{|\delta m|}{m_K}} \tag{2.12}$$

The interaction Lagrangian for ψ can then be written out as

$$\begin{aligned}\mathcal{L} &= C_1\frac{2}{f_\pi^2\Delta^2}(\partial_0\psi)^4 + C_3\frac{2}{f_\pi^2\Delta^2}(\partial_0\psi)^2(\nabla\psi)^2 + C_2\frac{2}{f_\pi^2\Delta^2}(\nabla\psi)^4 \\ &\quad + C_1\frac{8\mu_K\sin\varphi}{f_\pi\Delta^2}(\partial_0\psi)^3 + C_3\frac{4\mu_K\sin\varphi}{f_\pi\Delta^2}(\partial_0\psi)(\nabla\psi)^2.\end{aligned} \tag{2.13}$$

At this point we specialize to a particular form of the interaction lagrangian, with

the following relationship among the three coupling constants.

$$C \equiv C_1 = C_2 = -\tfrac{1}{2}C_3. \tag{2.14}$$

This reduces the number of coupling constants from three to one. The remainder of our calculation is for this special case, adopted because it leads to a particularly simple interaction lagrangian which is similar to that written down for the superfluid phonon in Refs. [66, 71],

$$\mathcal{L}_{int} = \frac{\lambda}{4f_\pi^4}(\partial_\mu\psi\partial^\mu\psi)^2 + \frac{g}{2f_\pi^2}(\partial_0\psi)(\partial_\mu\psi\partial^\mu\psi) \tag{2.15}$$

where

$$\lambda = 8C\frac{f_\pi^2}{\Delta^2} \qquad \text{and} \qquad g = 16\sin(\varphi)C\,\frac{\mu_K f_\pi}{\Delta^2} \tag{2.16}$$

2.3 Mean Free Path

In this section we discuss the mean free path of the Goldstone kaons in the CFL-K^0 phase. We expect that hydrodynamics will be applicable to neutron star oscillations when the mean free path is well below the kilometer scale, since neutron star radii are about 10 km.

We study two definitions of the mean free path, which we call the "shear mean free path" $l^{\rm shear}$ and the "scattering mean free path" $l^{\rm scat}$. The shear mean free path is based on the value of the shear viscosity itself, and is probably the physically relevant quantity for deciding when hydrodynamic calculations of shear viscosity are valid. The scattering mean free path which is given in appendix A is the average distance between collisions of the Goldstone kaons, including co-linear scattering events. Since co-linear scatterings do not contribute to the shear viscosity itself, it seems likely that

this quantity is not the relevant one for finding the limits of validity of shear viscosity calculations.

Shear mean free path

We take our definition of the shear mean free path from Ref. [71], where it is referred to as λ_B,

$$l^{\rm shear} = \frac{\eta}{n\,\langle p\rangle} \tag{2.17}$$

here η is the shear viscosity, $\langle p\rangle$ is the thermal average momentum, and n is the boson density,

$$\langle p\rangle = 2.7\,T/\nu\ , \tag{2.18}$$

$$n = \int \frac{d^3p}{(2\pi)^3} f_p = \zeta(3)\frac{T^3}{\pi^2\nu^3}\ . \tag{2.19}$$

where ν is the speed of the Goldstone bosons (given for kaons by eq. (2.11)).

This already allows us to make an estimate of the maximum shear viscosity that Goldstone kaons can provide, since it follows that $\eta \approx 0.3\nu^{-4}T^4 l^{\rm shear}$, so the maximum shear viscosity that could possibly occur in a neutron star at temperature T is when $l^{\rm shear} \approx 1$ km, i.e.

$$\eta_{\rm max} \approx \frac{T^3}{\nu^4}\frac{T}{7\times 10^{-16}\ {\rm MeV}}\ . \tag{2.20}$$

For Goldstone kaons it is quite possible to get $\nu \approx 0.1$ by using small values of δm. Using this value we find the following upper limits: at $T = 0.01$ MeV, $\eta_{\rm max} \sim 10^{11}$ MeV^3; at $T = 0.1$ MeV, $\eta_{\rm max} \sim 10^{15}$ MeV^3; at $T = 1$ MeV, $\eta_{\rm max} \sim 10^{19}$ MeV^3.

For superfluid phonons [66] we can make more definite statements because there is less uncertainty about the parameters appearing in these expressions. The shear viscosity is $\eta = 1.3\times 10^{-4}\mu_q^8/T^5$ and the speed ν is generally assumed to take its

perturbative value $1/\sqrt{3}$ [66], in which case we immediately find that

$$l_H^{\rm shear} \approx 4 \times 10^{-5} \frac{\mu_q^8}{T^9} \tag{2.21}$$

So phonon hydrodynamics becomes invalid in neutron stars when $l_H^{\rm shear} \gtrsim 1$ km, i.e. for $\mu \approx 500$ MeV we require $T \gtrsim 1$ MeV (10^{10} K), and at a temperature of 1 MeV the phonon shear viscosity is 5×10^{17} MeV^3. The calculation of the scattering mean free path which is determined by the two-body interaction cross section is given in appendix A.

2.4 Shear Viscosity

The shear viscosity η is the coefficient of the traceless part of the viscous stress tensor δT_{ij}, which is a small deviation from equilibrium of the spatial components of the energy momentum tensor T_{ij} for a fluid with pressure P and energy density ϵ,

$$\begin{aligned} T_{ij} &= T_{ij}^{(eq)} + \delta T_{ij} \\ T_{ij}^{(eq)} &= (P+\epsilon) V_i V_j - P\delta_{ij} \\ \delta T_{ij} &= -\eta V_{ij} + \cdots \end{aligned} \tag{2.22}$$

where V_{ij} is given by

$$V_{ij} = \partial_i V_j + \partial_j V_i - \frac{2}{3}\delta_{ij} \nabla \cdot \mathbf{V} \tag{2.23}$$

and the ellipsis in the equation for δT_{ij} stands for other dissipative terms arising from phenomena such as bulk viscosity and thermal conductivity. $\mathbf{V}(\mathbf{x}, t)$ is the fluid velocity at a given position and time. The stress-energy tensor and the viscosity can

be calculated using kinetic theory [72]. For a system of identical bosonic particles with dispersion relation E_p,

$$T_{ij}(\mathbf{x},t) = \nu^2 \int \frac{d^3p}{(2\pi)^3} \frac{p_i\, p_j}{E_p} f_p(\mathbf{x},t) \ . \tag{2.24}$$

where ν is the velocity of the Goldstone kaon (see eq. (2.11)). The full distribution function is given by

$$f_p(\mathbf{x},t) = \frac{1}{e^{p_\mu u^\mu(\mathbf{x},t)/T} - 1} = f_p^0 + \delta f_p(\mathbf{x},t) \tag{2.25}$$

where $u^\mu(\mathbf{x},t)$ is the 4-velocity of the fluid, and δf_p is a small departure from the equilibrium Bose-Einstein distribution

$$f_p^0 = \frac{1}{e^{E_p/T} - 1} \ . \tag{2.26}$$

For shear viscosity we are interested in deviations from equilibrium arising from a shear flow, so we write the deviation from equilibrium as

$$\begin{aligned} \delta f_p(\mathbf{x},t) &= -\frac{\chi(p,\mathbf{x},t)}{T} f_p^0(1+f_p^0) \\ \chi(p,\mathbf{x},t) &= g(p)\, p_{kl}\, V_{kl}(\mathbf{x},t), \end{aligned} \tag{2.27}$$

where

$$p_{kl} = p_k\, p_l - \frac{1}{3}\delta_{kl} p^2. \tag{2.28}$$

Substituting eq. (2.27) into eq. (2.24) and eq. (2.22) we find

$$\delta T_{ij}(\mathbf{x},t) = -\nu^2 \int \frac{d^3p}{(2\pi)^3} \frac{p_i\, p_j}{E_p} \frac{g(p)\, p_{kl}}{T} f_p^0(1+f_p^0)\, V_{kl}(\mathbf{x},t). \tag{2.29}$$

Using the definition of V_{ij} (Eq. 2.23) one can write δT_{ij} (Eq. 2.22) in the following form

$$\delta T_{ij} = -\frac{\eta}{2}[\delta_{ik}\delta_{jl} + \delta_{il}\delta_{jk} - \frac{2}{3}\delta_{ij}\delta_{kl}]V_{kl}, \tag{2.30}$$

Comparing this to eq. (2.29) gives

$$\frac{\eta}{2}[\delta_{ik}\delta_{jl} + \delta_{il}\delta_{jk} - \frac{2}{3}\delta_{ij}\delta_{kl}] = \nu^2 \int \frac{d^3p}{(2\pi)^3}\frac{p_i\, p_j}{E_p}\frac{g(p)\, p_{kl}}{T} f_p^0(1 + f_p^0). \tag{2.31}$$

Then, by contracting the tensor on the left hand side with respect to the pairs of indices i, k and j, l we can determine the shear viscosity in terms of the function $g(p)$,

$$\eta = \frac{4\,\nu^2}{15\,T}\int_p p^4\, f_p^0(1 + f_p^0)\, g(p), \tag{2.32}$$

where we have adopted the notation

$$\int_p = \int \frac{d^3p}{2\,E_p\,(2\,\pi)^3}. \tag{2.33}$$

Using the fact that $p^4 = \frac{3}{2}p_{ij}\, p_{ij}$ (see Eq. 2.28) one can write an alternate form of the shear viscosity which will be used later,

$$\eta = \frac{2\,\nu^2}{5\,T}\int_p f_p^0(1 + f_p^0)\, g(p) p_{ij} p_{ij}. \tag{2.34}$$

To solve for the viscosity, we need to find a form for $g(p)$. To do so, we can use the Boltzmann equation given in the absence of external forces by

$$\frac{df_p}{dt} = \frac{\partial f_p}{\partial t} + \mathbf{V}\cdot\nabla f_p = C[f_p]\ . \tag{2.35}$$

where $C[f_p]$ is the collision operator. The left-hand side of the equation above can be

written as [72]

$$\frac{df_p}{dt} = \nu \frac{f_p^0}{2\,p\,T}(1 + f_p^0)\, p_{ij}\, V_{ij} \ . \tag{2.36}$$

Again, this specific form assumes that we are only interested in shear flows. Thermal gradients and bulk flows would give additional terms on the right hand side of eq. (2.36). It is this form that also helped motivate the structure of the ansatz in eq. (2.27).

The collision operator $C[f_p]$ should contain any possible collision terms for the kaons. We will restrict ourselves to the terms lowest order in the coupling constants as more vertices are suppressed because each vertex brings in more powers of $1/f_\pi$ or $1/\Delta$ (see eq. (2.15) and eq. (2.16)). Also, we will ignore the $1 \leftrightarrow 2$ processes because for a particle with a linear dispersion relation such processes must be co-linear, so they do not involve momentum transfer that would contribute to the shear viscosity. Finally we are left with the collision operator for 2-body scattering given by [71]

$$C_{2\leftrightarrow 2} = \frac{1}{2E_p} \int_{k,k',p'} (2\pi)^4 \delta^4(P + K - P' - K') |\mathcal{M}|^2 D_{2\leftrightarrow 2} \tag{2.37}$$

Where $P = (E_p, \mathbf{p}) = (p_0, \mathbf{p})$ and K are the four momenta of the two incoming particles and P', K' are the four-momenta of the two outgoing particles in the $2 \leftrightarrow 2$ scattering process. $\mathcal{M}$ is the $2 \leftrightarrow 2$ scattering amplitude and $D_{2\leftrightarrow 2}$ contains the distribution functions and is given by

$$D_{2\leftrightarrow 2} = f_{p'}\, f_{k'}(1 + f_p)(1 + f_k) - f_p\, f_k(1 + f_{p'})(1 + f_{k'}). \tag{2.38}$$

We can also linearize the distributions as $D \approx D^0 + \delta D$ using our definition of δf_p in eq. (2.27). D^0 would make the collision integral vanish by detailed balance. One can

then write

$$\delta D_{2\leftrightarrow 2} = \frac{1}{T} f_p^0 \, f_k^0 (1 + f_{p'}^0)(1 + f_{k'}^0) \left(\chi(p) + \chi(k) - \chi(p') - \chi(k')\right) \tag{2.39}$$

and the collision integral as

$$\begin{aligned} C_{2\leftrightarrow 2} &\approx \frac{f_p^0}{2E_p T} \int_{k,p',k'} (2\pi)^4 \delta^4(P + K - P' - K') |\mathcal{M}|^2 f_k^0 (1 + f_{p'}^0)(1 + f_{k'}^0) \\ &\quad \left[g(p) p_{ij} + g(k) k_{ij} - g(k') k'_{ij} - g(p') p'_{ij}\right] V_{ij} \\ &\equiv \frac{1}{2E_p T} F_{ij}[g(p)] V_{ij} \end{aligned} \tag{2.40}$$

Using eq. (2.36) and the Boltzmann equation, we can conclude that

$$\nu^2 f_p^0 (1 + f_p^0) \, p_{ij} = F_{ij}[g(p)] \tag{2.41}$$

One can then use this equation and eq. (2.34) to get another expression for the shear viscosity in terms of collision term

$$\eta = \frac{2}{5T} \int_p g(p) p_{ij} F_{ij}[g(p)] \tag{2.42}$$

The process now is to evaluate η from eq. (2.32) and eq. (2.42), and ensure that they give the same answer. Formally, this is equivalent to solving the Boltzmann equation directly. Ensuring that the two forms are equal is quite non-trivial and is typically done by expanding $g(p)$ using an orthogonal set of functions, [73, 74]

$$g(p) = p^n \sum_{s=0}^{N} b_s B_s(p) \ . \tag{2.43}$$

This expansion introduces two new parameters: N, the order of the polynomial approximation; and n, which we call the minimum-exponent parameter, because the

lowest power of p that occurs in the polynomial expansion is p^n. The correct result is obtained in the limit $N \to \infty$ for any value of n. However, as we will see, the rate of convergence with increasing N is strongly dependent on the minimum-exponent parameter n.

The polynomials $B_s(p)$ are defined such that the coefficient of the highest power p^s is 1 and they obey the orthogonality condition [71]

$$\int_p f_p^0(1+f_p^0)\, p_{ij}\, p_{ij} p^n B_r(p) B_s(p) = A_r^{(n)} \delta_{rs} \ . \tag{2.44}$$

These conditions uniquely specify the $B_s(p)$ for all s, starting with $B_0(p) = 1$. From the orthogonality condition we find

$$A_0^{(n)} = \frac{2}{3}\int_p f_p^0(1+f_p^0) p^{4+n} = \frac{T^{6+n}}{6\pi^2\nu^{7+n}}\Gamma(6+n)\zeta(5+n) \ . \tag{2.45}$$

Using $g(p)$ from eq. (2.43) in eq. (2.32), and using the definition of $A_r^{(n)}$ from eq. (2.44), we get

$$\eta = \frac{2\,\nu^2}{5T} b_0 A_0^{(n)} \ . \tag{2.46}$$

An alternative expression for η follows from substituting $g(p)$ from eq. g-pnml into eq. (2.42),

$$\eta = \sum_{s,t=0}^{N=\infty} b_s b_t M_{st} \ , \tag{2.47}$$

where

$$\begin{aligned} M_{st} &= \frac{2}{5T}\int_{p,k,k',p'} (2\pi)^4 \delta^4(P+K-P'-K') |\mathcal{M}|^2 f_p^0 f_k^0 (1+f_{k'}^0)(1+f_{p'}^0)\ p^n B_s(p) p_{ij} \Delta_{ij}^t \ , \\ &= \frac{1}{10T}\int_{p,k,k',p'} (2\pi)^4 \delta^4(P+K-P'-K') |\mathcal{M}|^2 f_p^0 f_k^0 (1+f_{k'}^0)(1+f_{p'}^0)\ \Delta_{ij}^s \Delta_{ij}^t \end{aligned} \tag{2.48}$$

and

$$\Delta^t_{ij} = B_t(p)p^n p_{ij} + B_t(k)k^n k_{ij} - B_t(k')k'^n k'_{ij} - B_t(p')p'^n p'_{ij} \ . \tag{2.49}$$

The second line of eq. (2.48) uses the symmetry under relabeling the momenta of the legs in the scattering diagrams ($P \to K$, etc.), and can be used to demonstrate that the diagonal elements of M_{st} are positive definite. As we will see below, this ensures that the shear viscosity is also positive.

Requiring the two forms of η to be equal leads to a matrix equation for all the b_i's. From that we extract b_0,

$$b_0 = \frac{2\,\nu^2}{5T} A_0^{(n)} (M^{-1})_{00} \tag{2.50}$$

where $(M^{-1})_{00}$ means the first entry in the matrix inverse of M_{st}. Using this in eq. (2.46), we find

$$\eta = \frac{4\,\nu^4}{25T^2} (A_0^{(n)})^2 (M^{-1})_{00} \ . \tag{2.51}$$

As noted above, this expression becomes accurate in the limit $N \to \infty$, where the matrix M is of infinite size. It is known [66, 71] that the result for finite N rises with N, so for a matrix M_N, with finite dimension N, that obeys eq. (2.48),

$$\eta \geq \frac{4\,\nu^4}{25T^2} (A_0^{(n)})^2 (M_N^{-1})_{00} \tag{2.52}$$

We will see below that this expression converges rapidly with N for the optimal choice of the minimum-exponent parameter n.

The remaining task is to evaluate the integral in eq. (2.48). This requires the matrix elements for the $2 \leftrightarrow 2$ scattering process, $i\mathcal{M} = i\mathcal{M}_c + i\mathcal{M}_s + i\mathcal{M}_t + i\mathcal{M}_u$,

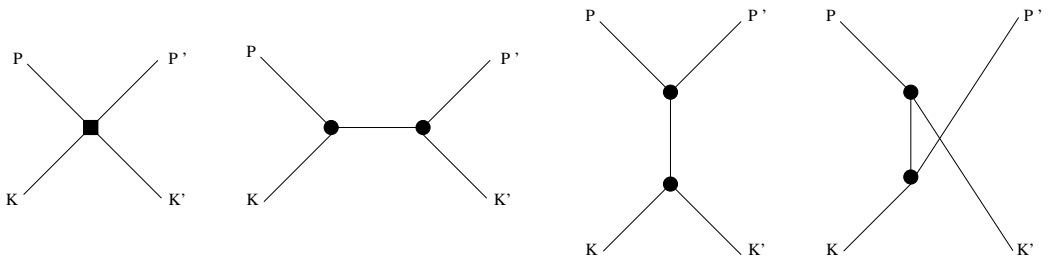

Figure 2.1: Feynman diagrams for the 2-body scattering amplitude. The black square is the 4-point contact interaction, the black circles are the 3-point vertices.

see Fig. 2.1, with the individual channels being given by

$$\begin{aligned} i\mathcal{M}_c &= \frac{\lambda}{f_\pi^4}\left[(P\cdot K)(P'\cdot K)+(P\cdot K')(P'\cdot K)+(P\cdot P')(K\cdot K')\right] \\ i\mathcal{M}_s &= \frac{g^2}{f_\pi^4}\left[2(p_0+k_0)P\cdot K+p_0K^2+k_0P^2\right]\left[2(p_0'+k_0')P'\cdot K'+p_0'K'^2+k_0'P'^2\right]G(P+K) \\ i\mathcal{M}_t &= i\mathcal{M}_s(P\leftrightarrow K') \\ i\mathcal{M}_u &= i\mathcal{M}_t(P\leftrightarrow K), \end{aligned} \tag{2.53}$$

where the last two lines in eq. (2.53) come from crossing symmetries and

$$G(Q)=\frac{1}{(q_0^2-\nu^2q^2)+i\,\mathrm{Im}\,\Pi(q_0,q)} \tag{2.54}$$

is the Goldstone kaon propagator. Note that to avoid the collinear singularities in our calculations we resum the kaon propagator including the one loop thermal damping. The imaginary part of the self energy, $\mathrm{Im}\,\Pi(\mathrm{q_0},\mathrm{q})$, is extracted after a one-loop computation (for more details see appendix A) [75, 66].

The 12-dimensional integral in eq. (2.48) can be simplified by eliminating the $\mathbf{p}'$ integral using the momentum-conserving delta-function. Then one can use the energy-conserving delta-function to eliminate the integral over the magnitude of k'. Three of the remaining 8 integrals can be eliminated by selecting the z-axis to lie along the vector $\mathbf{p}$, and noting that only the difference in the two remaining azimuthal

n	$N = 0$	$N = 1$	$N = 2$
-3	0.059	0.861	2.22
-2	1.59×10^5	2.01×10^5	2.02×10^5
-1	2.04×10^5	2.04×10^5	2.04×10^5
0	0.610	4.70	19.4

Table 2.2: Values of shear viscosity as a function of the order N of the polynomial approximation to $g(p)$, for different choices of the minimum-exponent parameter n. The calculated value rises towards the physical result as $N \to \infty$, and in this limit should be independent of n. We see that for $n = -1$ the result converges very rapidly as N rises, but for other values of n the convergence is slower.

angles matters. This leaves a 5-dimensional integral over the magnitudes of p and k, two polar angles corresponding to k and k' and one azimuthal angle. This can be evaluated numerically (see appendix C) using the *Vegas* Monte Carlo algorithm [**?**].

The results that we present below are obtained by setting the minimum-exponent parameter n to -1. This value is expected to give optimal convergence of the calculated shear viscosity to its physical value as a function of N because, as shown in appendix B, this term most strongly suppresses the co-linear scattering and therefore give the smallest collision term. The shear viscosity is inversely proportional to the collision term and since we have a variational procedure that says the answer we get is a lower bound, we are only interested in the largest value of the shear viscosity that we can calculate.

To check this reasoning we show in Table 2.2 results of calculations of the shear viscosity for different values of n and N. We see that for $n = -1$ the value of η at low N is already close to the maximum (asymptotic) value at $N = \infty$. For $n = -2$ the convergence is almost as good, achieving $\sim 1\%$ accuracy at $N = 2$. For other values of n the convergence is dramatically poorer. This behavior was also seen in Refs. [66, 71]. We conclude that we can achieve accuracy of better than 1% by choosing $n = -1$, and only keeping the first polynomial ($N = 0$), i.e. we set $g(p) = 1/p$.

2.5 Results

2.5.1 Analytic results

We now describe how the shear viscosity depends on the temperature and on the parameters of the effective lagrangian for the Goldstone kaon. The relevant parameters are the speed ν eq. (2.11) of the kaon and its interaction couplings λ and g eq. (2.15), which in turn depend on more basic parameters C, f_π, Δ, m_K eq. (2.16). Recall that we have assumed $|\delta m| \ll 1$, so in the expressions below, μ_K and m_K are usually interchangeable. One exception is the phonon speed ν, which occurs in the shear viscosity raised to the 11th power (see discussion after eq. (2.59)) so we use the full expression (the identity in eq. (2.11)) for it.

Before performing any numerical calculations, we can extract the temperature dependence of the shear viscosity. Because the co-linear scattering will not contribute to the answer, the propagator does not need to be regulated by the self-energy. Since the temperature only appears in the distribution functions and the self-energy, we can now factorize out the temperature dependence by rescaling all the momenta by the temperature. Doing so we find

$$M_{st} \sim T^{15+2\,n+s+t} \ . \tag{2.55}$$

where s and t are the indices of the matrix indicating how many terms we are keeping in our expansion for $g(p)$ and n is the minimum-exponent parameter (see eq. (2.43)). We also recall the temperature dependence of $A_r^{(n)}$ from eq. (2.44),

$$A_0^{(n)} \sim T^{n+6} \ . \tag{2.56}$$

Therefore, from eq. (2.51), we obtain the temperature dependence of the shear vis-

cosity

$$\eta \propto T^{-5} \ , \tag{2.57}$$

in agreement with previous results [66, 71]. The constant of proportionality in eq. (2.57) has mass dimension 8. In the case of the shear viscosity due to phonons there was only one possible scale, the quark chemical potential μ_q, so $\eta_H \propto \mu_q^8/T^5$. However, we have several scales (f_π, Δ, m_K) manifesting themselves in two coupling constants λ and g eq. (2.16). Which of these is most important depends on whether the scattering is dominated by the contact term or by the exchange of a virtual particle. The dimensionless parameter u that determines which scattering process dominates is

$$u = \frac{3g^2}{\lambda} = 96\, C\, \sin^2(\varphi) \left(\frac{\mu_K}{\Delta}\right)^2 , \tag{2.58}$$

where $\varphi = 2\sqrt{|\delta m|/m_K}$ eq. (2.12) and the 3 represents the 3 channels for virtual particle exchange. For typical values of δm, m_K, and Δ, this ratio can be bigger or smaller than 1. When $u \ll 1$, the contact term dominates, so the scattering amplitude is proportional to λ. When $u \gg 1$, the particle-exchange process dominates, so the scattering amplitude is proportional to g^2. The shear viscosity is inversely proportional to the scattering cross-section, so

$$\begin{aligned} u \ll 1: \quad & \eta = h_1(\nu) \frac{1}{C^2} \frac{f_\pi^4 \Delta^4}{T^5} \ , \\ u \gg 1: \quad & \eta = h_2(\nu) \frac{1}{C^4} \frac{f_\pi^4 \Delta^8}{\sin^4(\varphi) \mu_K^4 T^5} \ , \end{aligned} \tag{2.59}$$

where h_1 and h_2 are dimensionless functions that depend only on the Goldstone kaon speed ν, which depends on δm and m_K. We can obtain their analytic form when $\nu \ll 1$. In that case, the leading-order behavior in both regimes is a ν^{11} power law (see appendix C). In general they must be calculated numerically, and the result

(with the ν^{11} power law scaled out) is shown in Fig. 2.4.

Finally, we note that the shear viscosity due to Goldstone kaons will be smaller than that due to the superfluid phonons, since f_π, Δ, and m_K are much less than μ_q.

2.5.2 Numerical results

To begin, we will confirm the temperature dependence predicted in the previous section. To do so, we will fix the mass of the kaon, $m_K = 4$ MeV, $f_\pi = 100$ MeV, $\Delta = 100$ MeV and $C = 1$. In Fig. 2.2, we show the viscosity as a function of temperature for a few values of δm. The data points are obtained by numerical evaluation of the 5-dimensional integral, whereas the lines show the fit to a T^{-5} power law eq. ((2.57)), which is independent of the regime of coupling constants' values. On the same plot, we show the contribution from the phonons [66]. As expected, the phonon shear viscosity is much larger. Most of the difference comes from the difference in magnitude of the coupling constants (the kaons coupling constant is larger) and the rest comes from a difference in the speed of the kaon and the phonon (the kaon's is smaller), which enters the expression for shear viscosity raised to a high power. Using the shear mean free path criterion $l^{\rm shear} < 1$ km (Sec. 2.3) for the validity of hydrodynamics for neutron star oscillations, we expect the phonons to be non-hydrodynamic at $T \lesssim 1$ MeV; with the parameter values given above, the Goldstone kaons become non-hydrodynamic at $T \lesssim 0.03$ MeV.

In Fig. 2.3 we show the shear viscosity as a function of the gap Δ, with $\delta m = -0.5$ MeV and $T = 1$ MeV. The other parameters have the same values as in Fig. 2.2. This illustrates the transition between the two regimes given in eq. (2.59). The crossover occurs at $u = 1$ which corresponds to $\Delta = 30$ MeV, which is indicated on the graph. As expected, we see that for large Δ ($u \ll 1$), $\eta \propto \Delta^4$; for small Δ ($u \gg 1$), $\eta \propto \Delta^8$.

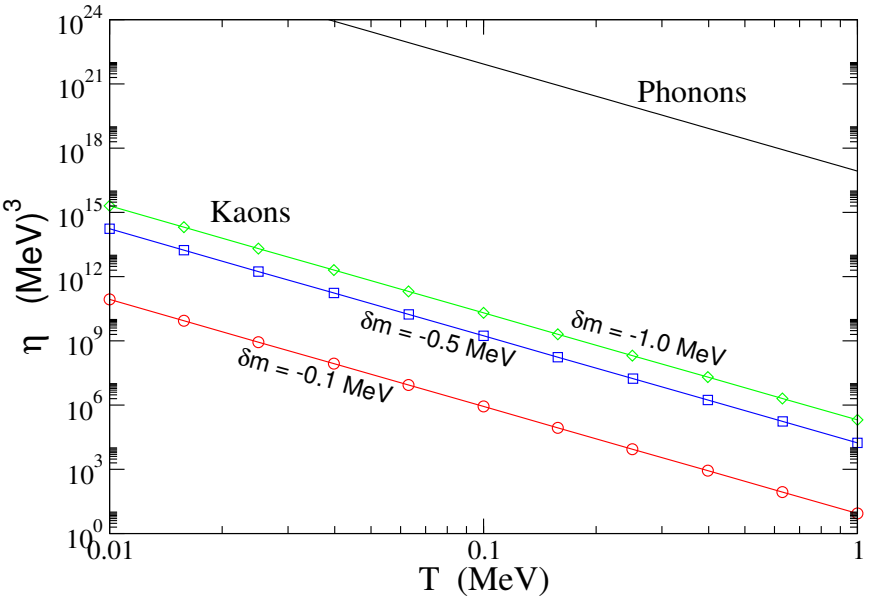

Figure 2.2: The shear viscosity as a function of temperature for kaons and phonons. For parameter values, see text. In the lower part of the graph, the points are numerical calculations and the straight lines are fits to the power law form given in eq. ((2.57)). The phonons' calculated shear viscosity is many orders of magnitude larger, although using the shear mean free path criterion (Sec. 2.3), we expect them to be non-hydrodynamic in neutron stars at $T \lesssim 1$ MeV.

In Fig. 2.4 we present the results of numerical calculation of $h_{1,2}(\nu)$ eq. (2.59). We have divided out the dominant behavior ν^{11} power law behavior (for details see appendix C). We see that the remaining ν dependence is very mild, so to a good approximation the shear viscosity is given by eq. (2.59) with

$$\begin{aligned} h_1(\nu) &\approx 3.44 \times 10^{-4} \nu^{11} \ , \\ h_2(\nu) &\approx 1.70 \times 10^{-8} \nu^{11} \ . \end{aligned} \tag{2.60}$$

To show how large the shear viscosity of CFL-K0 quark matter could be, we look at a case where the values of the parameters are pushed in the direction that yields a large value of η. We take $f_\pi, \Delta \approx 150$ MeV, $m_K \approx 4$ MeV, $\delta m \sim -1.0$ MeV, and $C \approx 0.2$. With these values we find that at $T = 0.1$ MeV (10^9 K) the shear mean free

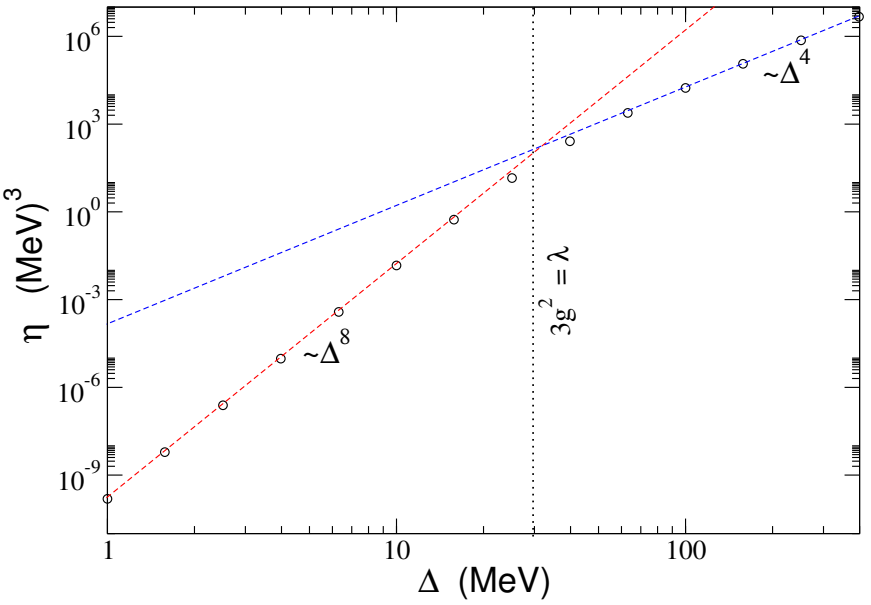

Figure 2.3: The shear viscosity as a function of Δ. (See text for parameter values.) The points are calculated numerically. The straight lines are fits to the power law behaviors of eq. (2.59).

path eq. (2.17) is 0.26 km, and $\eta = 1.7 \times 10^{13}$ MeV^3 $= 2.3 \times 10^{18}\,\mathrm{erg\,cm^{-1}s^{-1}}$. At this temperature the phonon's shear mean free path (see Sec. 2.3) is larger than the star, so the kaons provide the dominant contribution to the shear viscosity.

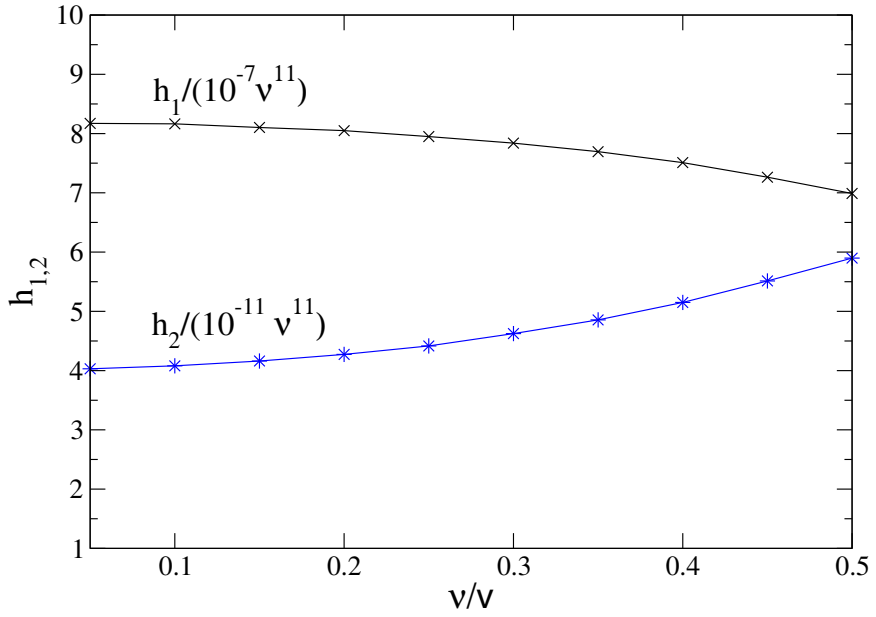

Figure 2.4: The functions $h_1(\nu)$ and $h_2(\nu)$ eq. (2.59). We scale out the ν^{11} power law behavior (see appendix C). On the x-axis we show ν in units of the kaon velocity $v \approx \sqrt{|\delta m|/m_K}$ in the non-kaon-condensed phase.

Finally, we check whether the regime of linear hydrodynamics is valid by evaluating the size of the corrections to the equilibrium stress-energy tensor. Linear hydrodynamics is appropriate if $\delta T_{ij} \ll T_{ij}$ eq. (2.22). (Note that this is different from the criterion of validity for hydrodynamics in general, discussed in appendix A.) This inequality becomes

$$\eta \ll V\ell(P+\epsilon) \tag{2.61}$$

where ℓ represents the length scale of the velocity gradients, and V is the typical fluid velocity which we assume is of order 1. If we use the energy density of free quark matter $\epsilon \approx 9\mu_q^4/(4\pi^2)$ which is of order 10^{10} MeV^4 at $\mu_q \approx 500$ MeV, (and $P \lesssim \epsilon$, which is typically the case), and use the length scale $\ell \sim 1$ km which is appropriate for oscillations of neutron stars, we find that linear hydrodynamics is valid as long as

$$\eta \ll 10^{25}\,\mathrm{MeV}^3 \tag{2.62}$$

which is easily obeyed by the values of the shear viscosity that we have calculated for the CFL-K0 phase.

2.6 Conclusions

In this chapter, we have calculated the shear viscosity arising from self-interaction of the Goldstone kaon mode in the CFL-K0 phase of quark matter. The shear viscosity from the other Goldstone mode, the superfluid phonon, has already been explored in Ref. [66]. We find the same T^{-5} temperature dependence that was found for the phonons in the CFL phase and for superfluid modes in a unitary Fermi gas [71]. Our final results are the approximate analytic expressions eq. (2.59), eq. (2.60) for the shear viscosity due to Goldstone kaons, and expressions eq. (2.17) and eq. (A.16) for

the "shear mean free path" and "scattering mean free path" of the Goldstone kaons.

Neutron star oscillations have a length scale in the kilometer range, so the phonon and Goldstone kaon fluids in a neutron star can only be described by hydrodynamics when their mean free paths are smaller than this. We argue that the shear mean free path is the appropriate quantity to use for this purpose (see Sec. 2.3).

Because the coupling constants for the Goldstone kaons are roughly an order of magnitude larger than those for the superfluid phonon, the shear viscosity and mean free path of the Goldstone kaon are both several orders of magnitude smaller than for the superfluid phonon (see Fig. 2.2). Using the shear mean free path (see Sec. 2.3), we find that the superfluid phonons in a neutron star are described by hydrodynamics at temperatures above about 1 MeV (10^{10} K). The Goldstone kaons are hydrodynamic down to lower temperatures: the exact threshold depends sensitively on the value of the constants in the effective action, but could easily be lower than the 0.01 to 0.05 MeV range at which our treatment becomes invalid because the weak-interaction mass of the Goldstone kaon [63] must then be taken in to account.

We conclude that, in the temperature range 0.01 MeV to 1 MeV, depending on the values of the coupling constants in their effective theory, Goldstone kaons may very well provide the dominant contribution to the shear viscosity in CFL-K0 quark matter.

There are several ways in which this work can be developed further. Firstly, we chose a specific form of the interaction lagrangian eq. (2.15) which has one coupling constant, rather than the most general form eq. (2.13) which has three; our calculation should be extended to the most general lagrangian. Secondly, it would be useful to extend our calculation to lower temperatures where, as noted above, one can no longer neglect the effects of weak interactions on the dispersion relation of the Goldstone kaon. It would also be interesting to study shear viscosity from light kaons

in the *non*-kaon-condensed CFL phase. These particles were found to give a large contribution to the bulk viscosity even at temperatures as low as a tenth of their energy gap [76, 77]. Thirdly, we neglected scattering between the Goldstone kaons and the superfluid phonons. It would be interesting to see if these processes shorten the phonon mean free path and make a significant contribution to the shear viscosity. Fourthly, even though our calculation is open to extension and improvement in the ways just described, it would be interesting to perform an analysis along the lines of Ref. [9] to see whether the shear viscosity of the Goldstone kaons can have a significant effect on the development of r-modes in a quark star or hybrid neutron star. Fifthly, as discussed in appendix A, we did not consider how the interactions themselves would alter the dispersion relation. This could affect the calculation of the mean free path at leading order in the induced non-linearity, but would provide a subleading correction to the shear viscosity. Finally, even when the superfluid phonons or Goldstone kaons are not in the hydrodynamic regime, they can still transfer momentum over long distances, and it is important to investigate how they could provide ballistic-regime damping (as opposed to hydrodynamic viscous damping) of neutron star oscillations.

Chapter 3

Large amplitude behavior of the bulk viscosity of dense matter

3.1 Introduction

The bulk viscosity of a given form of matter is a measure of the energy dissipated when it is subject to an oscillating cycle of compression and rarefaction. As we mentioned earlier in Sec. 1.3, a particularly important application of the bulk viscosity is in the damping of the r-mode oscillations of compact stars [41, 24, 42, 43, 44], which, at sufficiently low viscosity and high rotation rate, are unstable and can cause rapid spin-down of the star [50] via gravitational radiation. Bulk viscosity is known to be the dominant source for the damping of r-mode oscillations at high temperatures and low amplitudes. At low amplitudes the bulk viscosity is amplitude-independent, but since the r-mode is unstable its amplitude grows, and unless stopped by other mechanisms will quickly enter the "supra-thermal" regime where the bulk viscosity grows with amplitude [78, 79, 80], and may become large enough to stop the growth of the mode. The supra-thermal regime is characterized by $\mu_\Delta \gtrsim T$, where T is the temperature and μ_Δ is the amplitude of the oscillations in the chemical potential of

the quantity whose re-equilibration causes the viscous damping.

In this chapter which is based on Refs. [81, 82], we study the bulk viscosity of dense matter, taking into account non-linear effects that arise in the large amplitude "supra-thermal" region.

In section 3.2 we study the microscopic part of the problem via a comprehensive analysis of the bulk viscosity of dense matter. Since the precise phase structure and the equation of state of matter at high density is still unknown, we keep the dependence on those parameters as explicit as possible, and as well as numeric results we provide analytic approximations which prove to be surprisingly accurate. This allows us to obtain general results for the bulk viscosity valid for many different phases of matter, and enables us to estimate the involved uncertainties. In sections 3.3 and 3.4 we study in detail the cases of strange quark matter and equilibrated *npe*-matter, respectively, considering both modified and direct Urca processes in the hadronic case and we apply the results that we obtained in Sec. 3.2 to these cases. Yet, our general expressions can be applied to other equations of state and entirely different forms of strongly interacting matter. Finally in section 3.5 we give the conclusion and the outlook.

3.2 Bulk viscosity of dense matter

In this section we will derive the non-linear equations that determine the bulk viscosity due to weak interactions that interconvert the fermionic species that are present[1]. We will then solve it for arbitrary amplitudes. We focus on weak interactions because their equilibration rate is comparable to typical compact star oscillation frequencies: strong interactions make a negligible contribution at these frequencies because their

[1]We do not study bulk viscosity arising from the interconversion of bosons, such as the light mesons that occur in color-flavor-locked phases.

equilibration rate is much too fast.

The bulk viscosity of a given form of matter is defined by the response of the system to an oscillating compression and rarefaction. This corresponds to an oscillation in the densities of all exactly conserved quantities. We will assume that there is at least one such quantity whose density we call n_*. In compact stars it is typically the baryon number density. We will study the energy dissipated as a result of a small harmonic oscillation δn_* around its equilibrium value $\bar{n}_*$

$$n_*(\vec{r},t) = \bar{n}_*(\vec{r}) + \delta n_*(\vec{r},t) = \bar{n}_*(\vec{r}) + \Delta n_*(\vec{r}) \sin\left(\frac{2\pi t}{\tau}\right) , \tag{3.1}$$

where the amplitude of the oscillation is Δn_*, and we assume $\Delta n_* \ll \bar{n}_*$. The energy dissipation rate per volume in the fluid due to the oscillation is given by

$$\left(\frac{d\epsilon}{dt}\right)_{\text{diss}} = \zeta \left(\vec{\nabla}\cdot\vec{v}\right)^2 \tag{3.2}$$

where $\vec{v}$ is the local velocity of the fluid of the conserved quantity and the continuity equation for its particle number n_* reads

$$\frac{\partial n_*}{\partial t} + \vec{\nabla}\cdot(n_*\vec{v}) = 0\,. \tag{3.3}$$

In the hydrodynamic limit, density varies slowly enough so that density gradients can be neglected, and $\Delta n_*/\bar{n}_* \ll 1$, so averaging over a whole oscillation period $\tau = 2\pi/\omega$ gives the bulk viscosity as

$$\zeta \approx \frac{2}{\omega^2}\left\langle\frac{d\epsilon}{dt}\right\rangle_{\text{diss}} \frac{\bar{n}_*^2}{(\Delta n_*)^2}\,. \tag{3.4}$$

We will treat eq. (3.2) as our considered approximation for the bulk viscosity, so we calculate $d\epsilon/dt$ and use eq. (3.4) to obtain ζ in the hydrodynamic limit. At very

low ("subthermal") amplitudes, ζ is a constant, but in the "suprathermal" amplitude range, ζ becomes a function of the density fluctuation amplitude $\Delta n_*/\bar{n}_*$, or equivalently (via (3.3)) of $\vec{\nabla}\cdot\vec{v}/\omega$. This might be viewed as a breakdown in hydrodynamics, which is an expansion in powers of $\vec{\nabla}\cdot\vec{v}$, since one could view the density-dependence of ζ in the suprathermal regime as corresponding to the occurrence in (3.2) of terms that are higher order. However, the calculation remains under control: the suprathermal terms are calculable, and arise from deviations from local chemical equilibrium, so they are parametrically different from terms that arise from a failure to achieve local thermal equilibrium. Firstly, deviations from local thermal equilibrium induce corrections in powers of $\vec{\nabla}\cdot\vec{v}/\Lambda$, where Λ is a scale related to the the inverse relaxation time (cf. e.g. [83]), so, because $\omega \ll \Lambda$, such terms are intrinsically smaller than the suprathermal terms. Secondly, the coefficients of the suprathermal terms are enhanced by powers of C/T, where C is a susceptibility characterizing the particular form of strongly interacting matter, see eq. (3.15), which becomes large at low temperatures. Moreover, because we calculate $d\epsilon/dt$ to all orders in C/T, our computation captures *all* terms that arise from slow chemical equilibration of the conserved quantity that we study. In fact we obtain the full non-analytic density dependence of ζ, beyond the radius of convergence of an expansion in powers of $\vec{\nabla}\cdot\vec{v}/\omega$. The remaining higher-order terms in the expansion, which arise from corrections to the hydrodynamic assumption of local thermal equilibrium, have no special enhancement by factors of Λ/ω or C/T, and can be always neglected relative to the terms that we keep.

Using the relationship between fluctuations in volume and fluctuations of a conserved quantity,

$$\frac{dn_*}{n_*} = -\frac{dV}{V} \tag{3.5}$$

and the mechanical work done by a volume change

$$d\epsilon = -\frac{p}{V}dV \tag{3.6}$$

we can express the energy dissipation rate per volume averaged over one time period in terms of the induced pressure oscillation

$$\left\langle \frac{d\epsilon}{dt} \right\rangle_{\rm diss} = \frac{1}{\tau}\int_0^\tau \frac{p}{n_*}\frac{dn_*}{dt}dt\,. \tag{3.7}$$

To calculate the bulk viscosity we must calculate $p(t)$. We will assume that the bulk viscosity arises from beta-equilibration of fermionic species. We further assume that, in the absence of weak interactions, there would be s conserved species, and that there is a single channel of weak interactions that can perform interconversion of species, leaving $s-1$ exactly conserved fermion-number charges[2]. Subtracting the chemical potentials of the final state particles in the relevant weak channel from those of the initial state particles, we obtain the difference

$$\mu_\Delta \equiv \sum_i \mu_i - \sum_f \mu_f\ . \tag{3.8}$$

which is the quantity that is driven out of equilibrium by the driving density fluctuation, and whose re-equilibration leads to bulk viscosity. The quasi-equilibrium state can generally be described in terms of the driving density n_* and the ratio $x \equiv n_1/n_*$ where n_1 is the density of one of the particle species whose number is changed by the equilibration process. For small oscillation amplitudes $\Delta n_*/\bar{n}_* \ll 1$ the pressure can

[2]In this counting we exclude fermions like neutrinos, which escape from compact stars and so are effectively not conserved.

then be expanded around its equilibrium value $\bar{p} = p\,(\bar{n}_*)$

$$p = \bar{p} + \left.\frac{\partial p}{\partial n_*}\right|_x \delta n_* + \left.\frac{\partial p}{\partial x}\right|_{n_*} \delta x\,, \tag{3.9}$$

where δx is the deviation of x from its beta-equilibrium value. The t-independent part $\bar{p}$ as well as the term proportional to the driving density fluctuation δn_* do not contribute to the viscosity integral. The remaining susceptibility can be rewritten

$$\left.\frac{\partial p}{\partial x}\right|_{n_*} = \bar{n}_*^2 \left.\frac{\partial \mu_\Delta}{\partial n_*}\right|_x . \tag{3.10}$$

Because of weak interactions, x depends on time,

$$\delta x(t) = \int_0^t \frac{dx}{dt'} dt' \ . \tag{3.11}$$

From Eqs. (3.4),(3.7),(3.9),(3.10),(3.11),

$$\zeta = \frac{1}{\pi} \frac{\bar{n}_*^3}{\Delta n_*} \int_0^\tau \frac{\partial \mu_\Delta}{\partial n_*} \int_0^t \frac{dx}{dt'} dt' \cos(\omega t)\, dt\,. \tag{3.12}$$

We want to point out already at this point that, in contrast to the harmonic driving density oscillation δn_* with amplitude Δn_*, the induced chemical potential fluctuation $\delta\mu_\Delta$ around the vanishing equilibrium value can have a more complicated anharmonic form.

The fluctuations of the density ratio can be obtained from an analogous expansion of the chemical potential fluctuation

$$\delta\mu_\Delta = \left.\frac{\partial \mu_\Delta}{\partial n_*}\right|_x \delta n_* + \left.\frac{\partial \mu_\Delta}{\partial x}\right|_{n_*} \delta x \tag{3.13}$$

which yields a linear equation relating μ_Δ and δx

$$\frac{d\mu_\Delta}{dt} = C\omega\frac{\Delta n_*}{\bar{n}_*}\cos(\omega t) + B\bar{n}_*\frac{dx}{dt}\,, \tag{3.14}$$

with the susceptibilities

$$C \equiv \bar{n}_*\left.\frac{\partial\mu_\Delta}{\partial n_*}\right|_x \quad , \quad B \equiv \frac{1}{\bar{n}_*}\left.\frac{\partial\mu_\Delta}{\partial x}\right|_{n_*} \tag{3.15}$$

To obtain the temperature and amplitude dependence of the bulk viscosity, we now discuss the general form of the beta equilibration rate. We define the net equilibration rate

$$\Gamma^{(\leftrightarrow)} \equiv \Gamma^{(\rightarrow)} - \Gamma^{(\leftarrow)} = \bar{n}_*\frac{\partial x}{\partial t}\,, \tag{3.16}$$

where we use the convention that $\Gamma^{(\rightarrow)}$ is the rate for the process where n_1 is decreased, and $\Gamma^{(\leftarrow)}$ is the rate for the inverse process. We study equilibration processes where the net rate takes the general form

$$\Gamma^{(\leftrightarrow)} = -\tilde{\Gamma}T^\kappa\mu_\Delta\left(1 + \sum_{j=1}^{N}\chi_j\left(\frac{\mu_\Delta^2}{T^2}\right)^j\right)\,. \tag{3.17}$$

where N is the highest power of μ_Δ arising in the rate. In terms of dimensionless variables

$$\varphi \equiv \omega t \quad , \quad \mathcal{A}(\varphi) \equiv \frac{\mu_\Delta(t)}{T} \tag{3.18}$$

the differential equation for the chemical fluctuation eq. (3.14) can be written as

$$\frac{d\mathcal{A}}{d\varphi} = d\cos(\varphi) - f\mathcal{A}\left(1 + \sum_{j=1}^{N}\chi_j\mathcal{A}^{2j}\right)\,, \tag{3.19}$$

with the prefactors of the driving and feedback term given by

$$d \equiv \frac{C}{T}\frac{\Delta n_*}{\bar{n}_*} \quad , \quad f \equiv \frac{B\tilde{\Gamma}T^{\kappa}}{\omega}\,. \tag{3.20}$$

Note that the feedback term involves both linear and non-linear parts which are controlled by a single parameter f and that its particular form is determined by the constants χ_j which parametrize the particular weak rate. The viscosity is then finally given by

$$\begin{aligned}\zeta = &-\frac{\tilde{\Gamma}CT^{\kappa+1}}{\pi\omega^2}\frac{\bar{n}_*}{\Delta n_*} \\ &\cdot \int_0^{2\pi}\int_0^{\varphi} \mathcal{A}(\varphi')\left(1+\sum_{j=1}^{N}\chi_j\left(\mathcal{A}(\varphi')\right)^j\right)d\varphi'\cos\left(\varphi\right)d\varphi\,.\end{aligned} \tag{3.21}$$

where $\mathcal{A}\left(\varphi; d, f\right)$ is the periodic solution to eq. (3.19). Alternatively, using eq. (3.14), eq. (3.12) can also be written in an alternative form that involves only a single integral

$$\zeta = \frac{TC}{\pi\omega B}\frac{\bar{n}_*}{\Delta n_*}\int_0^{2\pi}\mathcal{A}\left(\varphi\right)\cos\left(\varphi\right)d\varphi\,, \tag{3.22}$$

In terms of a Fourier expansion of the periodic scaled chemical potential fluctuation

$$\mathcal{A}(\varphi) = \sum_{n=1}^{\infty}\left(a_n\sin\left(n\varphi\right) + b_n\cos(n\varphi)\right) \tag{3.23}$$

we see that the only components of $\mathcal{A}(\varphi)$ that contribute to the viscosity are the fundamental Fourier modes. Interestingly, whereas in eq. (3.21) it is the component in phase with the driving density oscillation, in eq. (3.22) it is the component that lags behind by a phase of $\pi/2$. This suggests that a truncated Fourier ansatz may provide a reliable approximation for the viscosity: we will explore this idea in Sec. 3.3. Before we discuss the general solution of these equations in detail, let us consider its

asymptotic limits.

Sub-thermal limit

In the limit $\mu_\Delta \ll T$ corresponding to $\mathcal{A} \ll 1$ the non-linear terms can be neglected

$$\left(\frac{d}{d\varphi} + f\right)\mathcal{A} = d\cos(\varphi)\ . \tag{3.24}$$

Since this equation is linear, the fluctuation $\mathcal{A}$ must be harmonic and only the $n = 1$ terms in the Fourier ansatz eq. (3.23) are present. Inserting this ansatz yields the solution for the required Fourier coefficients

$$a_1 = \frac{d}{1+f^2}\ , \quad b_1 = \frac{fd}{1+f^2}\,. \tag{3.25}$$

Inserted in eqs. (3.21) and (3.22) this yields the general sub-thermal result, denoted by a superscript $<$, for the bulk viscosity of an arbitrary form of matter which shows the characteristic resonant form

$$\zeta^{<} = \frac{C^2\tilde{\Gamma}T^\kappa}{\omega^2 + (B\tilde{\Gamma}T^\kappa)^2} = \zeta^{<}_{max}\frac{2\omega B\tilde{\Gamma}T^\kappa}{\omega^2 + (B\tilde{\Gamma}T^\kappa)^2}\,. \tag{3.26}$$

As long as the combination of susceptibilities C^2/B does not vary too quickly with temperature, the sub-thermal viscosity has a maximum

$$\zeta^{<}_{max} = \frac{C^2}{2\omega B} \quad \text{at} \quad T_{max} = \left(\frac{\omega}{\tilde{\Gamma}B}\right)^{\frac{1}{\kappa}}\ . \tag{3.27}$$

Intermediate regime

According to eq. (3.20) at sufficiently low temperature and high frequency one has $f \ll d$ and there can be an intermediate regime where over a range of amplitudes

$\mathcal{A} \ll (d/f)^{1/(2N+1)}$ the feedback terms are negligible [78], and eq. (3.19) reduces to

$$\frac{d\mathcal{A}}{d\varphi} \approx d\cos(\varphi) \quad \Rightarrow \quad \mathcal{A} = d\sin(\varphi) \tag{3.28}$$

Correspondingly the regime of the parameter d, where this approximation is valid and thereby the result for the viscosity is independent of the parameter f, is given by

$$f \ll d \ll f^{-\frac{1}{2N}} \tag{3.29}$$

so that such an intermediated regime is only realized for $f \ll 1$.

The simple result for $\mathcal{A}$ allows a straightforward evalution of the integral in eq. (3.21) and yields in this intermediate regime where the amplitude is directly proportional to the density fluctuation, denoted by the superscript $\sim$, a general analytic result for the viscosity[3]

$$\zeta^{\sim} = \frac{C^2\tilde{\Gamma}T^{\kappa}}{\omega^2}\left(1 + \sum_{j=1}^{N}\frac{(2j+1)!!\chi_j}{2^j\,(j+1)!}\left(\frac{C}{T}\frac{\Delta n}{\bar{n}}\right)^{2j}\right) \tag{3.30}$$

At small density amplitudes the first term in the parentheses dominates which corresponds to a low temperature approximation of the subthermal result eq. (3.26). At large amplitudes the highest term in the sum dominates, resulting in a density dependence $\sim (\Delta n/\bar{n})^{2N}$ whereas the temperature dependence precisely cancels.

Finally, taking into account that on one hand the non-linear terms in eq. (3.30) are negligible in the subthermal regime and on the other hand in the regime $f > 1$, i.e. $T > T_{max}$, where the resonant denominator eq. (3.25) in the subthermal result becomes relevant, the condition eq. (3.29) is not fulfilled anyhow, the two results can

[3]Note that this result cannot be obtained using eq. (3.22) since the derivation of the latter equation depends on the assumption that the feedback terms are non-vanishing.

be combined to an expression that is valid in both regimes

$$\zeta^{\lesssim} = \zeta^{<} + \theta(T_{max} - T)\frac{C^2\tilde{\Gamma}T^{\kappa}}{\omega^2}\sum_{j=1}^{N}\frac{(2j+1)!!\chi_j}{2^j\,(j+1)!}\left(\frac{C}{T}\frac{\Delta n}{\bar{n}}\right)^{2j} \tag{3.31}$$

Supra-Thermal limit

The suprathermal limit, $\mu_\Delta \gg T$, corresponds to $\mathcal{A} \gg 1$. Since the feedback term in the differential equation is restraining, this limit can only be reached in the limit of large driving terms $d \gg 1$. In this case only the largest power of $\mathcal{A}$ is relevant and eq. (3.19) reduces to

$$0 = d\cos(\varphi) - \chi_N f\mathcal{A}^{2N+1} \;\Rightarrow\; \mathcal{A} \sim \left(\frac{\Delta n_*}{\bar{n}_*}\right)^{\frac{1}{2N+1}}. \tag{3.32}$$

The viscosity scales correspondingly in this limit as

$$\zeta \sim \left(\frac{\Delta n_*}{\bar{n}_*}\right)^{-\frac{2N}{2N+1}} \tag{3.33}$$

and decreases at very large amplitudes.

General solution

After these limiting cases we will discuss the qualitative aspects of the general solution eq. (3.22). Due to the non-linearity of the differential equation (3.19) this requires a numeric solution. Yet, for each weak channel, characterized by the constants χ_j, such a solution as a function of the two independent variables d and f has to be performed only once and is then valid for any equation of state and includes the complete dependence on the underlying parameters in eq. (3.20). The qualitative behavior of the solution as a function of the two independent parameters d and f is shown for hadronic matter with modified Urca process in fig. 3.1. Turning up the feedback term at fixed driving term increases the phase shift of the waveform from 0 to

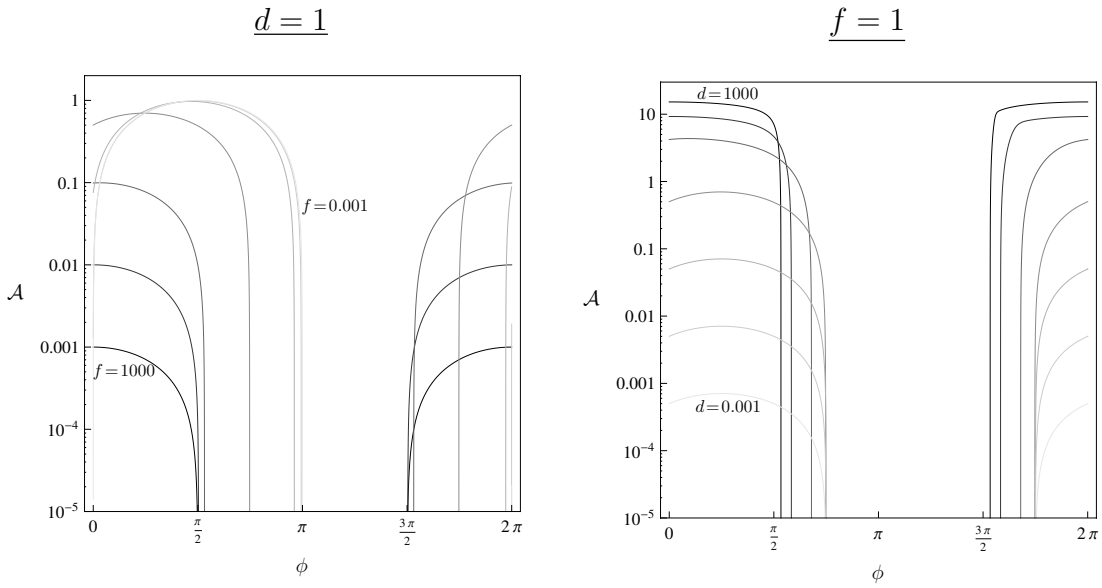

Figure 3.1: Waveform $\mathcal{A}(\phi) = \mu_\Delta(\omega t)/T$ for different values of the two independent parameters. We show only the positive half-wave, on a logarithmic scale. *Left panel:* Fixed driving term $d = 1$, with varying feedback term $f = 0.001, 0.01, \cdots, 1000$. At small values of f the chemical potential fluctuation is basically in phase corresponding to the approximation eq. (3.28). As f rises, the phase lag increases from zero towards $\pi/2$, but at the same time the amplitude decreases as $1/f$. *Right panel:* Fixed feedback term $f = 1$, with varying driving term $d = 0.001, 0.01, \cdots, 1000$. As d rises, the phase lag rises from $\pi/4$ to $\pi/2$ and the waveform becomes increasingly anharmonic, approaching a square wave in the limit.

$\pi/2$ and at the same time decreases the amplitude, but the waveform stays harmonic. In contrast, turning up the driving term at fixed feedback increases the amplitude towards the supra-thermal regime $\mathcal{A} > 1$ and the waveform becomes increasingly anharmonic. Recall, however, that only the phase shifted harmonic component in the Fourier expansion contributes to the viscosity eq. (3.22).

Motivated by the above expression eq. (3.27) for the maximum in the sub-thermal regime the general result can be written in the form

$$\zeta = \zeta^{<}_{max}\,\mathcal{I}(d,f) = \frac{C^2}{2\omega B}\mathcal{I}(d,f) \tag{3.34}$$

where the dimensionless function $\mathcal{I}$ that includes the non-trivial parameter depen-

dence is given by

$$\mathcal{I}(d,f) \equiv \frac{2}{\pi d}\int_0^{2\pi} \mathcal{A}(\varphi;d,f)\cos(\varphi)d\varphi\,, \tag{3.35}$$

or the analogous expression using eq. (3.21), where depending on the parameters either of the two forms can be more suitable for a numerical evaluation. The expression $\mathcal{I}$ can then be tabulated as a function of the independent parameters d and f. We believe that presenting our results in this form will make them easier to apply to calculations of r-mode damping, where the complete parameter dependence is required. The computation of the damping time of the mode involves an integral over the star of an expression that involves the bulk viscosity which varies throughout the star because of its dependence on the amplitude of the mode and the susceptibilities, both of which are position-dependent. The function $\mathcal{I}(d,f)$ encapsulates the dependence of the bulk viscosity on the position-dependent parameters, allowing straightforward evaluation of the damping time integral.

The function $\mathcal{I}(d,f)$ is shown in fig. 3.2 for two examples: a model of strange quark matter and a model of hadronic matter; details of the models are discussed below. We see that the function has the same qualitative form in both cases. It has a global maximum value of 1, reached in the sub-thermal limit and a line of local maxima along a parabola in the d-f-plane. Thus the maximum value (3.27) of the sub-thermal viscosity is also the maximum in the general case and depends only on the equation of state, the density and the frequency but is independent of the weak rate. The weak rate influences, however, at what temperatures and amplitudes the local maxima are reached. As seen from eq. (3.20), the parameter d is directly proportional to the amplitude, so that at moderate feedback an amplitude increase does initially not affect the viscosity at all, corresponding to the amplitude-independent sub-thermal result. But once the amplitude becomes sufficiently large we enter the supra-thermal regime and the viscosity increases strongly by orders of magnitude until it reaches

its maximum. The size of the amplitude $\mathcal{A}$ is denoted in fig. 3.2 by the darkness of shading of the surface. This qualitative behavior has already been observed in [78] but we find that at even higher amplitudes the viscosity decreases again according to the limiting behavior eq. (3.33). In contrast, at large feedback the viscosity becomes basically amplitude independent over the relevant parameter range as described by the sub-thermal result.

Let us now discuss the dependence of the viscosity on the underlying parameters in eq. (3.20). An amplitude increase (keeping all other variables fixed) results in a linear increase in the variable d as shown by the dashed (blue) curves in fig. 3.2. An increase in temperature changes the viscosity along a line shown by the solid (red) curves. In order to assess the frequency and amplitude dependence we must take into account the prefactor in eq. (3.34). This prefactor, given by the maximum viscosity in the subthermal regime, is shown in fig. 3.3, for the hadronic model of fig. 3.2(a). It exhibits a monotonic increase with density and inverse angular frequency. An increase in angular frequency therefore changes the viscosity via a change of $\mathcal{I}$ towards the negative f-direction and furthermore via the overall prefactor featuring an additional $1/\omega$ dependence. A density increase has an even more indirect impact since it depends on the detailed form of the susceptibilities $C(\bar{n}_*)$ and $B(\bar{n}_*)$ which likewise arise in the prefactors of the viscosity. These dependencies will be studied in more detail below.

3.3 Strange quark matter

3.3.1 General features

It has been suggested that the true ground state of matter at high densities may be strange quark matter [22, 23] consisting of u, d and s quarks. In that case self-

(a) Hadronic matter, modified Urca process (b) Quark matter, non-leptonic process

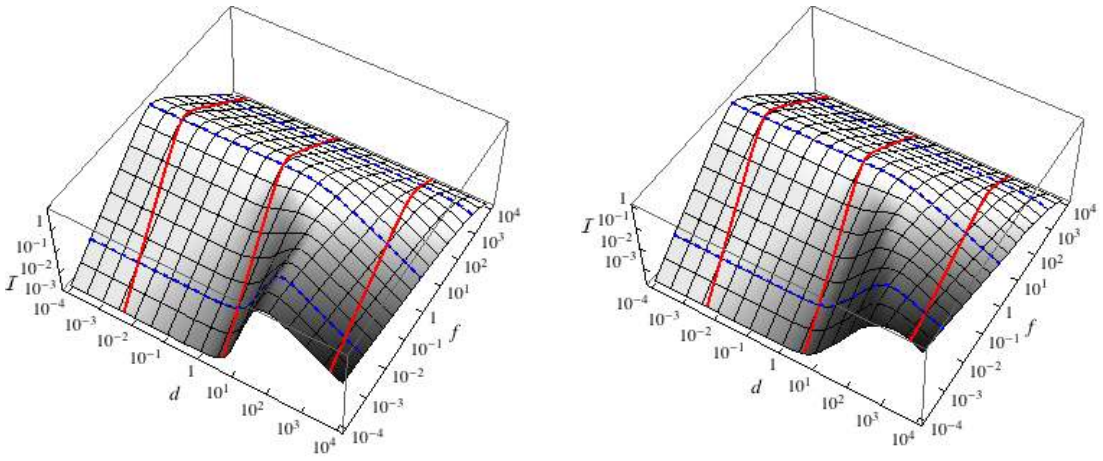

Figure 3.2: The function $\mathcal{I}$ arising in the general solution eq. (3.34) for two models of dense matter. Left panel: hadronic matter with modified Urca equilibration. Right panel: quark matter with the non-leptonic equilibration process eq. (3.36). The function has a global maximum of 1 reached asymptotically for $d \to 0, f = 1$ and a line of slowly decreasing local maxima along a parabola in the d-f plane. The shading of the surface denotes the size of the amplitude $\mathcal{A}$ so that dark shades of grey represent the supra-thermal regime. Eq. (3.20) relates d and f to underlying physical parameters such as temperature T and amplitude. An amplitude increase (keeping all other variables fixed) results in a linear increase in the variable d as shown by the dashed (blue) curves. An increase in temperature changes the viscosity along a line shown by the solid (red) curves.

bound strange stars could exist. In this section we apply the results obtained above to strange quark matter, which is both an interesting physical scenario and a useful introductory example in which one can make illuminating simplifications which are not possible for the case of hadronic matter discussed in the next section. The bulk viscosities of various forms of strange quark matter have previously been analyzed [78, 66, 84, 85, 86, 76, 65, 87, 88, 89], and the influence of strong magnetic fields has recently been discussed [90].

The dominant channel in unpaired strange quark matter is the non-leptonic flavor changing process

$$d + u \leftrightarrow s + u \ . \tag{3.36}$$

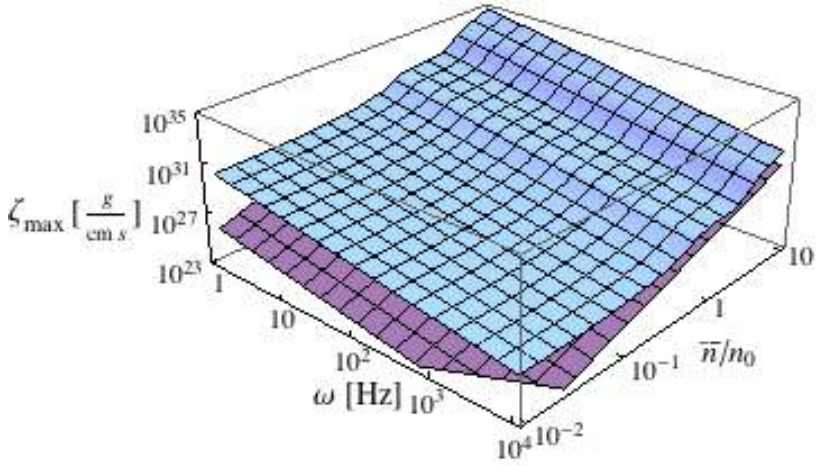

Figure 3.3: The maximum viscosity in the supra-thermal limit eq. (3.47) of hadronic matter (upper surface) and a hadronic gas (lower surface) as a function of baryon density and angular frequency. This represents also the analytic prefactor of the general expression in eq. (3.22). The corresponding plot for strange quark matter eq. (3.53) would be trivial since it does not depend on the density to leading order and only shows the analytic $1/\omega$ dependence.

The corresponding quark Urca processes, which involve leptons, are parametrically suppressed in the ratio T/μ_q. The conserved quantity that tracks the driving oscillation can be chosen as the baryon number, with density $n = \frac{1}{3}(n_s + n_d + n_u)$. The equilibrating chemical potential eq. (3.8) carries in this case the quantum numbers of neutral K-mesons and is therefore denoted by

$$\mu_K \equiv \mu_s - \mu_d \tag{3.37}$$

The rate of the non-leptonic process eq. (3.36) is given by [91]

$$\Gamma_q^{(\leftrightarrow)} = -\frac{16}{5\pi^5} G_F^2 \sin^2\theta_C \cos^2\theta_C \mu_d^5 \mu_K \left(4\pi^2 T^2 + \mu_K^2\right) \tag{3.38}$$

From this expression one can directly obtain the equilibration rate parameters $\tilde{\Gamma}$, κ and χ_i in the parameterization eq. (3.17). Their values are given in the first row of

table 3.1.

Matter/Channel	$\tilde{\Gamma}\left[\mathrm{MeV}^{(3-\kappa)}\right]$	κ	χ_1	χ_2	χ_3
quark non-leptonic	$6.59\times10^{-12}\left(\frac{\mu_d}{300\ \mathrm{MeV}}\right)^5$	2	$\frac{1}{4\pi^2}$	0	0
hadronic direct Urca	$5.24\cdot10^{-15}\left(\frac{x\,n}{n_0}\right)^{\frac{1}{3}}$	4	$\frac{10}{17\pi^2}$	$\frac{1}{17\pi^4}$	0
hadronic modified Urca	$4.68\cdot10^{-19}\left(\frac{x\,n}{n_0}\right)^{\frac{1}{3}}$	6	$\frac{189}{367\pi^2}$	$\frac{21}{367\pi^4}$	$\frac{3}{1835\pi^6}$

Table 3.1: Weak interaction parameters describing the considered damping process. Here μ_q is the quark chemical potential, n is the baryon density, n_0 nuclear saturation density and x the proton fraction.

3.3.2 Analytic approximation

Since in this case only cubic non-linearities arise, it is possible to obtain an approximate analytic solution to the non-linear equation (3.19) that goes beyond the simple approximation eq. (3.30). Taking into account the above observation that only the leading Fourier coefficient in the expansion of the chemical potential oscillation contributes to the bulk viscosity it is natural to seek such a solution via a Fourier ansatz up to a given order O

$$\mathcal{A}(t) = \sum_{n=-O}^{O} \tilde{\mathcal{A}}_n \mathrm{e}^{in\omega t} \tag{3.39}$$

where the complex form is used to simplify the computation. In principle, the amplitude of the leading Fourier mode will depend on the truncation order O, but analytically solving eq. (3.19) via a computer algebra system to order $O = 2$ we find that the coefficients $\tilde{\mathcal{A}}_{\pm2}$ vanish identically. Correspondingly anharmonicities do not directly contribute to the viscosity and are even absent to next to leading order so that we can restrict our analysis to the leading order $O = 1$. Although such a parameterization

neglects any anharmonicities it properly captures both the amplitude and the phase shift of the oscillation even in the large amplitude regime. Due to the reality of the solution there is only one independent complex Fourier exponent determined by a non-linear algebraic equation. In the case of quark matter where $\chi_i = 0$ for $i > 1$ and only the leading non-linear term $\chi\,(\mu_K/T)^3$ is present an analytic solution of this equation is possible. In this case we can decompose the amplitude into real and imaginary parts $\tilde{\mathcal{A}}_1 = A_R + iA_I$, obeying coupled equations

$$fA_R\big(1 + 3\chi(A_R^2 + A_I^2)\big) + A_I = -d/2 \tag{3.40}$$

$$fA_I\big(1 + 3\chi(A_R^2 + A_I^2)\big) - A_R = 0 \tag{3.41}$$

Note that an analytic solution is only possible because the quark matter equations are cubic; other forms of matter with higher order non-linearities in eq. (3.17) require a numeric solution. The above system of algebraic equations has a lengthy analytic solution which we refrain from giving here because, as we will see below, it can be very accurately approximated by a much simpler expression (E.3) constructed from a combination of the solutions in the sub-thermal and supra-thermal regimes. Therefore we now concentrate on the supra-thermal case, denoted by the index $>$, where the temperature-dependent term can be neglected,

$$\begin{aligned}\mathcal{A}^{>}(\varphi) &= 2A_R\cos(\varphi) - 2A_I\sin(\varphi)\\ &= -\frac{3d}{2}\left(\frac{(q(z)^2-1)^2}{\sqrt{3}z\,q(z)^2}\cos(\varphi) + \frac{q(z)^2-1}{z\,q(z)}\sin(\varphi)\right),\end{aligned} \tag{3.42}$$

where the dimensionless quantity z is defined by

$$z \equiv \frac{9\sqrt{3}}{8}\chi d^2 f = \frac{9\sqrt{3}\chi}{8}\frac{\tilde{\Gamma}C^2 B}{\omega}T^{\kappa-2}\left(\frac{\Delta n_*}{\bar{n}_*}\right)^2 \tag{3.43}$$

and

$$q(z) \equiv \left(\sqrt{z^2+1} - z\right)^{\frac{1}{3}} . \tag{3.44}$$

Eq. (3.22) then yields the approximate analytic result for the bulk viscosity in the supra-thermal regime

$$\zeta^{>} \approx \frac{2}{3\sqrt{3}} \frac{C^2}{B\omega}\, h\left(\frac{9\sqrt{3}\chi}{8} \frac{\tilde{\Gamma} C^2 B}{\omega} T^{\kappa-2} \left(\frac{\Delta n_*}{\bar{n}_*}\right)^2\right) \tag{3.45}$$

in terms of the dimensionless function

$$h(z) = \frac{9}{4z}\left(\left(\sqrt{z^2+1}-z\right)^{\frac{2}{3}} + \left(\sqrt{z^2+1}+z\right)^{\frac{2}{3}} - 2\right) . \tag{3.46}$$

This function has a maximum at $z_{max} = 3\sqrt{3}$. Since $h(z_{max}) = 3\sqrt{3}/4$, the corresponding maximum value of the viscosity is

$$\zeta^{>}_{max} = \frac{2}{3\sqrt{3}} \frac{C^2}{B\omega}\, h(z_{max}) = \frac{C^2}{2B\omega} \tag{3.47}$$

which strikingly is the same expression as in the sub-thermal limit eq. (3.27). Correspondingly the bulk viscosity has a universal upper bound ζ_{max} that is *independent* of the particular weak damping process. It is directly proportional to the oscillation period with a coefficient that only depends on the response of the strongly interacting matter. However, the corresponding temperature (3.27) and amplitude

$$\left(\frac{\Delta n_*}{\bar{n}_*}\right)_{max} = \sqrt{\frac{8\omega}{3\chi\tilde{\Gamma} T^{\kappa-2} C^2 B}} \tag{3.48}$$

at which this maximum is reached both depend on the weak rate.

Knowing the upper bound ζ_{max} and the functional behavior in the extreme sub-thermal and supra-thermal limits as well as the additive form eq. (3.31) in the low

temperature regime, allows us to give a simple parameterization of the full function for all temperatures and amplitudes. We construct a weighted sum of the analytic results in the sub-thermal eq. (3.26) and the supra-thermal regime eq. (3.45),

$$\zeta_{par} \approx \zeta^{<} + \theta(T_{max} - T)\frac{\zeta_{max} - \zeta^{<}}{\zeta_{max}}\zeta^{>} = \frac{C^2}{2B\omega}\left(\frac{2\omega\tilde{\Gamma}BT^{\kappa}}{\omega^2 + \tilde{\Gamma}^2B^2T^{2\kappa}}\right. \tag{3.49}$$
$$\left. + \theta\left(\left(\frac{\omega}{\tilde{\Gamma B}}\right)^{\frac{1}{\kappa}} - T\right)\frac{4}{3\sqrt{3}}\frac{\left(\omega - \tilde{\Gamma}BT^{\kappa}\right)^2}{\omega^2 + \tilde{\Gamma}^2B^2T^{2\kappa}}h\left(\frac{9\sqrt{3}\chi}{8}\frac{\tilde{\Gamma}BC^2T^{\kappa-2}}{\omega}\left(\frac{\Delta n_*}{\bar{n}_*}\right)^2\right)\right)$$

Studies of the damping of compact star oscillations previously took into account only the first, sub-thermal term in the parameterization eq. (3.49). The simple analytic form allows one to conveniently extend these studies in order to include large amplitude effects encoded in the second term. The small deviations of the simplified parameterization eq. (3.49) from the exact value of the bulk viscosity are negligible compared to the considerable uncertainties inherent in such a damping analysis. Evaluation of this expression requires knowledge of the susceptibilities B and C that depend on the equation of state.

3.3.3 Models of quark matter

We now apply the results derived above to some simple models of quark matter. We start with the simplest model, free quarks in a "confining bag". We will call this a "quark gas" (QG). We consider a 3-flavor quark and electron gas, with massless electron, up and down quarks and strange quark of mass m_s with pressure

$$p_{QG} = \frac{1}{4\pi^2}\left(\mu_d^4 + \mu_u^4 + \mu_s p_{Fs}^3 - \frac{3}{2}m_s^2\mu_s p_{Fs}\right.$$
$$\left. + \frac{3}{2}m_s^4\log\left(\frac{\mu_s + p_{Fs}}{m_s}\right)\right) - \mathcal{B} + \frac{\mu_e^4}{12\pi^2} \tag{3.50}$$

where the strange quark Fermi momentum is given by $p_{Fs}^2 = \mu_s^2 - m_s^2$. Here $\mathcal{B}$ is the phenomenological bag constant that is important for the equilibrium composition of a strange star, but does not affect transport properties like the bulk viscosity. The equilibrium state is determined from eq. (3.50) by taking into account charge neutrality and weak equilibrium with respect to both the explicitly considered non-leptonic channel as well as the quark Urca channel.

In quark matter there are multiple channels for beta equilibration: as well as the nonleptonic channel (3.36) there are Urca channels which convert d or s quarks in to u quarks and electrons, and emit neutrinos. However, at temperatures and oscillation frequencies of interest for compact star physics the Urca rates are much slower, and their contribution to the bulk viscosity is heavily suppressed. This means that the fractions x_u and x_e remain constant during the oscillation. The required susceptibilities then are given by

$$C_q = \bar{n}\left(\frac{\partial \mu_s}{\partial n} - \frac{\partial \mu_d}{\partial n}\right)_{x_s, x_u, x_e}, \tag{3.51}$$

$$B_q = \frac{1}{\bar{n}}\left(\frac{\partial \mu_s}{\partial x_s} - \frac{\partial \mu_d}{\partial x_s}\right)_{n, x_u, x_e}. \tag{3.52}$$

Taking into account charge neutrality, the above equation of state yields to leading order in m_s/μ_q the susceptibilities given in table 4.2 (for the case $c = 0$).

According to eq. (3.47) the maximum viscosity of a quark gas is given by

$$\zeta_{max} \approx \frac{m_s^4}{12\pi^2 \omega} \tag{3.53}$$

which depends on density only through possible density-dependence of the strange quark mass.

In Fig. 3.4 we give a comparison between the parameterization eq. (3.49) and

	B [MeV^{-2}]	C [MeV]
quark matter (gas: c=0)	$\frac{2\pi^2}{3(1-c)\mu_q^2}\left(1+\frac{m_s^2}{12(1-c)\mu_q^2}\right)$	$-\frac{m_s^2}{3(1-c)\mu_q}$
hadronic matter	$\frac{8S}{n}+\frac{\pi^2}{\left(4\left(1-2x\right)S\right)^2}$	$4(1-2x)\left(n\frac{\partial S}{\partial n}-\frac{S}{3}\right)$
free hadron gas	$\frac{4m_N^2}{3\left(3\pi^2\right)^{\frac{1}{3}}n^{\frac{4}{3}}}$	$\frac{\left(3\pi^2 n\right)^{\frac{2}{3}}}{6m_N}$

Table 3.2: Strong interaction parameters describing the response of various models of dense matter. In the case of hadronic matter with baryon density n a quadratic ansatz in the proton fraction x parameterized by the symmetry energy S eq. (3.61) is employed. The expressions for a free hadron gas are given to leading order in n/m_N^3, and for quark matter with quark chemical potential μ_q using eq. (3.54) to next to leading order in m_s/μ_q. The parameter c takes into account interaction effects within the employed quark matter model and vanishes for an ideal quark gas.

the full numeric solution. We show the amplitude dependence of the viscosity of strange quark matter for a range of temperatures These results are analogous to those given by Madsen in his initial analysis of supra-thermal effects [78]. The analytic solution features the qualitative form that has been observed for the general result in fig. 3.2 and shows a striking agreement with the full solution in the physically relevant region of amplitudes below the maximum. Note that for temperatures around T_{max} the parametrization eq. (3.49) overestimates the viscosity for amplitudes above $(\Delta n/\bar{n})_{max}$, as can be seen for the $T = 10^9$ K curve in fig. 3.4. However, if such amplitudes are reached then suprathermal bulk viscosity is overwhelmed, and other physics will have to be invoked to stop the growth of the mode.

We now examine the sensitivity of our results to uncertainties in the quark matter equation of state. We use an extension of the phenomenological parameterization proposed in [14] that allows us to study the behavior of the equation of state around chemical equilibrium. Expanding the ideal gas pressure to quartic order in m_s, the

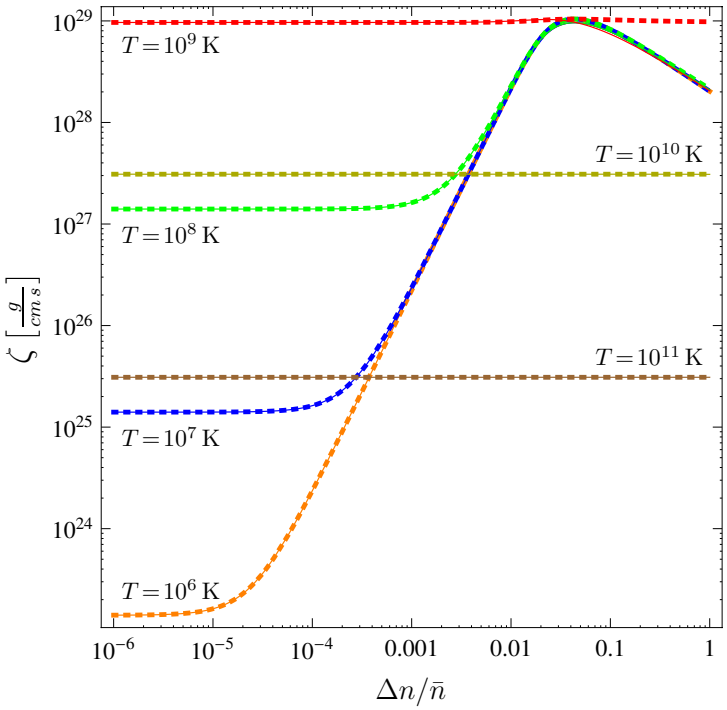

Figure 3.4: The viscosity of a strange quark gas as a function of the amplitude of the density oscillation $\Delta n/\bar{n}$ for different temperatures. The plots are given for an intermediate density $\bar{n} = 2n_0$ and a frequency $\omega = 8.4$ kHz corresponding to the oscillation frequency $\omega = 4/3\,\Omega$ of the quadrupole r-mode of a millisecond pulsar. The viscosity increases with the given temperatures starting from 10^6 K (bottom) to 10^9 K (top) and then decreases again. The thick, dashed curves represent the analytic model parametrization eq. (3.49) and the thin, full curves beneath them give the full numeric result. Clearly the parametrization is very accurate in the relevant regime below the maximum. At high temperatures the viscosity does not reach the supra-thermal regime for any physical value of the amplitude, hence the horizontal lines for $T \geqslant 10^{10}$ K.

m_s-independent quartic terms in the individual quark are modified

$$\begin{aligned} p_{par} =& \frac{1-c}{4\pi^2}\left(\mu_d^4+\mu_u^4+\mu_s^4\right) - \frac{3m_s^2\mu_s^2}{4\pi^2} \\ &+ \frac{3m_s^2}{32\pi^2}\left(3+4\log\left(\frac{2\mu_s}{m_s}\right)\right) - \mathcal{B} + \frac{\mu_e^4}{12\pi^2} \end{aligned} \tag{3.54}$$

where c is a new parameter which incorporates some effects of strong interactions between the quarks and m_s can parametrize here, in addition to corrections arising from the strange quark mass, also other interaction effects, like the pairing gap in color superconducting matter [14].

The bulk viscosity is sensitive (via the susceptibilities) to the parameters c and m_s, but not to the bag constant. We show in fig. 3.5 the effect on the bulk viscosity of varying c and m_s within their expected range of values, at twice nuclear saturation density and a temperature $T = 10^8$ K. We calculate the bulk viscosity for an angular frequency of the oscillation of $\omega = 8.4$ kHz (corresponding to the r-mode of a pulsar with a period of 1 ms). We find that the uncertainty amounts to more than an order of magnitude. In contrast to the equilibrium composition of strange stars which proved to be strongly dependent on the parameter c [14], in the present case the effective strange quark mass has a larger impact.

Finally we show in fig. 3.6 the dependence of the viscosity of a quark gas on the density of the matter and the frequency of the oscillation. The density dependence is most pronounced in the sub-thermal regime and becomes basically irrelevant in the supra-thermal regime, in accordance with the density-independence of the maximum of the viscosity eq. (3.53). Further, we see that the viscosity increases strongly with frequency, according to the $1/\omega$-dependence of the maximum eq. (3.53) which arises as a prefactor in eq. (3.49). Therefore, the results for a millisecond-pulsar given here in all other figures present a lower limit for the viscosity, whereas the damping of

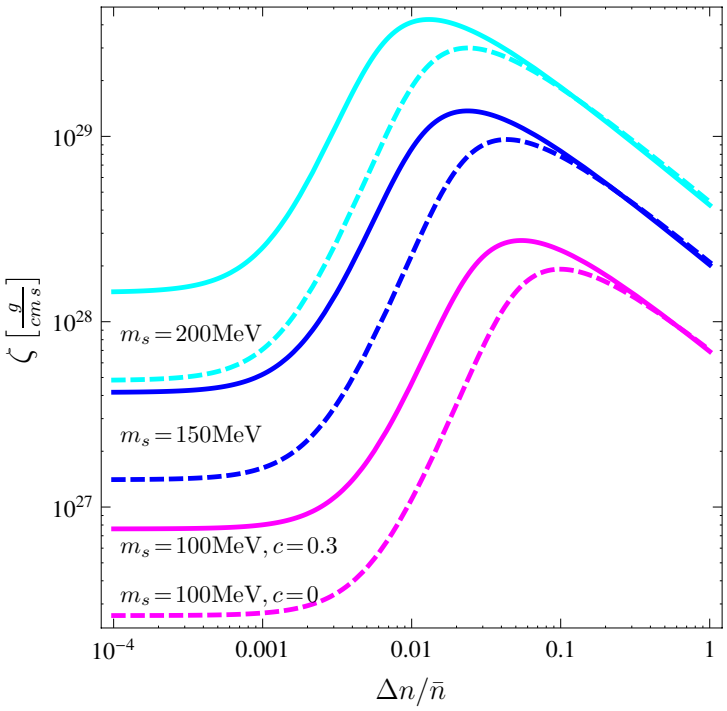

Figure 3.5: The dependence of the viscosity on parameters of the equation of state of strange quark matter using the simple parameterization eq. (3.54). We show the amplitude dependence at $T = 10^8$ K for $\omega = 8.4$ kHz and $\bar{n} = 2n_0$. Dashed curves are for $c = 0$, solid curves are for $c = 0.3$. We show $m_s = 100\,\mathrm{MeV}$ (lowest two curves, magenta), $m_s = 150\,\mathrm{MeV}$ (middle two curves, blue) and $m_s = 200\,\mathrm{MeV}$ (highest two curves, cyan).

slower rotating stars is much faster.

3.4 Hadronic matter

3.4.1 General features

The bulk viscosity has been calculated for various phases of nuclear matter (unpaired, superfluid, kaon-condensed etc) with flavor equilibration via either direct or modified Urca processes [7, 92, 93, 94, 95, 96]. The leptonic contribution has recently been calculated [97], and hyperonic matter has also been studied [53, 98, 99, 100]. We

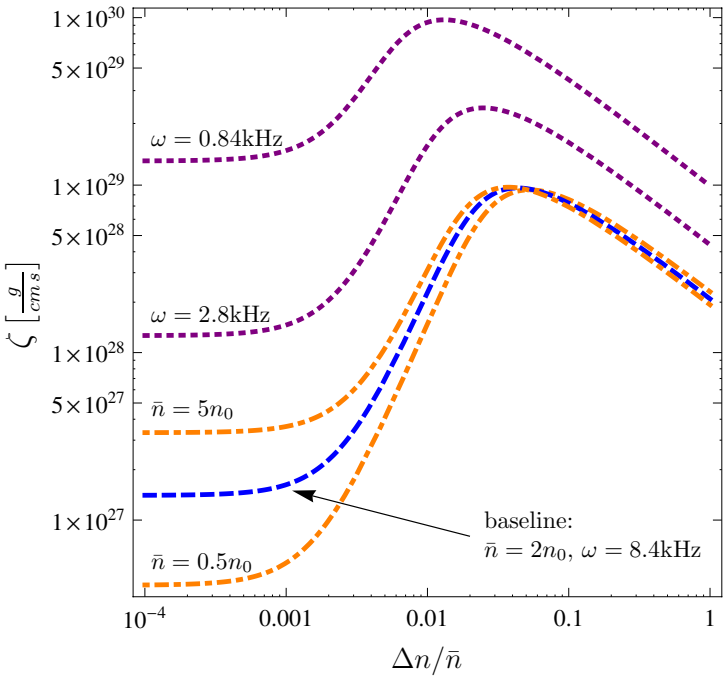

Figure 3.6: The dependence of the viscosity of quark matter on the density and oscillation frequency, using the phenomenological equation of state eq. (3.54) with $m_s = 150\,\mathrm{MeV}$ and $c = 0$, at $T = 10^8\,\mathrm{K}$. The dashed (blue) "baseline" curve is for $\bar{n} = 2n_0$ and a high angular frequency $\omega = 8.4$ kHz corresponding to a millisecond pulsar. The dot-dashed (orange) curves show the variation from the baseline with density: a low value $\bar{n} = 0.5n_0$ and a high value of $\bar{n} = 5n_0$. The dotted (purple) curves give the variation from the baseline with angular frequency: a lower value $\omega = 0.84\,\mathrm{kHz}$ and an intermediate value $\omega = 2.8\,\mathrm{kHz}$.

concentrate on the simplest case of non-superfluid hadronic *npe* matter. We note however, that the generic properties of our results also apply to more complicated forms of matter like hyperonic and/or superfluid nuclear matter. In the case of hadronic matter we assume that weak equilibration occurs via the Urca channel

$$p + e^- \to n + \nu_e \quad , \quad n \to p + e^- + \bar{\nu}_e \tag{3.55}$$

There are two qualitatively different cases depending on whether the direct process is possible or only the modified version where a bystander nucleon is necessary to satisfy

energy-momentum conservation. The latter represents a particular strong interaction vertex correction to the above process. However, from the point of view of the weak interaction these different processes belong to the same channel. Taking into account baryon number and charge conservation $\delta n_p - \delta n_e = 0$, the driving baryon number density oscillation yields here the oscillating chemical potential difference

$$\mu_I \equiv \mu_n - \mu_p - \mu_e \ . \tag{3.56}$$

where the notation reflects that the equilibrating quantity in this case is isospin.

Taking into account the effect of supra-thermal oscillation amplitudes requires the non-linear μ_I-corrections to the corresponding rates. These have been given for hadronic matter in [101, 7, 102] in the standard case that only modified Urca processes are allowed

$$\begin{aligned}\Gamma^{(\leftrightarrow)}_{hm}\mu_I = -3.5 \cdot 10^{13} \frac{\mathrm{ergs}}{\mathrm{cm^3 s}} \left(\frac{x\,n}{n_0}\right)^{\frac{1}{3}} \frac{T_8^8}{11513} \\ \cdot \left(14680 \frac{\mu_I^2}{\pi^2 T^2} + 7560 \frac{\mu_I^4}{\pi^4 T^4} + 840 \frac{\mu_I^6}{\pi^6 T^6} + 24 \frac{\mu_I^8}{\pi^8 T^8}\right)\end{aligned} \tag{3.57}$$

and in the enhanced case when direct Urca processes dominate [101, 103]

$$\begin{aligned}\Gamma^{(\leftrightarrow)}_{hd}\mu_I = -4.3 \cdot 10^{21} \frac{\mathrm{ergs}}{\mathrm{cm^3 s}} \left(\frac{x\,n}{n_0}\right)^{\frac{1}{3}} \frac{T_8^6}{457} \\ \cdot \left(714 \frac{\mu_I^2}{\pi^2 T^2} + 420 \frac{\mu_I^4}{\pi^4 T^4} + 42 \frac{\mu_I^6}{\pi^6 T^6}\right)\end{aligned} \tag{3.58}$$

where T_8 is the temperature in units of 10^8 K. Here we use the expressions given in [101], but we note that the hadronic rates depend on model assumptions for the behavior of the strong interaction at high density (see [102, 103]) and thereby involve uncertainties. These expressions yield the parameter values given in table 3.1. There

are major differences between these hadronic rates and the corresponding one for strange quark matter. In quark matter, non-leptonic processes are naturally allowed and only particles that have a Fermi surface (quarks in this case) are involved. In contrast in hadronic matter such processes are absent (unless hyperons are present) and equilibration must proceed via semi-leptonic processes involving particles with no Fermi surface (neutrinos in this case) giving a much stronger temperature dependence. As noted before the simple analytic approximation suitable for strange quark matter is not applicable here. Nevertheless we will see that many qualitative aspects of that solution obtain in the general case. We note that although the prefactors of the non-linear terms decrease strongly as the power of μ_I/T rises, it is not sufficient to neglect them since they enter the non-linear differential equation (3.19) where they dominate at sufficiently large amplitudes.

According to eq. (3.15), the susceptibilities for hadronic matter are

$$C_h = \bar{n} \left(\left.\frac{\partial \mu_n}{\partial n}\right|_{x_n} - \left.\frac{\partial \mu_p}{\partial n}\right|_{x_n} - \left.\frac{\partial \mu_e}{\partial n}\right|_{x_n} \right) , \tag{3.59}$$

$$B_h = \frac{1}{\bar{n}} \left(\left.\frac{\partial \mu_n}{\partial x_n}\right|_{n} - \left.\frac{\partial \mu_p}{\partial x_n}\right|_{n} - \left.\frac{\partial \mu_e}{\partial x_n}\right|_{n} \right) . \tag{3.60}$$

Computing these quantities requires the equation of state of dense neutron matter. We will perform calculations using two model equations of state of nuclear matter. The first one is the "hadron gas", consisting of an electrically neutral beta-equilibrated mixture of free neutrons, protons, and electrons. The second one is "APR hadron matter", using the well-known model by Akmal, Pandharipande and Ravenhall [11] which relies on a potential model that reproduces scattering data at nuclear densities. As a low density extension of the APR data we use the equation of state given by Baym, Pethick and Sutherland [12, 13]. In order to make it easy to apply our general results to other equations of state, we implement the APR equation of state using

the simple parameterization employed in [104] to approximate the dependence of the energy per particle on the proton fraction x by a quadratic form

$$E(n,x) = E_s(n) + S(n)(1-2x)^2 \tag{3.61}$$

where E_s and S are the corresponding energy for symmetric matter and the symmetry energy. We perform a global quartic fit to the APR prediction for symmetric and pure neutron matter E_n which then yields the symmetry energy as

$$S(n) = E_n(n) - E_s(n) \tag{3.62}$$

and the complete pressure including the electron contribution reads

$$p(n,x,\mu_e) = n^2\left(\frac{dE_s(n)}{dn} + \frac{dS(n)}{dn}(1-2x)^2\right) + \frac{\mu_e^4}{12\pi^2} \tag{3.63}$$

In the absence of oscillations the β-equilibrium condition $\mu_I = 0$ yields the electron chemical potential as

$$\mu_e = 4\,(1-2x)\,S(n) \tag{3.64}$$

and the requirement of charge neutrality $n_p = n_e$ allows us to determine the proton fraction $x(n)$ so that the pressure becomes a function of the baryon density alone. With these explicit expressions the susceptibilities in table 4.2 can be computed and the general results in section 3.2 can be employed. In the following we will discuss the numerical results for the bulk viscosity of nuclear matter, comparing it with those for one particular model of quark matter, the one given by eq. (3.54) with $m_s = 150$ MeV and $c = 0.3$.

3.4.2 Sub-thermal case

When $\mu_\Delta \ll T$ we obtain from the analytic expression eq. (3.26) the results shown in fig. 3.7 where the bulk viscosity of strange quark matter discussed in the previous section is also included for comparison. Here and in the following plots we study matter at twice nuclear saturation density, $\bar{n} = 2n_0$, and a compression cycle with a high angular frequency $\omega = 8.4$ kHz corresponding to an r-mode in a pulsar with a period of 1 ms. We see in fig. 3.7 that the maximum bulk viscosity of hadronic matter as a function of temperature (or equivalently as a function of angular frequency) is roughly an order of magnitude smaller than the maximum value for strange quark matter. This is unrelated to the beta-equilibration rate: the maximum viscosity depends according to eq. (3.27) on the relevant susceptibilities of the matter in question.

Other features of the plot do depend on the equilibration rate. As we expect from (3.26), quark matter achieves its maximum viscosity at the lowest temperature, and has less suppression at low temperatures. This is because the nonleptonic equilibration only involves two particles in the initial and final state, each of which has a large Fermi momentum $\sim \mu_q$ and hence large phase space factors. This leads to a low $\kappa = 2$ and a large value of $\tilde{\Gamma}$ (table 3.1). Thus the suppression at low temperature is only T^2, and, according to eq. (3.27), $T_{\max}$ is relatively low. The next fastest is the direct Urca process in nuclear matter, which involves more particles (including neutrinos which have no Fermi surface and thus very little phase space) and therefore has a higher κ and lower $\tilde{\Gamma}$, giving it stronger T^4 suppression at low temperatures, and a higher $T_{\max}$. The slowest is the modified Urca process in nuclear matter, which involves additional spectator nucleons, raising κ to 6 and further lowering $\tilde{\Gamma}$, raising $T_{\max}$, and increasing the low-T suppression to T^6.

Note that the right-most solid and dashed curves in fig. 3.7, for hadronic matter with modified Urca equilibration, correspond roughly to the leftmost of the three

solid (red) curves in fig. 3.2(a) that run along the surface from front to back.

We draw two important conclusions from fig. 3.7. First, we have retained the full resonant structure of the viscosity compared to previous analyses [7, 103] where a low temperature approximation $\tilde{\Gamma} B T^{\kappa} \ll \omega$ was used. This allows us to see that the viscosity decreases again at large temperatures and the maximum (3.27) occurs at millisecond-scale frequencies at potentially physically relevant temperatures of the order 10^{10} K for direct Urca and 10^{11} K for modified Urca. This means that the resonant structure may be important in some astrophysical applications and from eq. (3.27) it is clear that it becomes increasingly important at lower frequencies. Second, we see in fig. 3.7 that for nuclear matter there is a considerable difference between the solid curves which are based on an interacting equation of state [11, 12, 13] and the dashed curves which are for a free gas[4] of nucleons and electrons. These models have different susceptibilities B and C, and the main effect of this is a vertical shift of the whole curve. The shift in $T_{\rm max}$ is smaller because of the square root in eq. (3.27). Hadronic matter with interactions has been considered (with a more simplified equation of state) in [103, 92] but many analyses [45, 50, 9] rely on the simple analytic result[5] given by Sawyer [7] which is based on the free gas expression. We see that these differ by roughly a factor of three for the given density of $\bar{n} = 2n_0$, but according to fig. 3.3 this difference can increase strongly both at lower and higher density.

[4]Note that strictly speaking there are no modified Urca processes in an ideal hadron gas. Yet, for comparison with previous studies we use here the interacting matter expression for the rate but the ideal gas expressions for the strong susceptibilities.

[5]Note that the numerical prefactor given in [7] is too large by two orders of magnitude, see also [8].

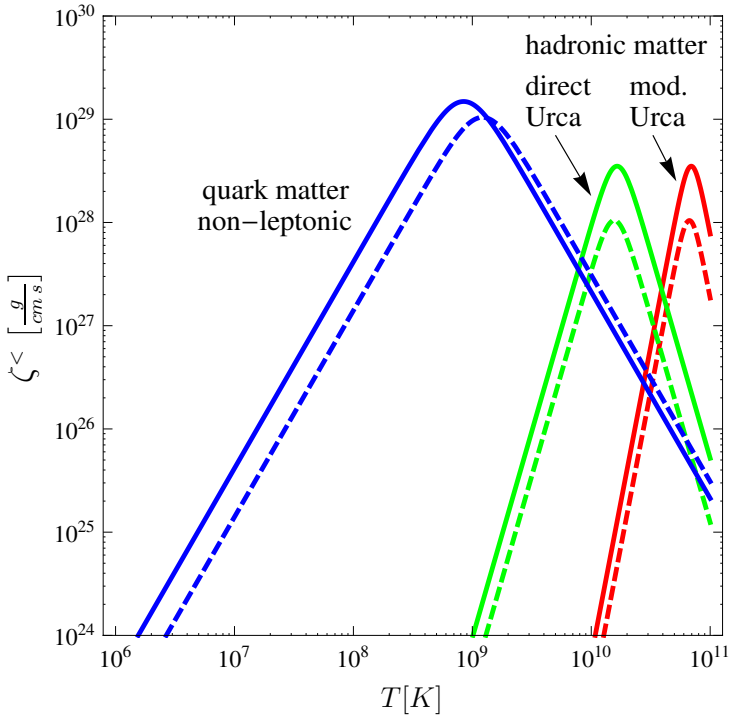

Figure 3.7: The sub-thermal approximation to the viscosity in the low amplitude limit as a function of temperature for $\omega = 8.4$ kHz and $n = 2n_0$. The curves forming the right-hand (red) peak represent the standard case of hadronic matter with modified Urca processes. The curves forming the middle (green) peak are for hadronic matter when direct Urca process are allowed. The curves forming the left-hand (blue) peak are for strange quark matter with non-leptonic processes. The dashed curves are for the free hadron and free quark models; the solid curves are for APR hadron matter, and interacting quarks eq. (3.54) with $m_s = 150\,\mathrm{MeV}$ and $c = 0.3$. With APR nuclear matter the bulk viscosity is ~ 3 times larger than for the free hadron gas used e.g. in [7, 8, 9].

3.4.3 The supra-thermal regime

Beyond the sub-thermal limit, in general a numeric evaluation of eqs. (3.19) and (3.22) is required. As discussed in sect. 3.2, the temperature and amplitude dependence of the bulk viscosity for a given form of matter can be expressed in terms of the function $\mathcal{I}(d, f)$ which was plotted in a form that is independent of the equation of state of hadronic matter with modified Urca processes in fig. 3.2.

Using this result, we show in fig. 3.8 plots of the amplitude dependence of the bulk viscosity at two temperatures (left panel: $T = 10^6$ K; right panel: $T = 10^9$ K) for the various forms of hadronic and quark matter considered in this chapter. Here solid lines again show the results for interacting matter whereas the dashed lines show the free hadron/quark gas results. The dotted lines, which are in most places invisible beneath the solid lines, show the analytic approximation eq. (3.30) valid in the intermediate regime.

Note that the right-most curves in fig. 3.8, for hadronic matter with modified Urca equilibration, correspond roughly to the foremost of the three dashed (blue) curves in fig. 3.2(a) that run along the surface from left to right.

At the lower temperature the viscosity reaches the supra-thermal regime already for small amplitudes, whereas at the higher temperature the sub-thermal regime extends to large amplitudes, giving a flat amplitude-independent plateau at low amplitudes. The stronger non-linear feedback in the hadronic cases leads to a significantly steeper rise that correlates with the largest power in eq. (3.17). Interestingly, despite these differences the maximum value reached by varying the amplitude is still roughly the same as the maximum value in the sub-thermal limit eq. (3.27), as has been analytically found in the case of strange quark matter. This is important since it means that oscillations are approximately equally damped at all temperatures once the amplitude becomes sufficiently large. The maximum arises for amplitudes of the order

0.01, 0.1 and 1 for strange quark matter and hadronic matter with direct and modified Urca, respectively. Therefore the simple analytic expression eq. (3.30) provides a remarkably good approximation, at physical amplitudes and oscillation period close to a millisecond, for hadronic matter in general and in particular for modified Urca processes. As can be seen from fig. 3.6, at lower frequencies the maxima occur at lower amplitudes and correspondingly the non-linear saturation of the viscosity, described by the full numeric solution, becomes relevant. The supra-thermal enhancement of the bulk viscosity is so strong, particularly for hadronic matter, that it could well provide the main saturation mechanism for unstable r-modes, stopping their growth at amplitudes that are below the threshold for other competing saturation mechanisms (e.g. non-linear hydrodynamics) but large enough to allow spin-down of a neutron star via gravitational radiation on astrophysical time scales.

3.5 Conclusions

In this chapter we have studied the bulk viscosity of dense matter including its non-linear behavior at large amplitudes (suprathermal regime). In particular we give a general numerical solution for the bulk viscosity of degenerate matter in Sec. 3.2 that is valid for all types of matter where equilibration occurs via fermions as well as arbitrary equations of state and retains the full parameter dependence. This allows one to include these supra-thermal effects in a systematic r-mode analysis. Furthermore, we give an approximate analytic result for any arbitrary form of matter that is valid over a large part of the supra-thermal regime, as well as a refined version for strange quark matter with non-leptonic processes in Sec. 3.3 which is valid at all amplitudes. We found that the free hadron gas model of nuclear matter, used for example in [45, 50, 9] to compute the susceptibilities that enter the viscosity, is not accurate even in the

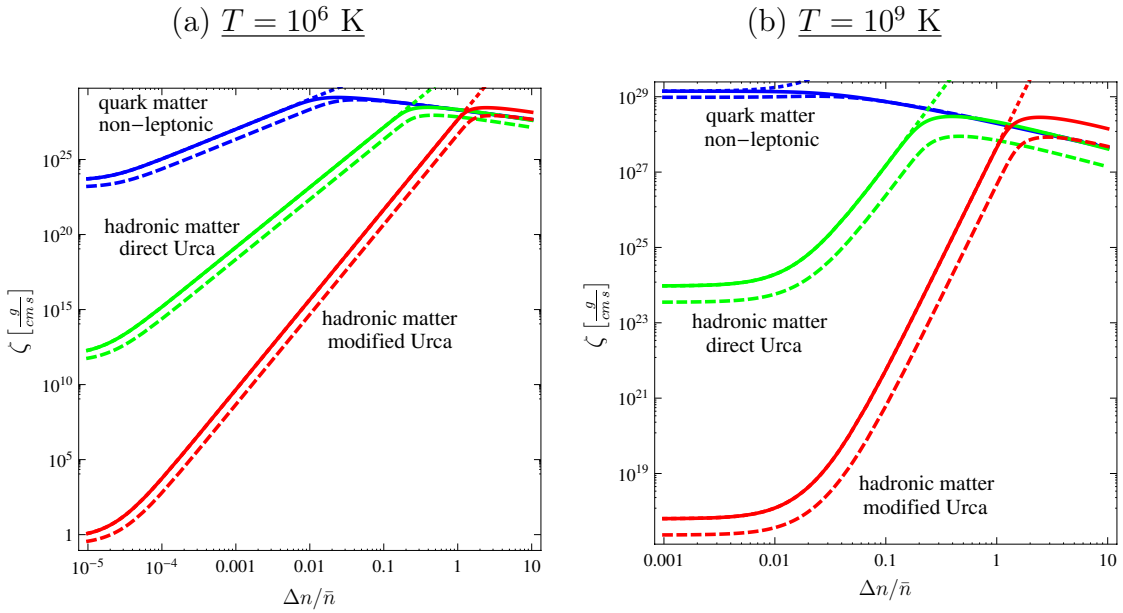

Figure 3.8: Comparison of the bulk viscosity of the different forms of matter studied in this work as a function of the density oscillation amplitude $\Delta n/\bar{n}$. The frequency is $\omega = 8.4$ kHz, corresponding to an r-mode in a millisecond pulsar and $\bar{n} = 2n_0$. Left panel: low temperature $T = 10^6$ K; right panel: high temperature $T = 10^9$ K. The dashed curves are for the free hadron and free quark models; the solid curves are for APR hadron matter, and interacting quarks eq. (3.54) with $m_s = 150\,\mathrm{MeV}$ and $c = 0.3$; for interacting matter the dotted curves which deviate just below the peak represent the approximation eq. (3.30). The bottom (red) curves represent the standard case of hadronic matter with modified Urca processes, the middle (green) curves are for hadronic matter when direct Urca process are allowed and the top (blue) curves are for strange quark matter with non-leptonic processes. Our calculations are valid only for $\Delta n/\bar{n} \ll 1$, but we show their extrapolation to higher amplitudes in order to compare with the qualitative general structure of the solution in fig. 3.2. Note that this plot uses a high oscillation frequency and that the viscosity is even larger at smaller values.

sub-thermal regime, and underestimates the viscosity. An analogous observation holds for models of interacting quark matter. Moreover, we find that the standard low temperature (high frequency) approximation is not applicable for temperatures around 10^{10} K and the full resonant form of the bulk viscosity is required. We confirm previous results for the amplitude-dependence of the bulk viscosity of strange quark matter [78] and find that these supra-thermal effects are parametrically even more important in nuclear matter, because of higher-order non-linearities in the amplitude-dependence of the Urca rate.

The most obvious application of our results is to the damping of unstable r-mode oscillations in neutron stars. As the amplitude of the mode enters the supra-thermal regime the viscosity will increase steeply above the sub-thermal result and can exceed it by many orders of magnitude, but eventually it reaches an upper bound that is completely independent of the particular weak damping process and depends only on susceptibilities of the dense matter in question. The viscosity then decreases at even larger amplitudes. We conclude that if r-mode growth is not stopped by the supra-thermal bulk viscosity before this maximum is reached then other non-linear dynamic effects [105, 106, 107, 108] will be required to stop it.

There are several other directions in which this work could be developed: Other equations of state for quark matter could be studied, for example the perturbative equation of state [109], and also other phases with different equilibration mechanisms. The same is true for the various equations of state and phases of hadronic matter. Our analysis was for the case of a single equilibration channel, and it would be interesting to extend it to multiple channels, which may be relevant to both hadronic and quark matter (see appendix A of [84] and [87]). In quark matter the non-Fermi liquid enhancement of the Urca rate [110] should further increase resonant effects. The application of our results to r-modes in neutron stars also raises interesting questions

concerning the correct treatment of the crust [111], and possible modification of the radial profile of the r-mode due to strong radial dependence of the bulk viscosity in layered stars such as hybrid stars.

Finally we note that at low temperatures the suprathermal enhancement of bulk viscosity becomes large, and the amplitude threshold for entering the suprathermal regime becomes low. This may not be relevant to the damping of r-modes because they are also damped by shear viscosity which becomes large at low temperature. But for other modes of compact stars [112], such as monopole pulsations [113], shear viscosity will not play such a significant role, and suprathermal bulk viscosity might be the dominant source of damping if external perturbations make the amplitude large enough. This might be relevant to old, cold, accreting stars in binary systems.

Chapter 4

Viscous damping of r-modes: Small amplitude instability

4.1 Introduction

In the previous chapter we studied the bulk viscosity of large amplitude oscillations and showed that the supra-thermal enhancement of the bulk viscosity is so strong that it could well provide the main saturation mechanism for unstable r-modes at finite amplitudes. In this chapter, however, we restrict ourselves to the subthermal regime $\mu_\Delta \ll T$, and study the viscous damping of the r-modes of compact stars and analyze in detail the regions where small amplitude modes are unstable to the emission of gravitational radiation. In the next section, Sec. 4.2, we explain different star models that will be used later on in this chapter and in the next chapter, and also we discuss the profile of the r-mode oscillations in neutron stars. Shear viscosity of quark matter and hadronic matter are given in Sec. 4.3. In Sec. 4.4 we present general expressions for the viscous damping times for arbitrary forms of interacting dense matter. In Sec. 4.5 we derive general semi-analytic results for the boundary of the instability regions of the r-modes, and also give the numerical results for the

instability regions for the considered star models. And finally the conclusions are given in Sec. 4.6.

4.2 Star models and r-modes

4.2.1 Static star models

The analysis of compact star oscillations and their damping requires as a first step the stable equilibrium configuration of the star. In this section we will discuss the considered star models that are used later on. We employ the general relativistic Tolman-Oppenheimer-Volkov (TOV) equations [38] to determine the equilibrium star configuration. This requires the equation of state of neutral and β-equilibrated dense matter. The recent measurement of a neutron star with the large mass $1.97 \pm 0.04\, M_\odot$ [4, 54] puts bounds on the equation of state of dense matter. We generally study equations of state that can accommodate such a heavy star. We consider three qualitatively different classes and study in each case both a star model with a standard value of $1.4\, M_\odot$ and one with a large mass $2\, M_\odot$:

1. Neutron stars (NS) are obtained for an equation of state that is hadronic at all relevant densities. Whereas the above maximum mass does not pose problems for neutron stars obtained from most hadronic equations of state, it seem nearly impossible to obtain such heavy stars which contain a significant amount of hyperonic matter [54]. Therefore we do not study this possibility here and consider only stars consisting of neutrons, protons and electrons as well as muons at sufficiently high density. We also neglect the possible presence of hadronic pairing which in general significantly reduces the bulk viscosity [92, 93]. Such pairing is only realized in certain shells within the star and as long as they are not large this might not qualitatively change the results obtained here. However,

the intricate dynamics of a two-component fluid can change this simplistic picture [114]. For our numerical results we employ the equilibrated equation of state by Akmal, Pandharipande and Ravenhall (APR) [11] which relies on a potential model that reproduces scattering data in vacuum supplemented by a model for three-body interactions in order to reproduce the saturation properties at nuclear densities. As a low density extension of the APR data we use the equation of state given by Baym, Pethick and Sutherland (BPS EoS) [12, 13]. Furthermore, we study in this class also a neutron star with an ultra-high mass $2.21\,M_\odot$ close to the mass limit for the APR equation of state, since in this case direct Urca interactions are possible in the interior of the star leading to a significantly enhanced weak rate, cf. e.g. [81].

2. Hybrid stars (HS) with an outer hadronic part and a core of quark matter are obtained from an equation of state where at some density the effective degrees of freedom change from hadrons to quarks. In general the equation of state of interacting quark matter is unknown and there are only hints from the perturbative regime [115, 116, 109] or model studies. We use the simple quartic parameterization for the equation of state of ungapped 3-flavor quark matter [14, 81] given by eq. 3.54 in the previous chapter.

$$p_{par} = \frac{1-c}{4\pi^2}\left(\mu_d^4+\mu_u^4+\mu_s^4\right) - \frac{3m_s^2\mu_s^2}{4\pi^2} + \frac{3m_s^4}{32\pi^2}\left(3+4\log\left(\frac{2\mu_s}{m_s}\right)\right) - \mathcal{B} + \frac{\mu_e^4}{12\pi^2} \tag{4.1}$$

where c, m_s and B are effective model parameters that incorporate some effects of the strong interactions between the quarks. From this equation of state we find the β-equilibrated and charge neutral ground state which depends on

a single quark number chemical potential μ_q. We use the general form since the computation of transport properties below requires susceptibilities around the equilibrium state. Within the parameterization eq. (4.1) the recent measurement of a heavy star strongly restricts the equation of state so that only equations of state that are strongly interacting ($c > 0.3$) are compatible [14, 54]. These are equations of state where the transition to quark matter is at rather low values of the baryon number $\lesssim 1.5\, n_0$, where n_0 is nuclear matter density, and we choose here one where it occurs at $1.5\, n_0$. Since the APR equation of state happens to be very similar to the above form eq. (4.1) so that even multiple transitions are possible [14], we do not expect the transition density to be a robust result that is independent of the considered equations of state. Therefore we study here in addition also two $1.4\, M_\odot$ hybrid star models obtained with quark equations of state that cannot accommodate a heavy star when combined with the APR equation of state. Ona has a small quark core, obtained for a transition density of $3.25\, n_0$, and the other a medium-sized quark core, obtained for a transition density of $3\, n_0$.

There are many possible phases of quark matter that feature various color superconducting pairing patterns. Here we do not explicitly study star models with pairing, but note that the parameterization eq. (4.1) can also describe superconducting matter. For our hybrid star models we make the assumption of local charge neutrality, excluding the possibility of a mixed phase and thereby circumventing the description of the wealth of possible geometric structures of such a mixture.

3. Strange stars (SS) that are self-bound could exist according to the strange matter hypothesis [23] that the true ground state of strongly interacting matter is 3-flavor quark matter. For strange stars we use the same equation of state

eq. (4.1), but use parameter sets that realize the strange matter hypothesis. In contrast to the case of hybrid stars large mass strange stars are possible even for $c = 0$ and due to our ignorance of the precise form of the interacting equation of state we choose this value to keep our model as simple as possible. For a strange quark mass of $m_s = 150$ MeV stable strange stars exist in this case for bag constants $B_{lim} < (158\,MeV)^4$, whereas heavy strange stars exist for this mass value only for bag constants $B \lesssim (140\,MeV)^4$. Lower effective quark mass values or changes in the quartic term ($c \neq 0$) relax these bounds.

We note already at this point that although the detailed parameters we chose here for our star models are rather arbitrary, we will give general analytic expressions below that will reveal the dependence of our main results on the various model parameters. The characteristic parameters of the considered star models are given in table 4.1. As is a well known property, the radii of the different models vary only moderately with the mass for masses of 1 to $2\,M_\odot$. The density profiles are shown in fig. 4.1. The core densities of these star models range from below $3\,n_0$ to more than $7\,n_0$. In contrast to neutron and hybrid stars that vary in density by 14 orders of magnitude, strange stars feature a roughly constant density profile.

	$M\,[M_\odot]$	$M_{core}\,[M_\odot]$	$R\,[km]$	$n_c\,[n_0]$	$\langle n\rangle\,[n_0]$	$\Omega_K\,[kHz]$
NS	1.4	(1.39)	11.5	3.43	1.58	6.02
	2.0	(1.99)	11.0	4.91	2.46	7.68
	2.21	0.85	10.0	7.17	3.37	9.31
SS	1.4	–	11.3	2.62	1.91	6.17
	2.0	–	11.6	4.95	2.43	7.09
HS	1.4 (S)	0.38*	10.8	5.89	1.85	6.61
	1.4(M)	0.66*	10.3	6.66	2.09	7.06
	1.4(L)	1.06	12.7	2.32	1.17	5.16
	2.0	1.81	12.2	4.89	1.84	6.62

Table 4.1: Results of the considered models of neutron stars (NS), strange stars (SS) and hybrid stars (HS). Shown are the mass of the star M, the mass of the core M_{core} (in the case of $2.21\,M_\odot$ neutron star, M_{core} is the mass of the region where direct Urca interactions are possible), the radius R, the baryon density at the center of the star n_c given in units of nuclear saturation density n_0, the average density $\langle n\rangle$ and the Kepler frequency Ω_K. The neutron stars were obtained by solving the relativistic TOV equations for catalyzed neutron matter using the APR equation of state [11] with low density extension [12, 13] and the strange stars with a quark gas bag model with $c = 0$, $m_s = 150\,MeV$ and a bag parameter $B = (138\,MeV)^4$. Large mass hybrid stars are only found when strong interaction corrections are considered, cf. [14], and we find a $2\,M_\odot$ star for $c = 0.4$, $m_s = 140\,MeV$, $B = (137\,MeV)^4$. The additional two $1.4\,M_\odot$ hybrid models with smaller cores, marked with an asterisk, result from equations of state that do not allow large mass models. They correspond to $c = 0$, $m_s = 150\,MeV$, $B = (164.5\,MeV)^4$ and $(171.5\,MeV)^4$ which are chosen to obtain transition densities of $3n_0$ and $3.25n_0$, respectively.

4.2.2 R-mode profile

In section 1.3 we introduced the r-mode oscillations of neutron stars. Here we will explain the calculations of the r-mode profile which is necessary in the computations of the damping time scales.

The analysis of the oscillation modes of compact stars requires the solution of the corresponding hydrodynamics equations [117]. Whereas the solution of the general relativistic equations for static star models is straightforward, the corresponding dynamic equations are more involved and explicit analytic expressions for the r-mode oscillation are only available in non-relativistic approximation. Yet numerical analyses of the general relativistic equations show that except for very compact stars the relativistic corrections are moderate [118, 119, 120]. In the non-relativistic case the current state of the art is the comprehensive analysis [43]. It might therefore seem more consistent to employ Newtonian equations for the static star models as well, but we prefer to perform the necessary approximation for the oscillation at least around the correct equilibrium configuration. In particular since we study heavy quark and hybrid stars where the different approximations could differ. In particular in the large amplitude regime, a consistent general relativistic analysis would clearly be desirable. Furthermore, so far these analyses assume that the oscillation modes are solutions of an ideal fluid. For these modes the damping is then computed in a second step.

R-modes are normal oscillations of rotating stars and correspondingly they require as a first step the solution of a uniformly rotating stellar model. Since neutron stars are cold, dense systems we assume a barotropic fluid where the pressure p is only a function of the energy density ρ. The hydrodynamic Euler equation for this spherical system, determining the enthalpy h and the equation for the gravitational potential Φ of the star, have to be solved with appropriate boundary conditions [43]. To simplify the demanding analysis a slow rotation expansion is performed and, since

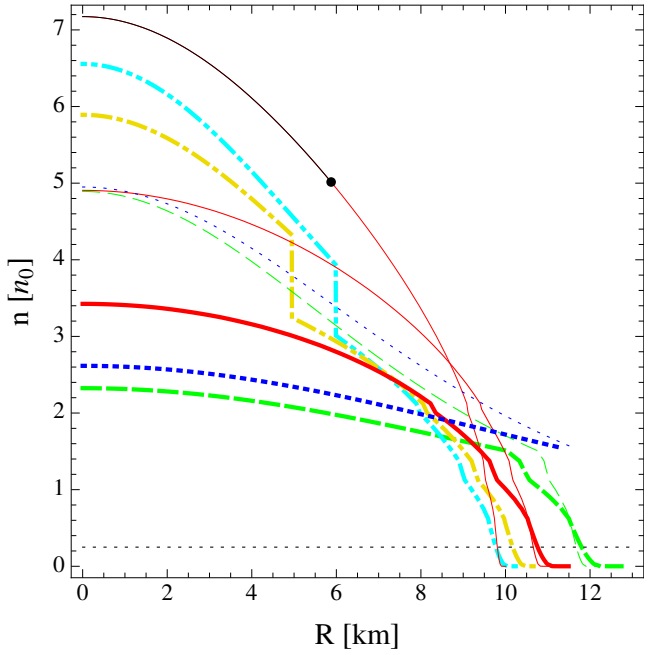

Figure 4.1: The density profiles of the star models considered in this work. The solid lines represent neutron star models with an APR equation of state, the dotted lines represent strange stars with a bag model equation of state and the dashed, dot-dot-dashed and dot-dashed lines represent hybrid star models with a large, medium and small quark matter core respectively. Thick lines represent $1.4\,M_\odot$ stars and thin lines represent massive $2\,M_\odot$ stars. In contrast to strange stars that are basically homogeneous, stars that contain hadronic matter have a very strong density dependence that extends over 14 orders of magnitude reflected by the near zero segments in this plot. The very thin solid curve presents the maximum neutron star model for the APR equation of state $\sim 2.2\,M_\odot$ where hadronic direct Urca processes are allowed to the left of the dot. The dotted horizontal line denotes the density $n = n_0/4$ chosen as the beginning of the crust whose contribution is not taken into account in the damping time integrals below.

the density fluctuation of the r-mode vanishes to leading order in the expansion, the computation of bulk viscosity damping times requires an expansion of h, Φ and of the energy density ρ to next-to-leading order

$$X(r, \cos\theta) = X_0(r) + X_2(r, \cos\theta) \left(\frac{\Omega^2}{\pi G \bar{\rho}_0} \right) + \cdots$$

where X stands for either of the three quantities, Ω is the angular velocity of the rotation and $\bar{\rho}_0$ the average energy density of the corresponding non-rotating star. The main effect of the rotational corrections is a flattening of the star due to centrifugal forces.

The next step is the search for eigenmodes of the rotating star in a linear low amplitude approximation, e.g. for the conserved baryon number $\Delta n \ll \bar{n}$. They can completely be described by the change in the gravitational potential $\delta\Phi$ and the hydrodynamical perturbation

$$\delta U = \frac{\delta p}{\rho} - \delta\Phi \, .$$

These are likewise expanded to next-to-leading order in Ω in the form

$$\delta X(r, \cos\theta) = R^2\Omega^2 \left(\delta X_0(r) + \delta X_2(r, \cos\theta) \, \frac{\Omega^2}{\pi G \bar{\rho}_0} + \cdots \right)$$

where δX stands again either for $\delta\Phi$ or δU and R is the radius of the static star. The potentials obey complicated differential equations with corresponding boundary conditions given in [43]. The boundary conditions require that the oscillation frequencies ω_r in the rotating and ω_i in the inertial frame are connected to the rotation frequency Ω via

$$\omega_r \equiv \omega = \kappa(\Omega)\Omega \quad , \quad \omega_i = \omega_r - m\Omega \tag{4.2}$$

where the parameter κ can likewise be expanded in Ω

$$\kappa = \kappa_0 + \kappa_2 \frac{\Omega^2}{\pi G \bar{\rho}_0} + \cdots$$

We study classical r-modes which are a one parameter class of eigenmode solutions, $l = m$, that are to leading order determined by $\kappa_0 = 2/(m+1)$ and given by

$$\delta U_0(\vec{r}) = \sqrt{\frac{m}{\pi\,(m+1)^3\,(2m+1)!}}\alpha \left(\frac{r}{R}\right)^{m+1} P^m_{m+1}(\cos\theta)\,\mathrm{e}^{im\varphi} \tag{4.3}$$

where P^m_{m+1} are associated Legendre polynomials and α is the dimensionless amplitude of the r-mode. There are different conventions for the amplitude α in the literature and we follow the convention for the amplitude given in [45] but take into account the corrections to the latter result in [43]. This convention is usually used in the literature and in this case the above expression breaks down for $\alpha > O(1)$. For more details on the r-mode expression see Appendix D. For the lowest r-mode that couples to gravitational waves with $m = 2$ the oscillation frequency in the inertial frame is given by $\omega_i = -4/3\,\Omega$, corresponding to a counter-rotating flow. The leading order gravitational potential obeys a differential equation that is given by eq. (4.9) and its analytic solution in the special case that the star is of uniform density is given in eq. (4.10). In general it requires a numeric solution and then completely determines the r-mode to this order.

At next-to-leading order there are two qualitatively different effects: First the connection between oscillation and rotation frequency as described by the parameter κ becomes non-linear via a non-vanishing value of κ_2 that has to be obtained numerically from a corresponding differential equation [43]. In fig. 4.2 the solution is shown for the star models discussed here. Whereas the corrections are small for quark stars, at large frequency they can become sizable for hadronic and hybrid stars. The

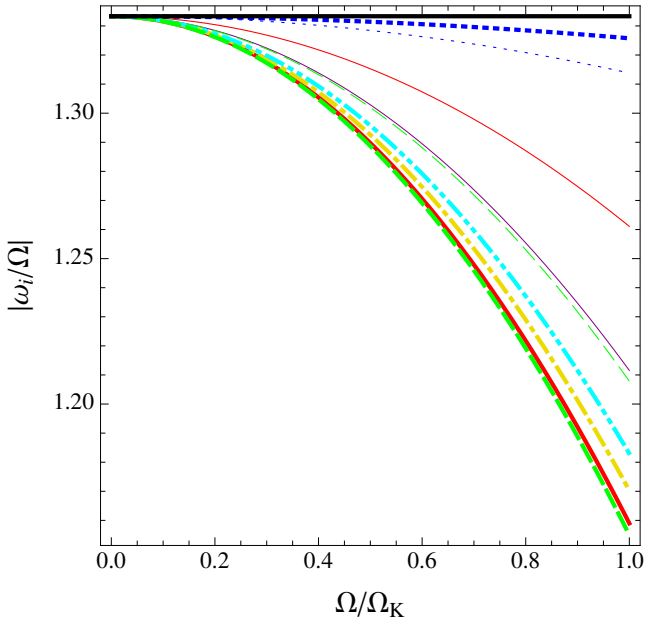

Figure 4.2: Connection of the oscillation frequency ω_i of the r-mode in the inertial frame to the rotation frequency of the considered star models to next to leading order in the Ω-expansion. The horizontal line shows the leading order result and the conventions for the other curves are the same as in fig. 4.1.

second effect is the change of the potentials arising as solutions of rather involved partial differential equations. At next-to-leading order they feature nontrivial radial and angular dependences that are not described by simple power laws or spherical harmonics anymore.

We are interested in the amplification of these modes due to gravitational radiation and their viscous damping which are described by the energy dissipation

$$\begin{aligned}\frac{dE}{dt} = &- \omega\left(\omega - m\Omega\right)^{2m+1} |\delta J_{mm}|^2 \\ &- \int d^3x \left(2\eta\delta\sigma^{ab}\delta\sigma_{ab} + \zeta\delta\sigma\delta\sigma^*\right)\end{aligned} \tag{4.4}$$

where η and ζ are the shear and bulk viscosity, respectively. The fluctuations δJ_{mm} and $\delta\sigma_{ab}$ couple to gravitational waves and shear viscosity, respectively. The fluctu-

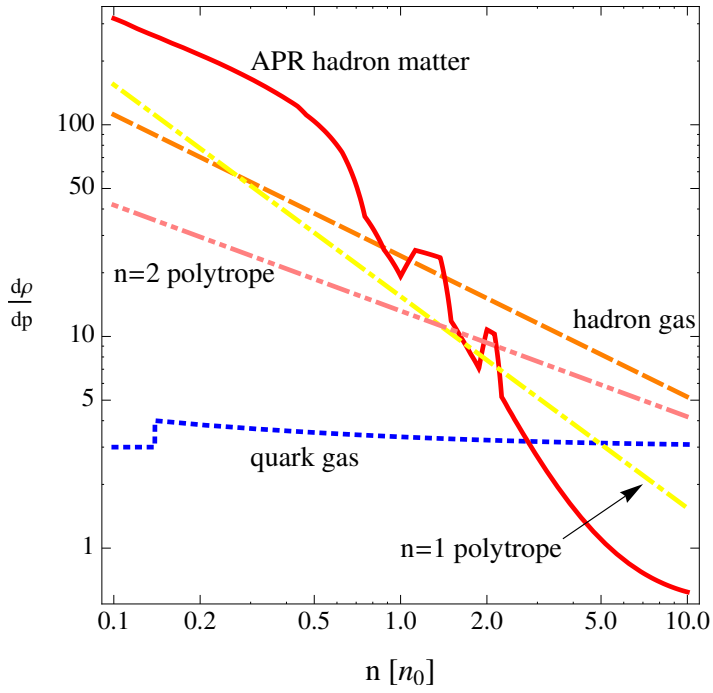

Figure 4.3: The density dependence of the inverse squared speed of sound $A \equiv d\rho/dp$ (which enters the r-mode profile multiplicatively) for the different forms of matter in table 4.2 as well as generic polytropic models. The solid line represents interacting APR matter, the dashed line a hadron gas and the dotted line shows the result for a quark gas. The structure at intermediate densities in the APR curve arises from phase transitions and the use of finite differences to compute the derivative, but due to the mild contribution of the denser inner regions of the star to the damping these, as well as the known problem that the APR equation of state becomes acausal at high density, have no influence on our results below.

ation $\delta\sigma \equiv \vec{\nabla} \cdot \delta\vec{v}$ of an r-mode oscillation which is subject to dissipation via bulk viscosity reads

$$\delta\sigma = -i\frac{2AR^2\Omega^3}{m+1}\left(\delta U_0 + \delta\Phi_0 + \cdots\right) + O\left(\Omega^5\right) \tag{4.5}$$

where A denotes the inverse speed of sound

$$A \equiv \left.\frac{\partial\rho}{\partial p}\right|_0 \tag{4.6}$$

evaluated at equilibrium and the dots represent several further terms of next-to-leading order in Ω given in [43]. The terms in the parenthesis depend on the expansion coefficients of the potentials and on the connection parameter κ, but are by virtue of the expansion independent of frequency. The fluctuation $\delta\sigma$ is finally connected to the fluctuations of energy $\Delta\rho$ and baryon number density Δn via their continuity equations

$$|\delta\sigma| = \left|\vec{\nabla}\cdot\delta\vec{v}\right| = \kappa\Omega\left|\frac{\Delta\rho}{\bar{\rho}}\right| = \kappa\Omega\left|\frac{\Delta n}{\bar{n}}\right|$$

Substituting δU_0 from eq. (4.3) in eq. (4.5) gives

$$\left|\frac{\Delta\rho}{\bar{\rho}}\right| = \left|\frac{\Delta n}{\bar{n}}\right| \approx \sqrt{\frac{4m}{(m+1)^3(2m+3)}}\frac{2}{(m+1)\,\kappa(\Omega)}\alpha A R^2\Omega^2 \cdot\left(\left(\left(\frac{r}{R}\right)^{m+1}+\delta\Phi_0\right)\left|Y^m_{m+1}(\theta,\phi)\right|+\cdots\right) \tag{4.7}$$

Following [9], in our numerical analysis we will consider the change of κ at second order, but because of the involved numerics [43], we will not take into account all explicit second order terms in eq. (4.5). A standard approximation [45] is to replace the Lagrangian density fluctuation by the Eulerian one which corresponds to neglecting the terms denoted by the ellipsis in eq. (4.7). E.g. the density fluctuation for a $m = 2$ r-mode reads then to leading order

$$\left|\frac{\Delta\rho}{\bar{\rho}}\right| \approx \left|\frac{\delta\rho}{\bar{\rho}}\right| = \sqrt{\frac{8}{189}}\alpha A R^2\Omega^2\left(\left(\frac{r}{R}\right)^3+\delta\Phi_0\,(r)\right)Y^2_3(\theta,\phi) \tag{4.8}$$

in terms of the spherical harmonics Y^2_3. However, we will give general semi-analytic expressions below that *are* valid to full next to leading order. These show that the influence of the neglected terms on important aspects of the instability regions is

rather mild. Here we give an analytic solution for the density fluctuation profile of the r-mode to leading order in Ω for a star of constant density. The part of the leading order density fluctuation eq. (4.8) that is generally not analytic is given by the change in the gravitational potential $\delta\Phi_0$ whose radial part $\delta\Phi_0(r)$ is defined by

$$\delta\Phi_0(\vec{r}) = \sqrt{\frac{m}{\pi\,(m+1)^3\,(2m+1)!}}\alpha\delta\Phi_0(r)\,P^m_{m+1}(\cos\theta)\,\mathrm{e}^{im\varphi}$$

It fulfills the differential equation [43]

$$\begin{aligned}\frac{d^2\delta\Phi_0}{dr^2} + \frac{2}{r}\frac{d\delta\Phi_0}{dr} + \left(4\pi G\rho\frac{d\rho}{dp} - \frac{(m+1)\,(m+2)}{r^2}\right)\delta\Phi_0 \\ = -4\pi G\rho\frac{d\rho}{dp}\left(\frac{r}{R}\right)^{m+1}\end{aligned} \tag{4.9}$$

with boundary conditions $\delta\Phi_0(0) = 0$ and

$$\left.\frac{d\delta\Phi_0(r)}{dr}\right|_{r=R} = -\left(\frac{1}{2} + \sqrt{\frac{1}{4} + (m+1)\,(m+2)}\right)\frac{\delta\Phi_0(R)}{R}$$

Here we specialize to the fundamental $m = 2$ r-mode where an analytic solution is possible for the idealized case $\rho = const.$ and $d\rho/dp = const.$ which is approximately realized for strange stars. The solution obtained with a computer algebra system reads

$$\begin{aligned}\delta\Phi_0(r) = -\frac{r^3}{R^3} \\ + \frac{7LR^2\left(\left(r^3 - 15L^2r\right)\cos\left(\frac{r}{L}\right) + 3L\left(5L^2 - 2r^2\right)\sin\left(\frac{r}{L}\right)\right)}{r^4\left(\left(3L^2 - R^2\right)\sin\left(\frac{R}{L}\right) - 3LR\cos\left(\frac{R}{L}\right)\right)}\end{aligned} \tag{4.10}$$

in terms of the intrinsic length scale

$$L \equiv \frac{1}{\sqrt{4\pi G\rho\frac{\delta\rho}{\delta p}}}$$

Unfortunately the above expression is rather ill behaved due to strong cancellations and not suitable for a direct evaluation. However, employing the series representations of the trigonometric functions it is possible to transform it into an alternative form

$$\delta\Phi_0(r) = g\left(\frac{r}{L}, \frac{R}{L}\right)\frac{r^3}{R^3}$$

in terms of hypergeometric functions

$$g(x,y) \equiv \frac{{}_0F_2\left(\frac{1}{2}, \frac{7}{2}+1; -\frac{x^2}{8}\right)}{{}_0F_2\left(\frac{1}{2}, \frac{5}{2}+1; -\frac{y^2}{8}\right)} - 1 \approx -\frac{x^2}{18} + \frac{y^2}{14} + \cdots$$

Correspondingly, $|g| < 0.07$ over the entire parameter range so that in view of the large uncertainties inherent in an r-mode analysis the gravitational potential term in eq. (4.8) can be neglected leaving a simple analytic expression for the r-mode profile of strange stars with approximately constant density

$$\left|\frac{\delta\rho}{\bar{\rho}}\right|_{SS} \approx \sqrt{\frac{8}{189}}\alpha A R^2\Omega^2\left(\frac{r}{R}\right)^3 Y_3^2(\theta,\phi)\,.$$

For our numerical analysis below we have made the approximation to neglect the additional second order corrections in the slow rotation expansion given by the ellipsis in eq. (4.7), which amounts to replacing the Lagrangian perturbation by the Eulerian perturbation, but we include the second order corrections to the frequency eq. (4.2). General analytic results show that this is a good approximation for the computation of the small amplitude instability regions.But in the next chapter we will see that, in obtaining a precise assessment of the damping time of large amplitude r-modes, the radial dependence of the density perturbation plays a vital role. The radius enters

eq. (4.7) explicitly and also via the density dependence of the inverse squared speed of sound A (fig. 4.3), and the radial density dependence of the star (fig.4.1). The radial variation of the density is moderate in a strange star, but much more pronounced in neutron stars where the r-mode amplitude grows strongly in the outer regions of the star.

4.3 Shear viscosity of dense matter

As we mentioned earlier, the bulk viscosity is the relevant damping mechanism for the growth of the r-modes at high temperatures and the shear viscosity is the relevant damping mechanism at low temperatures. Therefore to compute the viscous damping of the r-modes we need to have both bulk viscosity and shear viscosity for the considered form of matter. In the previous chapter we explained the bulk viscosity of dense matter in details and gave the results for different forms of matter. So in this section we give the shear viscosity results for the same forms of matter in order to compute the viscous damping times.

The shear viscosity arises from strong or electromagnetic interactions. In contrast to the bulk viscosity, the shear viscosity of dense matter is independent of the frequency of an external oscillation and approximately depends on temperature via a simple power law. Shear viscosity becomes large at low temperatures and therefore it is the dominant process for damping of the r-modes of cooler stars. Thereby, to leading order it can be parameterized as

$$\eta = \tilde{\eta} T^{-\sigma} \tag{4.11}$$

by simply factoring out the temperature dependence with exponent σ. In general several processes can contribute so that the full shear viscosity can approximately be

	A	B	C
hadronic matter	$m_N \left(\frac{\partial p}{\partial n}\right)^{-1}$	$\frac{8S}{n} + \frac{\pi^2}{(4(1-2x)S)^2}$	$4(1-2x)\left(n\frac{\partial S}{\partial n} - \frac{S}{3}\right)$
hadronic gas	$\frac{3m_N^2}{(3\pi^2 n)^{\frac{2}{3}}}$	$\frac{4m_N^2}{3(3\pi^2)^{\frac{1}{3}} n^{\frac{4}{3}}}$	$\frac{\left(3\pi^2 n\right)^{\frac{2}{3}}}{6m}$
quark matter (gas: $c = 0$)	$3 + \frac{m_s^2}{(1-c)\mu_q^2}$	$\frac{2\pi^2}{3(1-c)\mu_q^2}\left(1 + \frac{m_s^2}{12(1-c)\mu_q^2}\right)$	$-\frac{m_s^2}{3(1-c)\mu_q}$

Table 4.2: Strong interaction parameters, defined in eqs. (4.6) and (3.15), describing the response of the particular form of matter. In the case of interacting hadronic matter a quadratic ansatz in the proton fraction x parameterized by the symmetry energy S is employed. The expressions for a hadron and quark gas are given to leading order in n/m_N^3 respectively next to leading order in m_s/μ.

written as a sum of such power laws for the individual processes.

In the following we discuss the shear viscosity for the phases of dense matter presented in the considered classes of compact stars. We note however, that the general results given in this chapter likewise apply to more complicated forms of matter like hyperonic and/or superfluid nuclear matter as well as various forms of superconducting quark matter.

Further, the inverse speed of sound A, eq. (4.6), as well as the strong susceptibilities B and C, eq. (3.15), that parameterize the deviation from chemical equilibrium are required.

In previous r-mode analyses the shear viscosity in hadronic matter has been approximated by the contribution from strong hadron-hadron-scattering using the fit in [8] to the standard low density ($\lesssim n_0$) data given in [10]

$$\eta_n = 347 \rho^{\frac{9}{4}} T^{-2} \frac{\mathrm{g}}{\mathrm{cm\,s}} \tag{4.12}$$

where T is in units of Kelvin and ρ is given in $\mathrm{g/cm^3}$. Extrapolating this fit to high densities relevant for neutron stars overestimates the viscosity. The new evaluation in [121] shows instead that due to a non-Fermi liquid enhancement arising from the

Strong/EM process	$\tilde{\eta}\left[\mathrm{MeV}^{(3+\sigma)}\right]$	σ
quark scattering	$1.98\times10^{9}\alpha_s^{-\frac{5}{3}}\left(\frac{\mu_q}{300\,\mathrm{MeV}}\right)^{\frac{14}{3}}$	$\frac{5}{3}$
leptonic scattering	$1.40\times10^{12}\left(\frac{x\,n}{n_0}\right)^{\frac{14}{9}}$	$\frac{5}{3}$
nn-scattering	$5.46\times10^{9}\left(\frac{\rho}{m_N n_0}\right)^{\frac{9}{4}}$	2

Table 4.3: Parameters arising in the parameterization eq. (4.11) of the shear viscosity for different strong and electromagnetic interaction processes. The leptonic and quark scattering arises from a non-Fermi liquid enhancement due to unscreened magnetic interactions.

exchange of Landau-damped transverse photons, the main contribution to the shear viscosity of hadronic matter, at temperatures relevant to the spin-down evolution of the compact stars, comes from electron scattering and is given by

$$\eta_e = 4.26\times10^{-26}(x\,n)^{\frac{14}{9}}T^{-\frac{5}{3}}\frac{\mathrm{g}}{\mathrm{cm\,s}} \tag{4.13}$$

where T is in Kelvin and the baryon number density n is in units of cm^{-3}. In the calculation of η_e we have only considered electron-electron and electron-proton scattering and neglected the small effect of the muons to the shear viscosity. For densities larger than nuclear matter saturation density this electron contribution dominates over the hadronic one down to temperatures below 10^7 K. This region contains the part of the instability region that is relevant for the spin-down evolution of stars. Therefore in our main analysis we will completely neglect the hadronic component of the shear viscosity. However, we will compare with the previous form of the shear viscosity eq. (4.12) in order to discuss the effect of our improved analysis on the instability region[1].

[1]The leftmost part of the instability region below $\sim 10^7$ K only features an instability at very large frequencies. This part would only be relevant for old stars that are spun up by accretion, yet frequencies very close to the Kepler frequency are not reached via this mechanism anyway, cf. fig. 1.1, due to turbulent effects.

In the case of ungapped quark matter, the shear viscosity is dominated by quark-quark scattering, and in the limit of $T \ll q_D$, where q_D is the Debye wave number, it is given by [122]

$$\eta_q = \frac{1}{40\pi a}\left(\frac{2N_q}{\pi}\right)^{\frac{1}{3}} \alpha_s^{-\frac{5}{3}} \mu_q^{\frac{14}{3}} T^{-\frac{5}{3}} \tag{4.14}$$

where $\alpha_s = \frac{g^2}{4\pi}$ is the QCD coupling constant, $a \simeq 1.81$, $N_q = 3$ and μ_q and T are in units of MeV. The temperature dependence arises again from a non-Fermi liquid enhancement of the quark interaction. These expressions yield the parameters in the parameterization of the shear viscosity eq. (4.11) as given in table 4.3.

4.4 R-mode time scales

4.4.1 General expressions

The amplitude of the r-mode oscillations evolves with time dependence $\mathrm{e}^{i\omega t - t/\tau}$, where ω is the real part of the frequency of the r-mode and $1/\tau$ is the imaginary part of the frequency. The latter describes both the exponential rise of the r-mode driven by the Friedman-Schutz mechanism [49] and its decay due to viscous damping. We can decompose $1/\tau$ as

$$\frac{1}{\tau(\Omega,T)} = \frac{1}{\tau_G(\Omega)} + \frac{1}{\tau_B(\Omega,T)} + \frac{1}{\tau_S(T)}$$

where τ_G, τ_B and τ_S are gravitational radiation, bulk viscosity and shear viscosity time scales, respectively. The lowest of these individual time scales determines if the r-mode is unstable or damped. The damping time for the individual mechanisms is in general given by

$$\frac{1}{\tau_i} \equiv -\frac{1}{2E}\left(\frac{dE}{dt}\right)_i \tag{4.15}$$

and requires both the total energy of the r-mode

$$E = \frac{1}{2}\alpha^2 R^4 \Omega^2 \int_0^R \rho(r) \left(\frac{r}{R}\right)^{2m+2} dr \tag{4.16}$$

and the dissipated energy which is given by the corresponding part of eq. (4.4) [43]. For instance the dissipated energy eq. (4.4) due to the bulk viscosity reads

$$\left(\frac{dE}{dt}\right)_\zeta = -\kappa^2 \Omega^2 \int d^3x \left|\frac{\Delta\rho}{\rho}\right|^2 \zeta\left(\left|\frac{\Delta\rho}{\rho}\right|^2\right)$$

where the dependence of the bulk viscosity on the conserved number density fluctuation amplitude has been expressed in terms of the conserved energy density. If the star consists of several shells consisting of different forms of matter with different viscosity, as is the case for hybrid stars, neutron stars with a high density core where direct Urca reactions are allowed, etc., the integral consists of partial integrals over the individual shells s and the inverse viscous damping times can be written as

$$\frac{1}{\tau_i} = \sum_s \frac{1}{\tau_i^{(s)}}$$

Therefore, the contribution of the different shells enters additively. We will in the following expressions suppress the explicit label (s) but implicitly assume that the damping times consist of several contributions when different layers are present. With these expressions the individual r-mode time scales can be obtained. The time scale of the r-mode growth due to gravitational wave emission is given by [45]

$$\frac{1}{\tau_G} = -\frac{32\pi\,(m-1)^{2m}}{\left((2m+1)!!\right)^2}\left(\frac{m+2}{m+1}\right)^{2m+2} \tilde{J}_m G M R^{2m} \Omega^{2m+2} \tag{4.17}$$

with the radial integral constant

$$\tilde{J_m} \equiv \frac{1}{MR^{2m}} \int_0^R \rho(r)\, r^{2m+2} dr \tag{4.18}$$

Shear viscosity damping time

The damping time of an r-mode with angular quantum number m due to shear viscosity is given by

$$\frac{1}{\tau_S} = \frac{(m-1)\,(2m+1)}{\tilde{J}_m MR^{2m}} \int_0^R \eta\, r^{2m} dr$$

Using the parameterization eq. (4.11) this can be written as

$$\frac{1}{\tau_S} = \frac{(m-1)\,(2m+1)\,\tilde{S}_m \Lambda_{QCD}^{3+\sigma} R}{\tilde{J}_m MT^{\sigma}} \tag{4.19}$$

in terms of the dimensionless constant

$$\tilde{S}_m \equiv \frac{1}{R^{2m+1}\Lambda_{QCD}^{3+\sigma}} \int_{R_i}^{R_o} \tilde{\eta} r^{2m} dr \tag{4.20}$$

where R_i and R_o are the inner and outer radius of the corresponding shell, if there are several ones. This constant contains the complete dependence on the particular microscopic processes. To make this quantity dimensionless the generic scale Λ_{QCD} has been introduced that is chosen as $\Lambda_{QCD} = 1$ GeV for the numeric values. For the fundamental $m = 2$ r-mode the parameter $\tilde{S}$ is given for the different star models considered here in table 4.4.

Bulk viscosity damping time

The bulk viscosity damping time is given by

$$\frac{1}{\tau_B} = \frac{\kappa^2}{\alpha^2 \tilde{J}_m M R^2} \int d^3x \left|\frac{\Delta n}{\bar{n}}\right|^2 \zeta\left(\left|\frac{\Delta n}{\bar{n}}\right|^2\right) \tag{4.21}$$

where the bulk viscosity is in general a function of the amplitude [78, 81]. As has been noted before the strongly enhanced damping can provide a mechanism for the saturation of the r-mode as will be discussed elsewhere. Here we restrict ourselves to a study of the initial instability of small amplitude r-modes and in the subthermal regime the viscosity eq. (3.26) is independent of the r-mode amplitude. In this case only the angular integral over the density fluctuation enters and it is useful to define the angular averaged form

$$\begin{aligned}\delta\Sigma(r) &\equiv \frac{m+1}{2\alpha A R^2 \Omega^3} \sqrt{\frac{(m+1)^3 (2m+3)}{4m}} \left(\int d\Omega \, |\delta\sigma|^2\right)^{\frac{1}{2}} \\ &\underset{l.o.}{\longrightarrow} \left(\frac{r}{R}\right)^{m+1} + \delta\Phi_0 \end{aligned} \tag{4.22}$$

which reduces to the second line to leading order in the Ω-expansion, where the angular integral in eq. (5.1) is trivial due to the normalization of the spherical harmonics. The damping time in the subthermal regime is then given by

$$\frac{1}{\tau_B^<} = \frac{16m}{(2m+3)(m+1)^5 \kappa} \frac{R^5 \Omega^3}{\tilde{J}_m M} \mathcal{T}_m^< \left(\frac{T^\delta}{\kappa\Omega}\right) \tag{4.23}$$

where the dependence on all local quantities, like the equation of state, the weak rate, the density dependence of the particular star model and its r-mode profile is contained in the function

$$\mathcal{T}_m^<(b) \equiv \frac{b}{R^3}\int_{R_i}^{R_o} dr\, r^2 \frac{A^2C^2\tilde{\Gamma}}{1+\tilde{\Gamma}^2B^2b^2}\left(\delta\Sigma(r)\right)^2 \tag{4.24}$$

depending on a single external parameter and which has to be determined numerically for a given star model. In the asymptotic limits the damping time simplifies to

$$\frac{1}{\tau_B^<} \xrightarrow[f\ll 1]{} \frac{16m}{(2m+3)\,(m+1)^5\,\kappa^2}\frac{\Lambda_{QCD}^{9-\delta}\tilde{V}_m R^5\Omega^2T^\delta}{\Lambda_{EW}^4\tilde{J}_m M} \tag{4.25}$$

$$\frac{1}{\tau_B^<} \xrightarrow[f\gg 1]{} \frac{16m}{(2m+3)\,(m+1)^5}\frac{\Lambda_{EW}^4\Lambda_{QCD}^{\delta-1}\tilde{W}_m R^5\Omega^4}{\tilde{J}_m MT^\delta} \tag{4.26}$$

with the dimensionless constants

$$\tilde{V}_m \equiv \frac{\Lambda_{EW}^4}{R^3\Lambda_{QCD}^{9-\delta}}\int_{R_i}^{R_o} dr\, r^2A^2C^2\tilde{\Gamma}\,\left(\delta\Sigma(r)\right)^2 \tag{4.27}$$

$$\tilde{W}_m \equiv \frac{1}{R^3\Lambda_{EW}^4\Lambda_{QCD}^{\delta-1}}\int_{R_i}^{R_o} dr\, r^2\frac{A^2C^2}{\tilde{\Gamma}B^2}\left(\delta\Sigma(r)\right)^2 \tag{4.28}$$

Since the bulk viscosity originates from weak interactions here the second normalization scale Λ_{EW} is used with a generic value $\Lambda_{EW} = 100$ GeV. These normalization scales are only introduced to obtain dimensionless constants of order one and drop out of the final results for the damping times.

Finally, we want to stress that in these expressions for the r-mode time scales the complete local dependence on the star profile, the r-mode oscillation and the microscopic damping processes is contained in the few constant $\tilde{J}$, $\tilde{S}$, $\tilde{V}$ and $\tilde{W}$, but the dependence on the global parameters of the r-mode evolution [50] Ω and T is entirely explicit. These constants include in particular also the complete dependence

on the non-trivial radial and angular dependence of the full next-to-leading order expression for the r-mode[43]. Since to our knowledge results for the bulk viscosity in the crust of neutron stars are not yet available, we neglect the damping of the crust in our numerical analysis. It has, however, been argued that the shear viscosity of the crust could be crucial [123] and a more detailed study of this issue is definitely desirable.

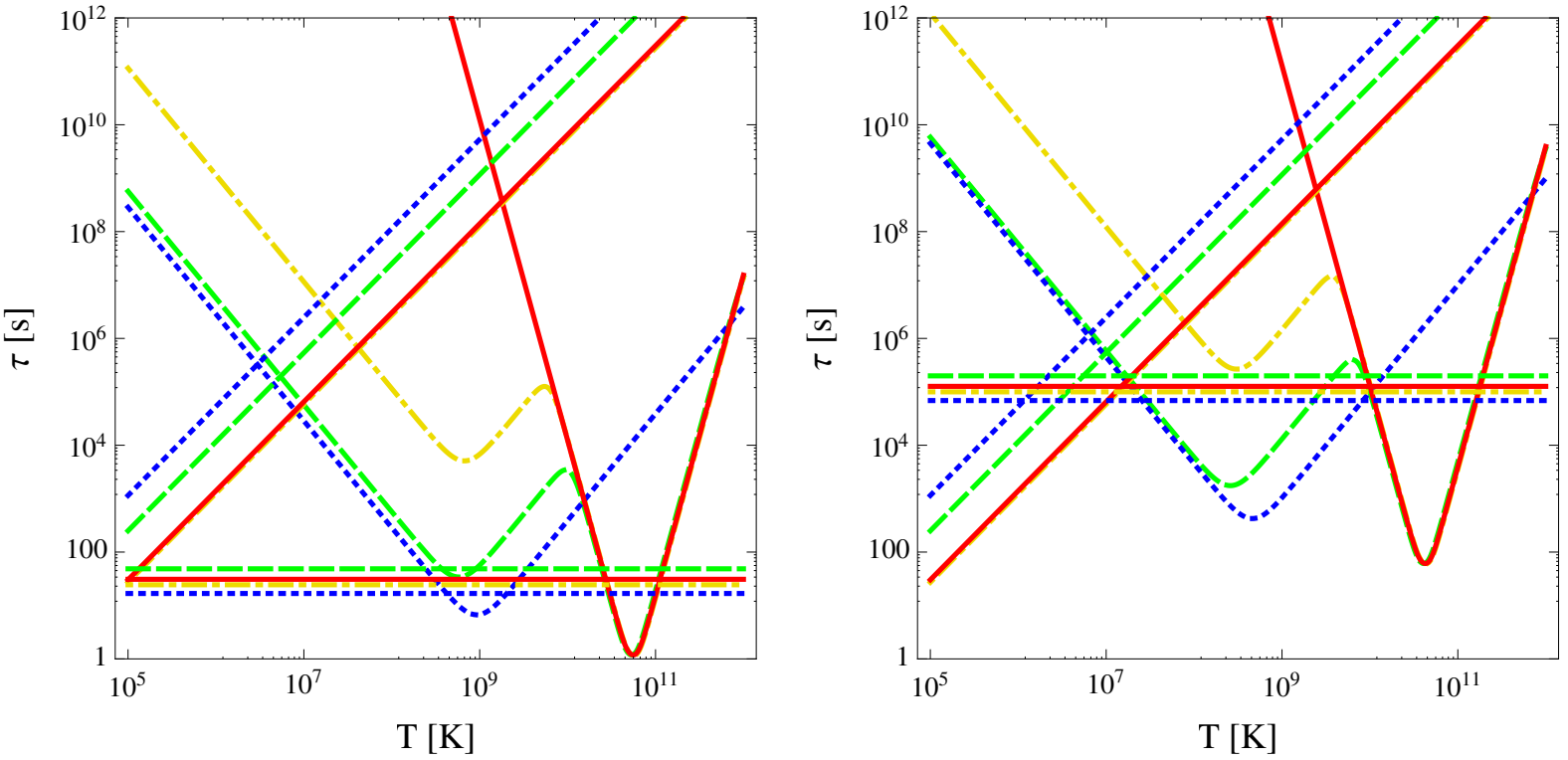

Figure 4.4: Damping times of the different $1.4\,M_\odot$ star models discussed in this work. Shown are a hadronic star with modified Urca processes (solid), hybrid stars with a small (dot-dashed) and large (dashed) quark core as well as a strange star (dotted). The horizontal curves give the time scale τ_G associated to the growth of the mode due to gravitational wave emission. The monotonically increasing curves show the damping time τ_S due to shear viscosity and the non-monotonic curves the damping time τ_B due to bulk viscosity. *Left panel:* Stars rotating at their Kepler frequency Ω_K. *Right panel:* Same for stars rotating at $\Omega_K/4$.

4.4.2 Results for the considered star models

Before we discuss the damping times for particular star models let us point out a few generic properties of the damping times that follow directly from the general expressions eqs. (4.17), (4.19) and (5.5). The gravitational time scale is independent of temperature and decreases strongly with frequency. The shear viscosity damping time increases with temperature and is independent of frequency. Because of the resonant behavior of the bulk viscosity, the corresponding damping time decreases with temperature, has a minimum and increases again at large temperatures. Furthermore, it also decreases with frequency, but slower than the gravitational time scale.

A numeric solution requires the integration over the star profiles to obtain the constants $\tilde{J}$, $\tilde{S}$ and the function $\mathcal{T}^{<}$, respectively the constants $\tilde{V}$ and $\tilde{W}$ describing its asymptotic behavior. The constants are given for the fundamental $m = 2$ r-mode of the various star models discussed in this work, and where applicable also for their different shells, in table 4.4. For the bulk viscosity of a $1.4\,M_{\odot}$ neutron star we compute the APR result employing the proper susceptibilities for interacting matter, as well the result when the susceptibilities are evaluated in the idealized case of a hadronic gas, as has been done previously [8, 7]. As can be seen the parameters in the interacting case are more than an order of magnitude larger, owing to the larger viscosity [81], which leads to a correspondingly smaller damping time. In the following we will consider only the proper interacting form unless otherwise noted.

star model	shell	$\tilde{J}$	$\tilde{S}$	$\tilde{V}$	$\tilde{W}$	$T_{min}[K]$	$\Omega_{min}[Hz]$	$T_{max}[K]$	$\Omega_{max}[Hz]$
NS $1.4\,M_\odot$	core	1.81×10^{-2}	7.68×10^{-5}	1.31×10^{-3}	1.61×10^{-6}	3.49×10^{9}	371	–	–
NS $1.4\,M_\odot$ gas			4.32×10^{-6}	1.28×10^{-4}	1.76×10^{-7}	3.70×10^{9}	226	–	–
NS $2.0\,M_\odot$		2.05×10^{-2}	2.25×10^{-4}	1.16×10^{-3}	1.72×10^{-6}	4.19×10^{9}	368	–	–
NS $2.21\,M_\odot$	d.U. core	2.02×10^{-2}	5.05×10^{-4}	1.16×10^{-8}	7.11×10^{-7}	2.03×10^{9}	493	–	–
	m.U. core			9.34×10^{-4}	1.55×10^{-6}				
SS eq. (4.1)	all	$\frac{3}{28\pi}$	$\frac{\hat{\eta}\mu_q^{14/3}}{5\Lambda_{QCD}^{14/3}\alpha_s^{5/3}}$	$\frac{\Lambda_{EW}^4\hat{\Gamma}m_s^4\mu_q^3}{9\Lambda_{QCD}^7(1-c)^2}$	$\frac{m_s^4}{4\pi^4\Lambda_{EW}^4\Lambda_{QCD}\hat{\Gamma}\mu_q^3}$	eq. (4.43)	eq. (4.42)	eq. (4.45)	eq. (4.44)
SS $1.4\,M_\odot$		3.08×10^{-2}	3.49×10^{-6}	3.53×10^{-10}	0.191	7.86×10^{6}	1020	1.01×10^{9}	8340
SS $2.0\,M_\odot$		2.65×10^{-2}	4.45×10^{-6}	3.38×10^{-10}	0.157	8.58×10^{6}	955	8.07×10^{8}	6600
HS $1.4\,M_\odot$ L	quark core	1.93×10^{-2}	2.19×10^{-6}	1.38×10^{-10}	1.03×10^{-2}	9.87×10^{6}	1170	5.83×10^{8}	7270^*
	hadr. core		6.72×10^{-6}	1.40×10^{-3}	1.51×10^{-6}	6.88×10^{9}	$1040^\dagger$	–	–
HS $1.4\,M_\odot$ S	quark core	1.68×10^{-2}	2.88×10^{-7}	7.96×10^{-13}	6.85×10^{-5}	1.01×10^{8}	1070	4.35×10^{8}	3690^*
	hadr. core		3.29×10^{-6}	1.25×10^{-3}	1.56×10^{-6}	3.61×10^{9}	$394^\diamond$	–	–
HS $2.0\,M_\odot$	quark core	2.00×10^{-2}	5.25×10^{-6}	3.76×10^{-10}	2.34×10^{-2}	7.73×10^{6}	1080	4.77×10^{8}	6310^*
	hadr. core		5.24×10^{-6}	1.07×10^{-3}	1.32×10^{-6}	7.65×10^{9}	$925^\dagger$	–	–

Table 4.4: Radial integral parameters and characteristic points of the instability region of a $m = 2$ r-mode for the star models considered in this work. The constant $\tilde{J}$, $\tilde{S}$, $\tilde{V}$ and $\tilde{W}$ are given by eqs. (4.18), (4.20), (5.7) and (4.28) using the generic normalization scales $\Lambda_{QCD} = 1$ GeV and $\Lambda_{EW} = 100$ GeV. The temperatures and frequencies are obtained with the analytic expressions for the minima eqs. (4.31), (4.32), (4.37) and (4.38) and for the maxima eqs. (4.34) and (4.35). The expressions for a generic strange star (or quark core) in terms of the parameters of the quark model equation of state eq. (4.1), using the constants $\hat{\Gamma}$ and $\hat{\eta}$ defined in eq. (4.41) are given as well. $(*)$ These values deviate significantly from the actual results due to the inappropriate approximation of constant radial profiles, whereas this idealization entirely fails for hadronic parts. $(\dagger)$ The second minimum arises from the competition of the bulk viscosity damping in the quark and the hadronic shell. $(\diamond)$ The second minimum arises from the competition of bulk and shear viscosity damping in the hadronic shell.

In the left panel of fig. 4.4 the numeric solution for the different time scales is shown as a function of temperature for $1.4\,M_\odot$ stars of the different classes considered here rotating at their Kepler frequency Ω_K. Shown are gravitational time scales (horizontal lines), the shear viscosity damping times (monotonically increasing curves) and bulk viscosity damping times (non-monotonic curves). The solid lines denote the neutron star model, the dotted lines a strange star and the dashed and dot-dashed lines show hybrid star models with a small and large quark core, respectively. Whereas damping due to shear viscosity dominates for strange and hybrid stars for $T \lesssim 10^7$ K and for neutron stars even for $T \lesssim 10^9$ K, the bulk viscosity damping time of the neutron and the strange star feature the generic resonant form, where the minima are around 10^9 K and 10^{11} K, respectively, and the higher gradients in case of the neutron star arise from the higher power of δ (tab. 3.1). It is clear that as a function of the core size the family of hybrid curves interpolates continuously between the two uniform star models. Correspondingly, for hybrid stars the contribution of the quark core dominates at low temperature, whereas the hadronic shell dominates at higher temperatures, which leads to a curve with two minima. For all star models at Ω_K the gravitational time scale is the lowest over a range of temperatures.

The right panel of fig. 4.4 shows the same plot at the lower frequency $\Omega_K/4$. As is clear from the general discussion the shear curves are unchanged whereas the gravitational curves and the bulk curves are shifted upwards compared to the left panel of fig. 4.4. Since the gravitational time scale moves upwards faster than the bulk viscosity curve, the instability region shrinks from both sides as the frequency is lowered. For hybrid stars with a large quark core the gravitational time scale can move above the minimum of the bulk viscosity arising from the quark core as the frequency is lowered and the instability region is divided by a stability window. Yet, for a hybrid star with a sufficiently small quark core the minimum can move above

the shear curve before the gravitational time scale can overtake it. In this case there would be no signature of the quark core and the instability regions of such a hybrid star and of the corresponding neutron star would look basically indistinguishable[2]. This is nearly the case for the small core hybrid star model denoted by the dot-dashed curve as will be discussed below.

4.5 R-mode instability regions

The boundary of the instability region is given by the condition $|\tau_G| = |\tau_V|$, where τ_V is the viscous damping time. This reads in terms of the individual contributions

$$\frac{1}{\tau_G} + \sum_s \left(\frac{1}{\tau_S^{(s)}} + \frac{1}{\tau_B^{(s)}} \right) = 0 \tag{4.29}$$

Since at the boundary the time scale of the gravitational instability is identical to the viscous time scale, the r-mode amplitude neither increases nor decreases. If the viscous damping time is shorter modes induced by external perturbations will quickly be damped away, whereas in the opposite case they are unstable and will initially grow. As will be shown in a second article the increase in the bulk viscosity at large amplitude can eventually saturate the r-mode, but here we will limit ourselves to the small amplitude regime and analyze the regions where small amplitude modes are unstable. In general eq. (4.29) has no analytic solution and has to be solved numerically. However there are various limiting cases for which analytic solutions exist and we will study them below.

[2]The fact that the volume of the neutron shell is slightly smaller is not significant for the damping times that vary over many orders of magnitude, so that the dashed curves in fig. 4.4 are invisible underneath the solid neutron star curves.

4.5.1 Analytic expressions

The boundary of the instability region eq. (4.29) can generally not be found analytically due to the occurrence of several terms with non-trivial temperature and frequency dependencies. Since the viscous damping times vary extremely strongly with temperature and frequency (fig. 4.4) in general there is over nearly the whole parameter space one component that clearly dominates the others in the sum. In such a case the equation can easily be solved analytically and yields analytic expressions for the different segments of the instability region. Although the numeric solution of eq. (4.29) is straightforward, these analytic expressions reveal the general dependence on the various unknown model parameters entering the r-mode analysis and therefore provide a measure for the uncertainty of these results in a situation where most properties of dense strongly interacting are basically unknown.

General semi-analytic expressions for the boundary of the instability region

Here we give the general semi-analytic expressions for the boundary of the instability region that are valid for arbitrary multipoles and can be applied to stars involving several shells. The only non-analytic input in these expressions enters via the radial integral constants $\tilde{J}$, $\tilde{S}$, $\tilde{V}$ and $\tilde{W}$ arising in the gravitational time scale, the shear viscosity time scale as well as the low and high temperature limit of the bulk viscosity time scale. In general these constants, which are given for the star models discussed in this work and the normalization scales $\Lambda_{QCD} = 1$ GeV and $\Lambda_{EW} = 100$ GeV in table 4.4, have to be computed numerically. However, since the dependence of many of the following results on these constants is surprisingly weak, these expressions are often essentially analytic.

On the low temperature side of the instability region the shear viscosity dominates

and neglecting the bulk viscosity yields the analytic result for the boundary in this region

$$\Omega(T) \xrightarrow[T \ll T_{min}]{} \left(\frac{(2m+1)\left((2m+1)!!\right)^2 (m+1)^{2m+2}}{32\pi (m+2)^{2m+2} (m-1)^{2m-1}} \cdot \frac{\tilde{S}_m \Lambda_{QCD}^{3+\sigma}}{\tilde{J}_m^2 G M^2 R^{2m-1} T^\sigma} \right)^{\frac{1}{2m+2}} \tag{4.30}$$

In the case of a hybrid star with two or more distinct shells one of them generally dominates and the above expression applies using only the contribution $\tilde{S}$ of the dominant shell as well as the corresponding exponent σ. The dominant contribution to the inverse shear viscosity damping time arises from the hadronic shell. Since the shear damping time increases monotonically with temperature whereas the bulk viscosity decreases in this regime monotonically, the minimum of the instability region is taken at the temperature where $\tau_S = \tau_B$. The minimum frequency is then obtained from $1/\tau_G + 2/\tau_B = 0$ and taking into account that at low frequency $\kappa \approx \kappa_0$ it yields

$$\Omega_{min} \approx \left(\left(\frac{m (m+1)^{2m-1} \left((2m+1)!!\right)^2}{4\pi (2m+3) (m+2)^{2m+2} (m-1)^{2m}} \right)^{\sigma} \cdot \left(\frac{\left((2m+1)!!\right)^2 (2m+1) (m+1)^{2m+2}}{16\pi (m-1)^{2m-1} (m+2)^{2m+2}} \right)^{\delta} \cdot \frac{\tilde{V}_m^\sigma \tilde{S}_m^\delta \Lambda_{QCD}^{3\delta+9\sigma}}{\tilde{J}_m^{2(\delta+\sigma)} \Lambda_{EW}^{4\sigma} G^{\delta+\sigma} R^{2m(\delta+\sigma)-\delta-5\sigma} M^{2(\delta+\sigma)}} \right)^{\frac{1}{2m(\delta+\sigma)+2\delta}} \tag{4.31}$$

whereas the corresponding minimum temperature is

$$T_{min} \approx \left(\frac{(2m+3)\,(2m+1)\,(m+1)^3\,(m-1)}{4m} \cdot \frac{\tilde{S}_m \Lambda_{EW}^4 \Lambda_{QCD}^{\delta+\sigma-6}}{\tilde{V}_m R^4} \right)^{\frac{1}{\delta+\sigma}} \Omega_{min}^{-\frac{2}{\delta+\sigma}} \tag{4.32}$$

Above the minimum the bulk viscosity dominates and increases until it reaches a maximum. Within a temperature range in between these two extrema shear viscosity can be neglected and the low temperature approximation to the bulk viscosity can be applied. In the general case the equation $1/\tau_B + 1/\tau_G = 0$ for the boundary cannot be solved analytically as a function of T due to the non-linear second order terms in Ω. However, it is possible to solve the equation analytically as a function of Ω which provides an equally valid parameterization of the segment in between the two extrema

$$T(\Omega) \xrightarrow[\Omega \ll \Omega_{max}]{\Omega_{min} \ll \Omega} \left(\frac{2\pi\,(2m+3)(m+2)^{2m+2}(m-1)^{2m}\kappa^2}{m\,(m+1)^{2m-3}\,((2m+1)!!)^2} \cdot \frac{\tilde{J_m}^2 \Lambda_{EW}^4 G M^2 \Omega^{2m}}{\tilde{V}_m \Lambda_{QCD}^{9-\delta} R^{5-2m}} \right)^{\frac{1}{\delta}} \tag{4.33}$$

Since there is no analytic expression for the bulk viscosity around the maximum only for the special case of constant density stars a result is possible. In this case the maximum frequency is

$$\Omega_{max} \xrightarrow[\text{dens.}]{\text{unif.}} \left(\frac{2\pi m \left(m+1\right)^{2m-2} \left(2m+3\right) \left((2m+1)!!\right)^2}{9 \left(2m+5\right) \left(m+2\right)^{2m+2} \left(m-1\right)^{2m}} \cdot \frac{\bar{A}^2 \bar{C}^2 \left(R_o^3 - R_i^3\right)}{G \bar{B} M^2 R^{2m-2}} \right)^{\frac{1}{2m-1}} \tag{4.34}$$

where R_i and R_o are the inner and outer radii of the dominant shell (0 and R for a homogeneous star) and bars denote average quantities over the shell in case the density is only approximately constant. The corresponding maximum temperature is

$$T_{max} \xrightarrow[\text{density}]{\text{uniform}} \left(\frac{2\Omega_{max}}{\left(m+1\right) \bar{\tilde{\Gamma}} \bar{B}} \right)^{\frac{1}{\delta}} \tag{4.35}$$

In general the constant density approximation is only valid for quark matter and the corresponding results in this case are given in the main text. However, for neutron stars the corresponding maximum is in general above the Kepler frequency anyway and therefore not physically interesting. Far above the temperature where the maximum is located the high temperature approximation to the bulk viscosity is valid and the boundary $1/\tau_B + 1/\tau_G = 0$ condition yields here

$$\Omega(T) \xrightarrow[T \gg T_{max}]{} \left(\frac{m \left(m+1\right)^{2m-3} \left((2m+1)!!\right)^2}{2\pi \left(2m+3\right) \left(m+2\right)^{2m+2} \left(m-1\right)^{2m}} \cdot \frac{\tilde{W}_m \Lambda_{EW}^4 \Lambda_{QCD}^{\delta-1} R^{5-2m}}{\tilde{J}_m^2 G M^2 T^{\delta}} \right)^{\frac{1}{2m-2}} \tag{4.36}$$

For homogeneous stars the present approximations cover nearly the entire boundary of the instability region. If the star has more than one layer, there may be a second minimum. Depending on the size of the layers here it can be either the bulk viscosity of the second layer that equals the dominant shear viscosity at the minimum, in

which case the above expressions hold, or the bulk viscosities of the different layers are identical $\tau_B^{(i)} = \tau_B^{(o)}$ which yields analogously

$$\Omega_{min}^{(B)} = \left(\left(\frac{m\left(m+1\right)^{2m-3}\left((2m+1)!!\right)^2}{\pi\left(2m+3\right)\left(m-1\right)^{2m}\left(m+2\right)^{2m+2}} \right)^{\delta^{(o)}+\delta^{(i)}} \cdot \left(\frac{m+1}{2}\right)^{2\delta^{(i)}} \frac{\Lambda_{QCD}^{9\delta^{(i)}-\delta^{(o)}} \left(\tilde{V}_m^{(o)}\right)^{\delta^{(i)}} \left(\tilde{W}_m^{(i)}\right)^{\delta^{(o)}}}{\Lambda_{EW}^{4\left(\delta^{(i)}-\delta^{(o)}\right)} G^{\left(\delta^{(o)}+\delta^{(i)}\right)} \tilde{J}_m^{2\left(\delta^{(o)}+\delta^{(i)}\right)}} \cdot \frac{R^{(5-2m)\left(\delta^{(o)}+\delta^{(i)}\right)}}{M^{2\left(\delta^{(o)}+\delta^{(i)}\right)}} \right)^{\frac{1}{2m\left(\delta^{(o)}+\delta^{(i)}\right)-2\delta^{(o)}}} \tag{4.37}$$

and the corresponding temperature is

$$T_{min}^{(B)} = \left(\frac{4}{\left(m+1\right)^2} \cdot \frac{W_m^{(i)} \Lambda_{EW}^8 \Lambda_{QCD}^{\delta^{(o)}+\delta^{(i)}-10}}{V_m^{(o)}} \right)^{\frac{1}{\delta^{(o)}+\delta^{(i)}}} \left(\Omega_{min}^{(B)}\right)^{\frac{2}{\delta^{(o)}+\delta^{(i)}}} \tag{4.38}$$

Low temperature boundary

As is clear from the analytic expressions for the damping times and confirmed by fig. 4.4 at low temperatures shear viscosity damping dominates. Furthermore, in the case of hybrid stars the damping due to hadronic shear viscosity dominates over the quark core. Comparing it with the gravitational time scale yields

$$\Omega\left(T\right) \xrightarrow[T \ll T_{min}]{} 1.12 \frac{\tilde{S}^{\frac{1}{6}} \Lambda_{QCD}^{\frac{7}{9}}}{\tilde{J}^{\frac{1}{3}} G^{\frac{1}{6}} M^{\frac{1}{3}} R^{\frac{1}{2}}} T^{-\frac{5}{18}} \quad \left(\text{NS and SS}\right)$$

where the irrational power arises from the Landau damping of the corresponding interactions that induce shear viscosity. Interestingly this expression depends only mildly on the constant $\tilde{S}$ that encodes the microscopic interaction. This segment of the boundary is important for old stars in binary systems that are spun up by accretion from a companion star and enter the instability region from below

Minimum of the instability region

Since the shear viscosity damping time monotonically increases with temperature whereas the bulk viscosity damping time monotonically decreases at low temperature there is a minimum of the instability boundary given by $\tau_B = \tau_S$. Due to the non-linear frequency dependence of the second order damping times an exact analytic solution is not possible. However, since these minima are located at frequencies far below the Kepler frequency it is according to fig. 4.2 a very good approximation to use the leading order frequency connection $\kappa = \kappa_0$ in which case an analytic solution is possible. For neutron stars it reads

$$\Omega_{min}^{(NS)} \approx 1.06 \frac{\Lambda_{QCD}^{\frac{99}{128}} \tilde{S}^{\frac{9}{64}} \tilde{V}^{\frac{5}{128}}}{R^{\frac{49}{128}} \tilde{J}^{\frac{23}{64}} G^{\frac{23}{128}} M^{\frac{23}{64}} \Lambda_{EW}^{\frac{5}{32}}} \tag{4.39}$$

$$T_{min}^{(NS)} \approx 1.89 \frac{\tilde{S}^{\frac{3}{32}} \Lambda_{QCD}^{\frac{1}{64}} \Lambda_{EW}^{\frac{9}{16}} G^{\frac{3}{64}} \tilde{J}^{\frac{3}{32}} M^{\frac{3}{32}}}{\tilde{V}^{\frac{9}{64}} R^{\frac{27}{64}}} \tag{4.40}$$

Note, the appearance of surprisingly low powers in these expressions. In particular, due to the arising 5/128 power a change of $\tilde{V}$ by an order of magnitude results only in a mild deviation of the minimum frequency of less than 10%, and even a very drastic change by three orders of magnitude does not change the result by more than 30%. Whereas the viscosity constants eqs. (5.7) and (4.28) can vary by many orders of magnitude for different classes of stars with different transport processes as can

be seen from tab. 4.4, they are generically of similar order of magnitude within a given class due to the identical parametric dependence on the microscopic physics. Recall, that the minimum of the instability region is of particular importance for the r-mode analysis since it determines to what frequency r-modes can spin down a star. It is needless to say that such an insensitivity of the minimum frequency on the microscopic physics is more than welcome in the present situation where there are still huge uncertainties on the underlying equation of state and the transport coefficients of dense matter. This presents one of the main results of this article.

In the general case studied in appendix 4.5.1 the $(2m(\delta+\sigma)+2\delta)/\sigma$-th root of the bulk viscosity constants $\tilde{V}_m$ arises in the expression for the minimum frequency eq. (4.31). For short-range (Fermi liquid) interactions the shear viscosity exponent is generically $\sigma = 2$ whereas it reduces to $\sigma = 5/3$ when long-ranged, only Landau-damped (non-Fermi liquid) gauge interactions are present. Since the rate of the weak interactions vanishes in equilibrium and requires phase space both for initial and final state particles in general $\delta \geq 2$. A similar argument should hold for processes mediated by Goldstone bosons in color superconducting phases. Therefore the above root is for all multipoles and corresponding processes higher than 11 so that change of the viscosity constants $\tilde{V}_m$ by an order of magnitude still changes the minimum only by at most $\sim 20\%$, making it very insensitive to them. This extends the finding obtained in an explicit comparison of various different neutron star models in [45] to general forms of matter and damping processes. This insensitivity is particularly interesting since these constants contain the complete dependence on the detailed second order r-mode profiles, so that the minimum frequency is hardly affected by the second order effects. This observation had already been made for the particular neutron star model studied in [43]. A similar statement holds for the dependence on the shear viscosity constants $\tilde{S}_m$, where the corresponding root is at least of 6th order

reached in the limit $\delta \gg \sigma$. The temperature of the minimum is more sensitive to these constants, as likewise observed in [45, 43], since it only involves the $(\sigma + \delta)$-th root.

Finally we give the explicit expression for the minimum frequency of strange stars with the general quark model equation of state eq. (4.1). The parameter dependence of the quark matter viscosity coefficients given in tables 3.1 and 4.3 can be factored out according to

$$\tilde{\Gamma}^{(q)} \equiv \hat{\Gamma}\mu_q^5 \quad , \tilde{\eta}^{(q)} \equiv \hat{\eta}\alpha_s^{-5/3}\mu_q^{14/3} \tag{4.41}$$

where $\hat{\Gamma}$ and $\hat{\eta}$ are pure constants, so that the minimum is located at

$$\Omega_{min}^{(SS)} \approx 2.23 \frac{\hat{\Gamma}^{\frac{5}{56}}\hat{\eta}^{\frac{3}{28}} m_s^{\frac{5}{14}} \mu_q^{\frac{43}{56}}}{G^{\frac{11}{56}}(1-c)^{\frac{5}{28}}\alpha_s^{\frac{5}{28}} R^{\frac{13}{56}} M^{\frac{11}{28}}} \tag{4.42}$$

$$T_{min}^{(SS)} \approx 2.78 \frac{\hat{\eta}^{\frac{3}{14}} G^{\frac{3}{28}} \mu_q^{\frac{1}{28}} (1-c)^{\frac{9}{14}} M^{\frac{3}{14}}}{\hat{\Gamma}^{\frac{9}{28}}\alpha_s^{\frac{5}{14}} m_s^{\frac{9}{7}} R^{\frac{27}{28}}} \tag{4.43}$$

Assuming that eq. (4.1) gives an estimate for the uncertainty in the unknown quark matter equation of state and estimating the uncertainty in the quadratic and quartic parameters m_s and $1 - c$ each by a factor of two and that in the strong coupling α_s generously by an order of magnitude, the minimum could vary here by roughly a factor of two owing to the uncertainty in the unknown microscopic dynamics. As noted before the quark model equation of state is also valid for color superconducting phases [14]. In this case the gap reduces the parameter m_s which would lower the minimum frequency and enlarge the instability region.

Intermediate boundary

Above the minimum the damping is dominated by the bulk viscosity and below its maximum it can be approximated by the asymptotic low temperature form eq. (4.25). The semi-analytic result to next-to leading order in Ω is given in the appendix, but because of the small effect of the next-to-leading order corrections of the oscillation frequency on the instability regions, observed above, we can simply neglect these and obtain

$$\Omega\left(T\right) \xrightarrow[T\ll T_{max}]{T\gg T_{min}} 0.360 \frac{\tilde{V}^{\frac{1}{4}} \Lambda_{QCD}^{\frac{9}{4}} R^{\frac{1}{4}}}{\tilde{J}^{\frac{1}{2}} \Lambda_{EW} G^{\frac{1}{4}} M^{\frac{1}{2}}} \cdot \begin{cases} \left(\frac{T}{\Lambda_{QCD}}\right)^{\frac{3}{2}} & \text{(NS)} \\ \left(\frac{T}{\Lambda_{QCD}}\right)^{\frac{1}{2}} & \text{(SS)} \end{cases}$$

This part of the instability boundary is important for the spin down of young compact stars since it determines where they hit the instability region during their initial fast cooling phase.

Maximum of the instability region for strange stars

Due to the resonant form of the bulk viscosity eq. (3.26) whose maximum eq. (3.27) translates into a minimum of the corresponding damping time, the instability region features a maximum if the corresponding frequency is below the Kepler frequency or otherwise splits into two parts. Since there is no analytic expression for the damping time in the vicinity of the maximum there is no general expression for the maximum. Yet, for hadronic matter the corresponding maximum frequency is usually above the Kepler frequency anyway so it is not relevant for physical applications. In contrast, for strange stars, where the maximum is generally below the Kepler frequency and important for the r-mode analysis, the density profile varies only mildly and can be approximated by a uniform density. In this case a general analytic expression for the maximum of the instability region is given in eqs. (4.34, 4.35) in appendix 4.5.1 and

reduces using the susceptibilities in tab. 4.2 to

$$\Omega_{max}^{(SS)} \approx 0.434 \frac{m_s^{\frac{4}{3}} R^{\frac{1}{3}}}{(1-c)^{\frac{1}{3}} G^{\frac{1}{3}} M^{\frac{2}{3}}} \tag{4.44}$$

$$T_{max}^{(SS)} \approx 0.210 \frac{(1-c)^{\frac{1}{3}} m_s^{\frac{2}{3}} R^{\frac{1}{6}}}{\hat{\Gamma}^{\frac{1}{2}} G^{\frac{1}{6}} \mu_q^{\frac{3}{2}} M^{\frac{1}{3}}} \tag{4.45}$$

where the tiny second order corrections to the oscillation frequency, cf. fig. 4.2, were neglected in this case. Note that analogous to the expression for the maximum of the viscosity of quark matter given in [81] the chemical potential drops out and therefore there is no ambiguity where to evaluate the susceptibilities in case the density distribution of the considered star model is not entirely constant. This gives for the dimensionless ratio

$$\frac{\Omega_{max}^{(SS)}}{\Omega_K} \approx 1.03 \frac{m_{150}^{\frac{4}{3}} R_{10}^{\frac{11}{6}}}{(1-c)^{\frac{1}{3}} M_{1.4}^{\frac{7}{6}}} \tag{4.46}$$

where m_{150}, $M_{1.4}$ and R_{10} are the effective strange quark mass in units of 150 MeV, the stars mass in units of $1.4\,M_\odot$ and the radius in units of 10 km, respectively.

Whereas the dependence on the parameter c, which in the perturbative regime is positive and thereby increases the maximum frequency, is comparatively mild, the dependence on the effective strange quark mass is significant and can within the probable uncertainty region $100\,\mathrm{MeV} \lesssim m_s \lesssim 200\,\mathrm{MeV}$ strongly change the position of the maximum frequency from values considerably below to values above the Kepler frequency. For superconducting matter the gap can reduce the effective parameter m_s. Whereas the maximum frequency of massive stars can be significantly lower, the radii of sufficiently massive strange stars do not vary much with mass along a mass-radius curve so that the dependence on the radius is mild despite the arising high

power. To judge the implicit dependence of the masses and radii on the equation of state it is useful to recall that the solution of the TOV equations for a uniform density star exhibits scaling with the bag constant $R/R_0, M/M_0 \sim \sqrt{B_0/B}$ [124]. Despite the uniform density approximation, the analytic result eq. (4.46) for the maximum, given in tab. 4.4, agrees nicely with the numeric results for the considered strange star models. The above expression can also be applied to the corresponding analysis of Jaikumar, et. al. [9]. Using their lower strange quark mass $m_s = 100$ MeV as well as their slightly smaller radius and taking into account that these authors erroneously used the angular velocity in the inertial frame to evaluate the bulk viscosity yields $\Omega_{max}^{(SS)}/\Omega_K \approx 0.47$ in very good agreement with the plot of the exclusion region shown in their fig. 4. When employing the proper angular velocity in the rotating frame, eq. (4.46), gives instead the corrected result $\Omega_{max}^{(SS)}/\Omega_K \approx 0.59$.

The analytic results section 4.5.1 to some extent also apply to the maxima of the instability regions of hybrid stars but in this case the agreement is less precise since the density profile of their quark core features a more pronounced radial dependence.

High temperature boundary

For completeness we also give the high temperature part of the boundary.

$$\Omega\left(T\right) \xrightarrow[T\gg T_{max}]{} 8.66\times 10^{-2}\frac{\tilde{W}^{\frac{1}{2}}\Lambda_{EW}^{2}R^{\frac{1}{2}}}{\tilde{J}\Lambda_{QCD}^{\frac{1}{2}}G^{\frac{1}{2}}M}\cdot\begin{cases}\left(\frac{\Lambda_{QCD}}{T}\right)^{3} & \text{(NS)}\\ \frac{\Lambda_{QCD}}{T} & \text{(SS)}\end{cases}$$

Due to the resonant behavior of the bulk viscosity which decreases again at large temperatures, the r-mode is unstable for all forms of matter at large temperatures above the corresponding boundary of the shell with the largest resonance temperature eq. (3.27). This part could be less relevant for the r-mode evolution since stars cool very fast initially and could leave this region before the r-mode can develop.

General properties of the analytic analysis

Finally let us note a few generic properties of these analytic results. Since the mass appears in the denominator in all these expressions, an increase of the mass of the star increases the instability region and moves it uniformly downward and slightly to the right in a $T - \Omega$-plot. The dependence on the radius is less uniform, but in general these expressions are less sensitive to the radius than to the mass of the star. Furthermore for a given equation of state the radius of a star varies very little for masses of 1 to $2\,M_\odot$. As already noted, the dependence of the minima of the instability region on the viscosity parameters is extremely mild. Due to the arising small powers $O\,(1/10)$ even a large variation of the viscosity parameters by three orders of magnitude within the set of possible equations of state for a given class of stars, like e.g. pure neutron stars would not change the minimum by more than a factor of two. In contrast the dependence of the maxima on the viscosity parameters is far more pronounced and as discussed above changes by more than a factor of two are here easily possible.

4.5.2 Numeric results

Let us now discuss the numeric results for the exclusion regions and compare them to the semi-analytic expressions obtained in the last section in order to assess the quality of the latter. Fig. 4.5 compares the expressions for particular segments of the instability region and for the extrema to the numeric solution. The left panel shows the results for a standard $1.4\,M_\odot$ neutron star model (solid) and a corresponding strange star model (dotted). The thick curves show the numeric results and the thin curves the analytic approximations and the dots denote the minima. Since we neglect the contribution from the neutron star crust there is only a single shell in each case. As can be seen, except for the regions around the extrema, the analytic

expressions for the different segments approximate the boundary of the instability region extremely well and are mostly hidden underneath the numeric curves. Yet, the extrema are in turn well described by the corresponding analytic expressions. As noted in [44, 117, 9], due to the resonant form of the bulk viscosity there is a stability window around 10^9 K where strange stars are not unstable against r-modes up to large frequencies. For the considered strange star model the maximum of the instability region is above the Kepler frequency so that two separate regions appear, but as discussed before the position of the maximum depends on the particular microscopic parameters. Due to the same qualitative resonant structure of the bulk viscosity there is also a second instability region at high temperatures $\gtrsim 10^{11}$ K for neutron stars that has previously been neglected due to the employed low temperature approximation to the hadronic bulk viscosity [8, 7]. Although the r-mode is initially unstable the naive expectation is that this should be irrelevant for the spin-down evolution since the star cools extremely fast at such high temperatures and might leave this region before r-modes can develop. Yet, since the interior of the star is initially opaque to neutrinos and the cooling is delayed this is not entirely clear and requires further study.

On the right panel of fig. 4.5 the comparison for the $1.4\,M_\odot$ hybrid star model is shown. Here there are contributions from the different layers, but strikingly the analytic approximation works even in this more complicated case. This plot shows nicely the generic structure of the boundary of the instability region, discussed in the previous subsection, when several shells are present that feature qualitatively different damping mechanisms. Around its resonant temperature the bulk viscosity damping mechanism of a given shell in general clearly dominates over those of the other shells. If the resonant temperatures of the different bulk viscosities are sufficiently separated there are several maxima, that define corresponding stability windows. Below each

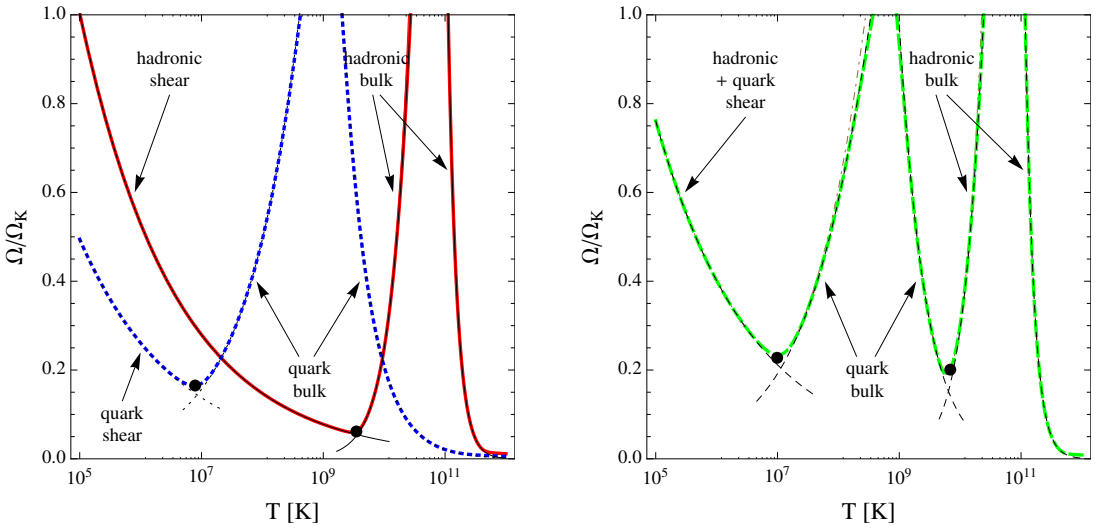

Figure 4.5: Comparison of the numeric results for the instability region (thick lines) with the various approximate semi-analytic expressions (thin lines and dots) presented in the text for the different classes of compacts stars. The dots present the results for the extrema and the thin lines which are valid away from the extrema represent the corresponding analytic results taking into account only the contribution from the dominant process and shell in the respective region. *Left panel:* Instability regions for the $1.4\,M_\odot$ neutron star (solid) and strange star model (dotted). *Right panel:* Same for the $1.4\,M_\odot$ hybrid star model. The thin dot-dashed curve on the right panel which deviates slightly close to the maximum is the leading order result without the frequency corrections in fig. 4.2, whereas the corresponding curves are indistinguishable on the left panel. Note that here in the following where the ratio Ω/Ω_K is plotted this ratio is taken with the respective Kepler angular frequency for each star model, see table 4.1, so that the same value of Ω/Ω_K corresponds to a different value of Ω for different curves.

of these maxima there is a minimum where a dominant mechanism is replaced by the next. However, in case two resonant temperatures are too close or a shell is too small to have a sizable impact, individual stability windows can be fully or partly washed out. We discuss such cases below.

Fig. 4.6 shows the exclusion region for the standard $1.4\,M_\odot$ neutron star model compared to approximations used previously in the literature. The solid curve shows our new result with shear viscosity due to the dominant Landau-damped lepton scat-

tering [121] and bulk viscosity due to modified Urca processes based on susceptibilities for interacting matter [81]. The dotted curve shows the exclusion region when using the result for the shear viscosity from the fit in [8] to the standard low density ($\lesssim n_0$) data from hadron-hadron-scattering given in [10]. Extrapolating this fit to high densities relevant for neutron stars overestimates the viscosity compared to its actual, subleading size [121], leading to the smaller exclusion region. The dashed curve shows the result when employing the previously used expression for the bulk viscosity [8, 7] which employs susceptibilities in the approximation of an ideal hadron gas, see table 4.2. It is again the insensitivity to the viscosity parameter $\tilde{V}$ discussed in the previous subsection that is responsible for the fact that these corrections, which change the damping time by more than an order of magnitude, have only such a mild effect on the exclusion region and the minimum eq. (4.39). It is interesting that the effect of the interactions is opposite to that of the 2nd order Ω-corrections [43]. The combined curve formed by the dotted and the dashed segment is the exclusion region that had previously been studied in the literature. As can be seen the combined effect of both corrections is to move the instability region to lower temperatures so that it extends to roughly 10^5 K. This is relevant for old stars at low temperatures that are spun up by accretion since the r-mode becomes unstable already at lower frequencies.

The left panel of fig. 4.7 compares the instability regions of the different $1.4\,M_\odot$ star models considered here and also includes the analytic results for the extrema. The minima in these plots corresponds to the maxima where two damping mechanisms cross in fig. 4.4 whereas the maxima in fig. 4.7 correspond to the minima in fig. 4.4. As can be seen the instability regions of the hybrid stars interpolate between the neutron star and the strange star curve as the size of the quark core increases, even though all these curves are based on rather different equations of state distinguished by the interaction parameter c, see table 4.1. The right panel of fig. 4.7 shows the

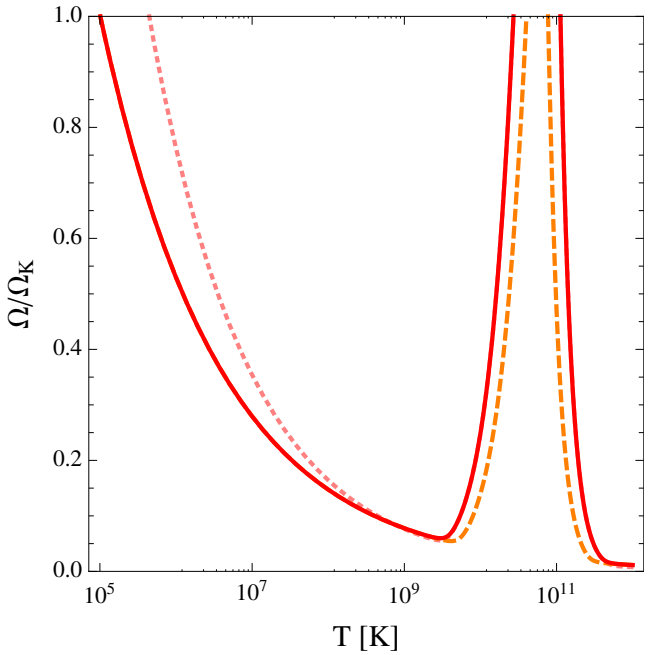

Figure 4.6: Modification of the instability region of a $1.4\,M_\odot$ neutron star due to improved approximations for the microscopic transport properties. The solid curve shows the standard neutron star model with shear viscosity due to the dominant Landau-damped lepton scattering and bulk viscosity based on the proper susceptibilities for interacting matter (as all other neutron star results in this work). The dashed curve shows the result when using the fit given in [8] to the density data $\lesssim n_0$ for the shear viscosity from hadron-hadron scattering obtained in [10]. The dotted line shows the result when employing the previously used expression neglecting interactions to the susceptibilities contributing to the bulk viscosity [8, 7].

instability regions for the $2\,M_\odot$ models discussed in this work. As has already been observed as a generic feature of the analytic analysis, the r-mode instability in heavy stars is enhanced and the boundary of the instability region moves slightly to lower frequencies. As predicted by the mass dependences of the analytic expressions this is most pronounced in the vicinity of the maxima and milder in the vicinity of the minima. The approximate analytic results for the maxima deviate slightly from the maxima of the numerical curves. The reason for this is that the uniform density approximation is not justified in this case due to the strong radial dependence of the

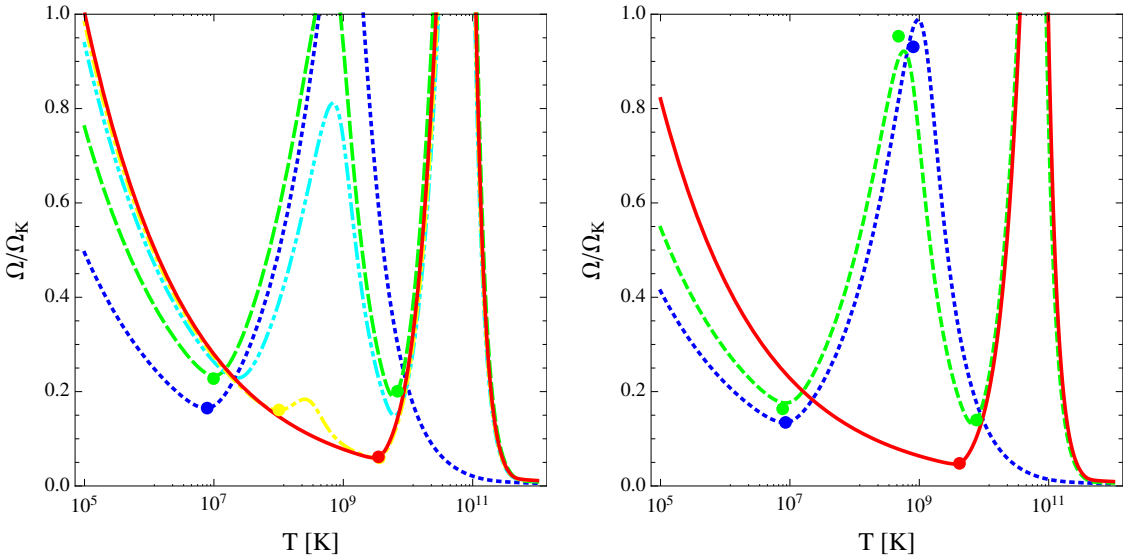

Figure 4.7: Instability regions for the different star models considered in this work. Shown are neutron star models with APR equation of state (solid), hybrid stars with a small (dot-dashed), a medium (dot-dot-dashed) and a large quark matter core (dashed) and strange star models (dotted) with an ideal gas equation of state. The dots show again the analytic estimates for the extrema. *Left panel:* $1.4\,M_\odot$ stars. *Right panel:* $2\,M_\odot$ stars, for which for the considered equations of state stars with smaller quark cores could not be found.

density profiles, see fig. 4.1.

Fig. 4.8 shows the instability region for an ultra-heavy neutron star $M \approx 2.2\,M_\odot$ denoted by the solid curve. Here, the instability region has grown to the point that the lower and the upper part are about to merge. For this star the densities that are reached are high enough that direct Urca processes are kinematically allowed within an inner core with radius of roughly $R/2$. The enhanced damping due to direct Urca bulk viscosity in the inner core leads to a notch at the right side of the instability region, as also found in [125]. Yet, the modification is rather mild in this case: the dashed curve shows the same star model when direct Urca processes are artificially suppressed. In the opposite extreme when direct Urca processes are artificially allowed in the entire core, shown by the dotted curve, the enhanced damping does lead to a significant change of the instability region. Moreover, the frequency of the

minimum of the instability region increases. Due to the resonant form of the bulk viscosity, however, the instability region does not uniformly shrink over the whole temperature range where bulk viscosity dominates, but the stability window moves to lower temperatures leaving the r-mode unstable at higher temperatures where it is otherwise stable in the presence of modified Urca processes. The temperature scales of the corresponding stability windows agree with the temperature scales of the resonant maximum of the bulk viscosity, see [81]. Direct Urca processes are very sensitive to the proton fraction of dense matter. Whereas the required fraction is roughly 14% in the case of the APR equation of state, reached at relatively high densities $\gtrsim 5n_0$, this could be different for other equations of state. In a case where the direct Urca core is larger but a modified Urca shell is still present so that both of them have a sizeable volume fraction, their combined damping could lead to a larger stability window, yet still at parametrically larger temperatures than the stability window of strange stars.

Fig. 4.9 shows the result for the higher multipoles for the different $1.4\,M_\odot$ star models. As can be seen, the right boundaries of the instability regions for the higher multipoles are extremely close to the boundary of the fundamental $m = 2$ mode. Correspondingly these modes could easily be excited once the evolution of a star enters the instability region. Each mode that is triggered would lead to a further enhancement of the spindown of the star and could change the evolution. This could be particularly relevant for young neutron stars that enter the instability region at high temperatures when the cooling is still fast but there are no strong reheating mechanisms which could prevent the star from substantially penetrating the instability region.

Fig. 4.10 finally compares our numeric results to astrophysical data. Although the rotation frequencies of pulsars are known to high accuracy, the relevant core

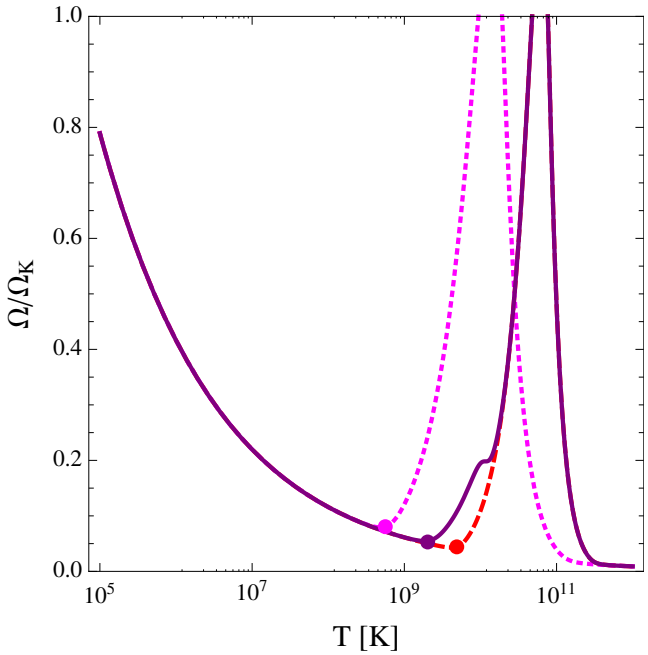

Figure 4.8: The instability region with direct Urca interactions is shown for the 2.21 $M_\odot$ maximum mass neutron star model (solid curve), where direct Urca processes are allowed in the inner core but only modified Urca processes in the layer surrounding it. For comparison the instability region is shown when direct Urca reactions are artificially suppressed (dashed curve) as well as when they are artificially allowed in the entire hadronic core (dotted curve).

temperatures are not known for most pulsars and involve large uncertainties even for those stars where estimates are available. The reason is that the temperature of the surface is indirectly inferred from the data and it is necessary to abstract from it the core temperature via models. Such an analysis has been performed for two low mass X-ray binary systems Aql X-1 and SAX J1808.4-3658 [126], where the pulsars accrete matter from companion stars. The horizontal lines give an optimistic estimate for the uncertainty of the temperature. As can be seen these data points are well within the instability region of neutron stars. This holds in particular for the faster one of the two pulsars, Aql X-1, which is right in the middle. Our analysis shows this statement cannot be undermined by the unknown equation of state. So if r-modes would spin

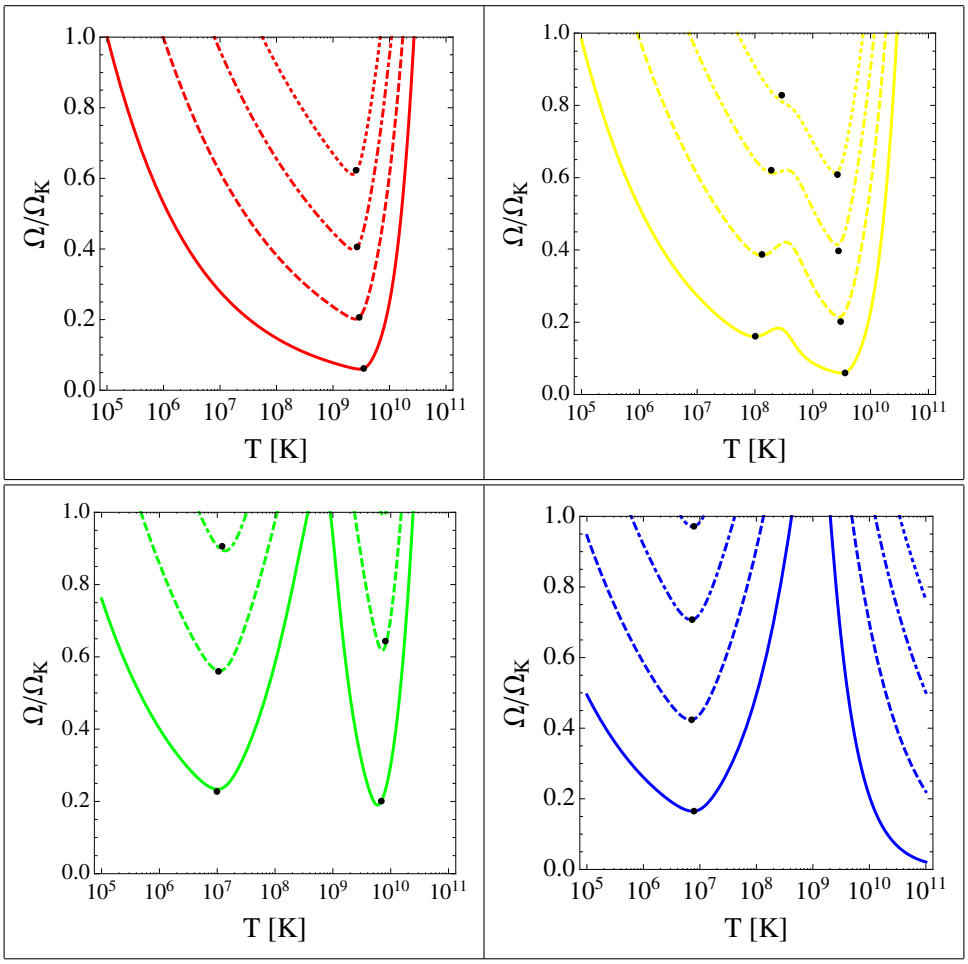

Figure 4.9: Instability regions for the first four multipole r-modes ($m = 2$ to 5) of the different $1.4\,M_\odot$ star models (top, left: neutron star; top, right: hybrid star, small quark core; bottom, left: hybrid star, large quark core; bottom right: strange star). The minima from eqs. (4.31) & (4.32), the second minima of the large core hybrid star from eqs. (4.37) & (4.38) and the maxima from eqs. (4.34) & (4.35) are denoted by the dots. For higher multipoles the size of the instability regions decreases and they move to higher rotation frequencies, so that all modes with $m \geq 7$ are entirely stable in the physical range of frequencies. In particular in the cases of neutron and hybrid stars the right boundaries of the instability regions of the higher multipoles are very close to the fundamental $m = 2$ mode, so that several modes can easily be excited if the evolution significantly enters the fundamental instability region.

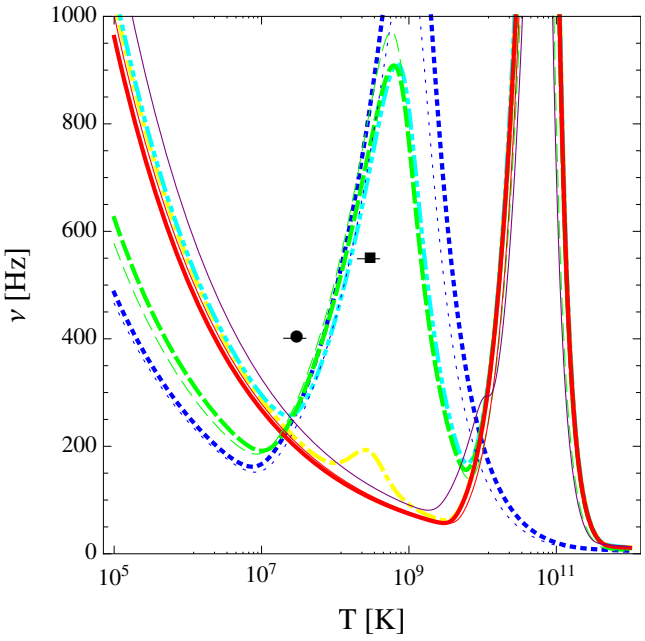

Figure 4.10: Comparison of the instability regions in absolute frequencies for the different star models considered in this work with the two low mass X-ray binaries Aql X-1 (filled square) and SAX J1808.4-3658 (open circle). The horizontal bar gives a partial measure for the error within the model computations which should be larger due to uncontrolled assumptions that are not considered in its size.

down stars so fast that the stars would leave the unstable region on time scales short compared to astrophysical ones these stars could not be pure neutron stars and would require some form of enhanced damping. Yet, in the case of strange stars and hybrid stars with a sufficiently large quark core, the data points are close to the boundary of the corresponding stability window and would be compatible in such a scenario[3]. As our results show, hybrid stars with a small quark core or neutron stars with enhanced hadronic direct Urca damping, in contrast, would not be sufficient.

[3]A potential problem with such an explanation of the data would be the observation of a very fast and at the same time very cold pulsar, since, after the accretion stops, stars within the stability window would re-enter the instability region due to cooling and correspondingly would have to spin down to a fraction of their Kepler frequency.

4.6 Conclusions

Using general expressions for the viscosities of dense matter we have derived semi-analytic results for the damping times of small amplitude r-mode oscillations and the boundary of the instability region. Our results show that the boundary of the instability region and in particular its minimum, which determines to what extent r-modes can spin down a fast star, are extremely insensitive to the quantitative details of the microscopic interactions that induce viscous damping. However, the instability regions can nevertheless effectively discriminate between qualitatively different classes of stars. In particular strange stars and hybrid stars with sufficiently large quark cores feature a stability window that cannot be reproduced with standard neutron stars without some admixture of exotic matter that provides enhanced damping. We find that the presence of some form of exotic matter does not automatically lead to a stability window since the instability region of hybrid stars with a sufficiently small quark core is almost indistinguishable from that of a neutron star. Similarly, the presence of neutron matter with direct Urca interactions will in most cases not considerably change the instability region. However, due to the demonstrated insensitivity of the instability regions to quantitative microscopic details, the clear determination of a very fast pulsar with $\Omega > 300$ Hz in the temperature range around 10^9 K could provide a convincing signature for some exotic form of matter. What remains to be shown in order to transform this into a strict signature is that the crust does not dominate the damping, and that r-modes do not saturate at amplitudes that are so small that the spindown takes billions of years in which case the instability region would not really present a no-go area. The second point requires a thorough understanding of the dynamical evolution of compact stars and a step towards this goal is taken in the next chapter where we show that the large amplitude behavior of the

bulk viscosity can saturate r-modes at amplitudes that are large enough for a fast spindown.

Chapter 5

Large amplitude saturation of the r-modes

5.1 Introduction

In the previous chapter we analyzed the instability regions of the r-mode oscillations. The main result of that chapter was that these regions vary greatly between qualitatively different classes of stars containing distinct phases of strongly interacting matter, but are extremely insensitive to unknown quantitative details of the equation of state and the transport properties within a given class. Therefore, a proper understanding of the r-mode dynamics could in the future provide robust signatures for the presence of exotic phases in compact stars.

Since exponentially growing r-modes will destroy the star if their growth is not stopped by some non-linear mechanism, the fact that fast spinning compact stars are observed suggests that such a non-linear damping mechanism is indeed present. More importantly, even if stopped at a finite amplitude, r-modes still strongly emit gravitational waves and could provide an extremely efficient mechanism for the spin-down of compact stars [50] and an interesting signal for terrestrial gravitational wave

detectors. Spin-down due to r-modes could explain the observed absence of fast-spinning young stars despite the fact that their creation during a supernova could naturally lead to a fast spinning remnant. For spin-down via r-modes the size of the saturation amplitude is crucial. If the amplitude α is too low, it takes too long to spin down the star; if the amplitude is too large, $\alpha > O(1)$, the r-mode would disrupt the star's structure, and even before this point the r-mode could be destroyed. If the r-mode amplitude saturates at an intermediate value, a fast spin-down is possible. Previously, various mechanisms for the large-amplitude behavior of r-modes have been suggested [105]. They include the coupling between different modes [108, 127], the decay into daughter modes and the eventual transformation of the r-mode energy into differential rotation [106, 107], friction between different layers of the star, and surface effects in the star's crust [123].

In this chapter, which is based on Ref. [128], we study an alternative mechanism that does not involve such complicated non-linear dynamical or structural effects. It is present already in a standard hydrodynamical description and exploits the fact that at large amplitudes the damping due to bulk viscosity increases dramatically with the amplitude [81, 79, 78, 129]. In this suprathermal regime, where the deviation from chemical equilibrium μ_Δ fulfills $\mu_\Delta \gtrsim T$, the viscous damping could overcome the initial gravitational instability and saturate the r-mode. However, as shown in chapter 3, the bulk viscosity has a maximum as a function of the amplitude and decreases again at even larger amplitudes. If the amplitude exceeds this critical value then the r-mode growth cannot be stopped by viscous damping and other non-linear dynamic effects [105, 106, 107, 127, 108] are required to saturate it. Nevertheless, we find that over a significant region of the parameter space the suprathermal enhancement is indeed sufficient to saturate the r-mode at a finite amplitude and the r-mode can then efficiently spin down the star. This is in contrast to certain non-linear hydrodynamical

effects where the r-mode could completely decay [107] and would not be able to cause an appreciable spin-down of the star.

For r-modes with amplitudes sufficiently below the maximum, we give general analytic expressions for the suprathermal damping time valid for various forms of dense matter. For r-modes with arbitrary amplitudes, where an analytic evaluation is not possible, we give a general expression for the bulk viscosity damping time that includes the complete parameter dependence required for the analysis of the star's evolution, encoded in a two-parameter function that can be numerically computed and tabulated for different star models. This offers an explicit framework for the consistent inclusion of the r-mode saturation into a star evolution analysis and supersedes previously necessary model assumptions [50]. We will analyze the same star models as in chapter 4. These include neutron stars, hybrid stars and strange stars. In addition, motivated by the recent observation of a $2M_\odot$ star [4, 54] we only study models that also yield heavy stars. Moreover, similar to the analytic results in chapter 3, we give approximate analytic expressions for the maximum saturation amplitude that exhibit the detailed parameter dependence on the equation of state and the transport properties of dense matter. In addition to the standard fundamental $m=2$ r-mode we also study the saturation of higher multipoles and find that they saturate at significantly lower amplitudes. In this work we concentrate on the effects of suprathermal bulk viscosity on the damping times (see chapter 4) and the suitably extended concept of the instability regions.

5.2 Bulk viscosity damping time scale

In the previous chapter we gave the expressions for the bulk viscosity damping time scales in the small amplitude limit. Here we give the general results for the bulk

viscosity time scales which are valid in the large amplitude limit as well. As we saw in the last chapter, the bulk viscosity damping time is given by [43]

$$\frac{1}{\tau_B} = \frac{\kappa^2}{\alpha^2 \tilde{J}_m M R^2} \int d^3x \left|\frac{\Delta\rho}{\bar{\rho}}\right|^2 \zeta\left(\left|\frac{\Delta\rho}{\bar{\rho}}\right|^2\right) \tag{5.1}$$

Using the general expressions for the bulk viscosity eqs. (3.34) and (3.35) and expressing the fluctuation in the conserved energy density $\Delta\rho/\bar{\rho}$ by the same fluctuation of the baryon density $\Delta n/\bar{n}$, gives for the damping time the general expression

$$\frac{1}{\tau_B} = \frac{4\pi\Omega^3}{(m+1)^2 \tilde{J}_m M R^2 \kappa} \sum_l \mathcal{T}^{(l)}(a,b)\,. \tag{5.2}$$

in terms of integrals over the individual shells. Defining the reduced density oscillation

$$\left(\frac{\Delta n}{\bar{n}}\right)_{\text{red.}} \equiv \frac{(m+1)\,\kappa(\Omega)}{2\alpha\Omega^2} \frac{\Delta n}{\bar{n}} \tag{5.3}$$

we can write

$$\begin{aligned} \mathcal{T}^{(l)}(a,b) \equiv & \int_{R_i^{(l)}}^{R_o^{(l)}} dr\, r^2 \int d\theta \sin\theta \left|\left(\frac{\Delta n}{\bar{n}}\right)_{\text{red.}}(r,\theta)\right|^2 \frac{C(r)^2}{B(r)} \\ & \cdot \tilde{\mathcal{I}}\left(aC(r)B(r)^{1/\delta}\tilde{\Gamma}(r)^{1/\delta}\left|\left(\frac{\Delta n}{\bar{n}}\right)_{\text{red.}}(r,\theta)\right|,\, bB(r)\tilde{\Gamma}(r)\right) \end{aligned} \tag{5.4}$$

depending on only two independent parameters

$$a \equiv \frac{\kappa_0 \alpha \Omega^2}{\kappa \omega^{1/\delta}} = \frac{2\alpha \Omega^{(2\delta-1)/\delta}}{(m+1)\,\kappa^{(\delta+1)/\delta}}$$
$$b \equiv \frac{T^\delta}{\omega} = \frac{T^\delta}{\kappa \Omega}$$

Note that in eq. (5.4) all local quantities can have different functional forms in different shells, as given in tables 4.2 and 3.1, but to make the expression readable we do not show the explicit suffixes (l). Whereas strange stars are basically homogeneous and consist of a single phase, the crust of neutron and hybrid stars is extremely inhomogeneous and complicated. Although there are no free protons and thereby no Urca processes, the ultra-heavy nuclei present in the inner crust as well as the clusters in potential pasta phases still feature analogous beta-processes. Since oscillations likewise push the system out of beta-equilibrium an analogous suprathermal enhancement of the bulk viscosity contribution from these phases is expected. However, there are to our knowledge no results for the bulk viscosity in the inner crust, yet [130]. Therefore we will in our numeric results given below neglect the contribution from the crust and only include the contribution from the core. The core does not have a sharply-defined boundary: we chose it conventionally to be at baryon density $n_0/4$ corresponding to the lowest point in the APR table, but check the dependence on this choice.

5.2.1 Approximate limits of the bulk viscosity damping time

In the subthermal regime $\mu_\Delta \ll T$ the bulk viscosity eq. (3.26) is independent of the r-mode amplitude, so the angular integral in eq. (5.1) is trivial. The damping time in the subthermal regime is then given by

$$\frac{1}{\tau_B^<} = \frac{16m}{(2m+3)(m+1)^5\kappa}\frac{R^5\Omega^3}{\tilde{J}_m M}\sum_l \mathcal{T}_m^{<(l)}\Big(\frac{T^\delta}{\kappa\Omega}\Big) \tag{5.5}$$

in terms of the one dimensional radial integral

$$\mathcal{T}_m^{<(l)}(b) \equiv \frac{b}{R^3}\int_{R_i^{(l)}}^{R_o^{(l)}} dr\, r^2 \frac{A^2C^2\tilde{\Gamma}}{1+\tilde{\Gamma}^2B^2b^2}\left(\Big(\frac{r}{R}\Big)^{m+1} + \delta\Phi_0\right)^2$$

This expression was used to study the small amplitude instability regions in chapter 4. Here we want to study the large-amplitude saturation and therefore it is useful to obtain an analytic expression that includes the large-amplitude enhancement of the bulk viscosity. In the intermediate, linear regime and for $f \ll 1$ the general analytic approximation for the bulk viscosity eq. (3.30) is valid. Since this local condition has to be fulfilled everywhere in the star, the global parameters a and b must be smaller than certain bounds that are determined by the particular properties of the considered stars. We recall from chapter 3 that the approximation is particularly useful for hadronic matter with modified Urca processes where it covers almost the entire range of physical local density amplitudes at millisecond frequencies. A plot of the regions of validity of the individual analytic approximations of the bulk viscosity for different forms of matter is given in [82]. Analogous to the low temperature/high frequency approximation in the subthermal regime eq. (5.5), in the intermediate, linear regime an explicit evaluation is possible. With the analytic expression for the bulk viscosity eq. (3.30) the angular integrals over the spherical harmonics arising in the r-mode profile take the form

$$\int d\Omega_{\theta\phi}\left|Y_{m+1}^m(\theta,\phi)\right|^{2n} = \frac{4\pi\,(2n-1)!!(m\,n)!}{(2(m+1)n+1)!!}\Big(\frac{(2m+3)!!}{4\pi\,m!}\Big)^n$$

and this yields a result that apart from the evaluation of the remaining radial integrals is analytic (see also [79, 80])

$$\frac{1}{\tau_B^{\sim}} = \frac{16\,(2m+1)!!\Lambda_{QCD}^{9-\delta}R^5T^\delta\Omega^2}{(m+1)^5(m-1)!\kappa^2\tilde{J}_m\Lambda_{EW}^4M}\sum_{j=0}^{N}\frac{((2j+1)!!)^2(m(j+1))!\chi_j\tilde{V}_{m,j}}{(j+1)!\,(2(m+1)(j+1)+1)!!} \cdot\left(\frac{2m\,(2m+1)!!}{\pi\,(m+1)^5\,m!\kappa^2}\frac{\Lambda_{QCD}^2R^4\alpha^2\Omega^4}{T^2}\right)^j \tag{5.6}$$

The dependence on all local parameters, like the equation of state, the weak rate, the density dependence of the particular star and its r-mode profile is contained in a few dimensionless radial integral constants (Λ_{EW} is a typical electroweak scale)

$$\tilde{V}_{m,j} \equiv \frac{\Lambda_{EW}^4}{\Lambda_{QCD}^{7-\delta+2(j+1)}R^3} \cdot\int_0^{\mathcal{R}}dr\,r^2\tilde{\Gamma}(r)\left(A(r)\,C(r)\left(\left(\frac{r}{R}\right)^{m+1}+\delta\Phi_0(r)\right)\right)^{2(j+1)} \tag{5.7}$$

but the dependence on the parameters of the r-mode evolution Ω, α and T is entirely explicit in eq. (5.6). The $j=0$ term in eq. (5.6) is precisely the approximate subthermal result eq. (5.5) in the considered approximation. The constants $\tilde{V}_j \equiv \tilde{V}_{2,j}$ for the fundamental r-mode are given for several stars in table 5.1. Although these parameters can vary significantly for different stars, it is quite striking that as far as the bulk viscosity is concerned, the complex details of the individual stars are encoded in a few constants. Note in particular that the parametric form eq. (5.6) remains valid for the full second order r-mode expression and only the constants eq. (5.7) are changed. At sufficiently large amplitudes the largest power in the sum in eq. (5.6) dominates and due to the connection $\delta=2N$ the bulk viscosity damping time becomes temperature independent in this approximation. Note also that the integrals $\tilde{V}_{m,N}$, as well as the general expression eq. (5.4) feature an extremely pronounced radial dependence, both due to the explicit radial dependence and the radial dependence of the inverse squared

speed of sound A, that strongly weights the outer parts of the star.

star model	shell	$\tilde{V}_0$	$\tilde{V}_1$	$\tilde{V}_2$	$\tilde{V}_3$	$\alpha_{sat}\,(\Omega_K)$
NS $1.4\,M_\odot$	core	1.31×10^{-3}	4.24×10^{-3}	2.02×10^{-2}	0.105	3.68
NS $1.4\,M_\odot$ gas		1.28×10^{-4}	5.52×10^{-5}	3.88×10^{-5}	3.03×10^{-5}	14.3
NS $2.0\,M_\odot$		1.16×10^{-3}	4.92×10^{-3}	3.25×10^{-2}	0.238	2.52
NS $2.21\,M_\odot$	d.U. core	1.16×10^{-8}	7.24×10^{-12}	5.39×10^{-15}	–	–
	m.U. core	9.34×10^{-4}	4.42×10^{-3}	3.39×10^{-2}	0.288	2.60
SS eq. (4.1)	all	$\frac{\Lambda_{EW}^4\hat{\Gamma}m_s^4\mu_q^3}{9\Lambda_{QCD}^7(1-c)^2}$	$\frac{\Lambda_{EW}^4\hat{\Gamma}m_s^8\mu_q}{15\Lambda_{QCD}^9(1-c)^4}$	–	–	eq. (5.10)
SS $1.4\,M_\odot$		3.53×10^{-10}	1.24×10^{-12}	–	–	1.16
SS $2.0\,M_\odot$		3.58×10^{-10}	9.70×10^{-13}	–	–	1.56
HS $1.4\,M_\odot$	quark core	1.38×10^{-10}	1.75×10^{-13}	–	–	2.25
	hadr. core	1.39×10^{-3}	4.70×10^{-3}	2.23×10^{-2}	0.116	3.66
HS $2.0\,M_\odot$	quark core	3.76×10^{-10}	7.75×10^{-13}	–	–	1.59
	hadr. core	1.07×10^{-3}	4.12×10^{-3}	2.31×10^{-2}	0.134	2.94

Table 5.1: Radial integral parameters and static saturation amplitude of a $m=2$ r-mode for the stars considered in this work. The constant $\tilde{J}$, $\tilde{S}$ and $\tilde{V}_i$ are given by eqs. (4.18), (4.20) and (5.7), respectively, using the generic normalization scales $\Lambda_{QCD}=1$ GeV and $\Lambda_{EW}=100$ GeV. Note that the subthermal parameter $\tilde{V}_0$ corresponds to $\tilde{V}$ in [15] where the subscript was omitted for simplicity and the strange star expressions are given to leading order in m_s/μ.

5.2.2 Results for the damping times

Using the expressions for the microscopic parameters given in tables 4.2 and 3.1 and the general expressions for the r-mode growth and damping time scales, eqs. (4.17), (4.19) and (5.2), we obtain the gravitational and viscosity time scales as a function of their dependent macroscopic parameters. These are given in fig. 5.1 for the cases of a neutron star with damping due to modified Urca reactions (left panel) and a strange star (right panel) by the solid lines as a function of temperature and for different amplitudes ranging from top to bottom from the subthermal result at infinitesimal amplitude to the extreme case $\alpha = 10$.

At sufficiently low temperature the strong increase of the bulk viscosity with the (local) amplitude $\Delta n/\bar{n}$ damps r-modes with large (global) dimensionless amplitude α at significantly shorter time scales. As found before from the analytic expression eq. (5.6), given by the dotted curves, the damping time is temperature independent in this low temperature and intermediate amplitude regime. In contrast, due to the generic form of the bulk viscosity, featuring a universal maximum, the damping of large amplitude r-modes is not enhanced at high temperatures. As a direct consequence of the subthermal maximum of the bulk viscosity [81], the corresponding "resonant" temperature where the damping time is minimal is at roughly 10^9 K for strange stars and 10^{11} K for neutron stars. Correspondingly, r-modes are entirely unstable at high temperatures. However, due to the strong suprathermal enhancement at low temperatures the damping undercuts the gravitational time scale at sufficiently large amplitude so that the r-mode growth will slow down and eventually saturate. The corresponding amplitudes are strikingly very similar for the two different classes of stars, as will be discussed in more detail below. At very large amplitudes $\alpha \sim O(10)$ the damping times decrease again at all temperatures as a consequence of the behavior of the bulk viscosity [81].

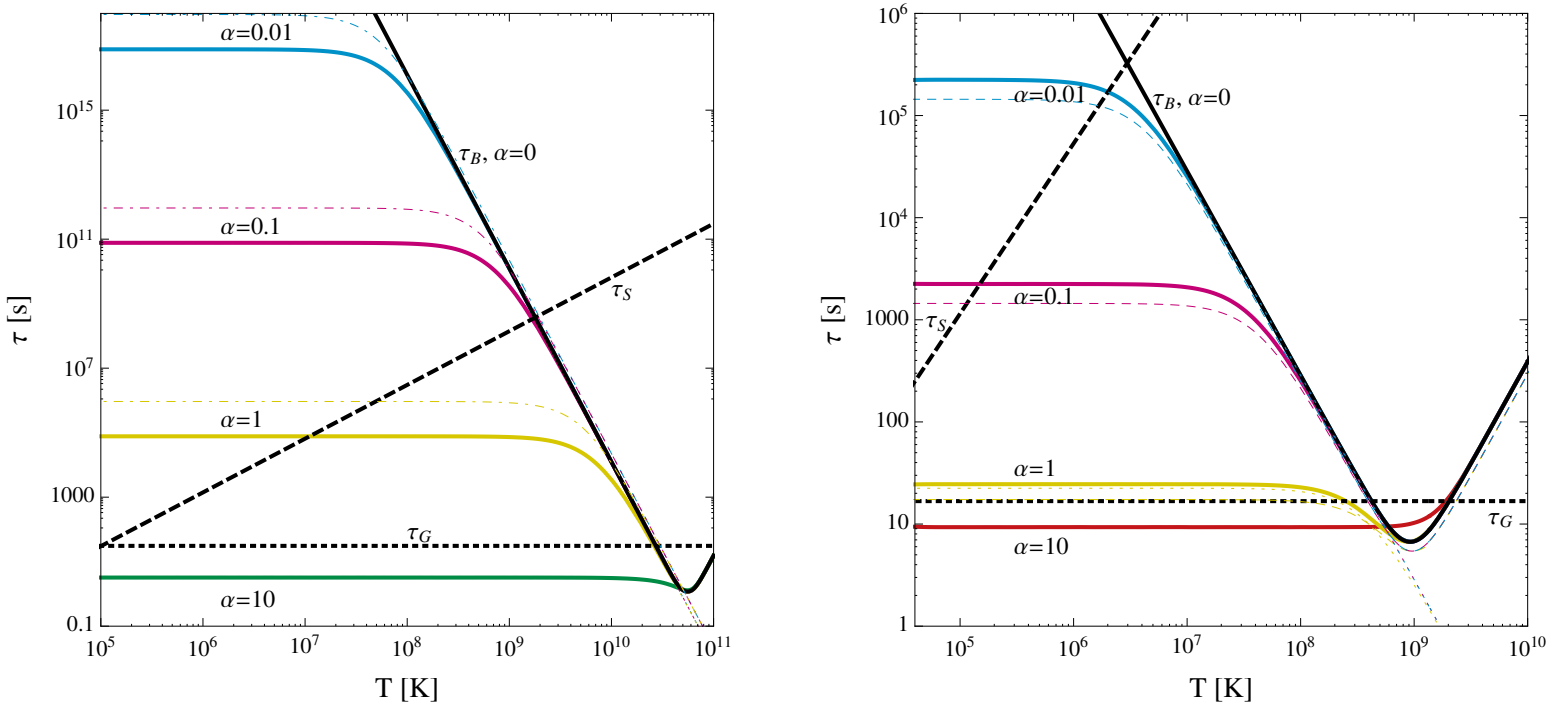

Figure 5.1: The relevant r-mode time scales for $1.4\,M_\odot$ stars rotating at their Kepler frequency. *Left panel:* Neutron star. *Right panel:* Strange star. The dotted horizontal line presents the time scale τ_G associated to the growth of the mode due to gravitational wave emission. The dashed rising curve shows the damping time τ_S due to shear viscosity. The damping time τ_B due to bulk viscosity is given for different dimensionless r-mode amplitudes $\alpha = 0$, 0.01, 0.1, 1 and 10 by the solid curves. The thin dotted curves correspond to the analytic linear approximation eq. (5.6) and are below the shown plot range for the largest amplitude. The thin dot-dashed curves on the left panel show the change when only a smaller core (ranging to a density of $n_0/2$ instead of $n_0/4$) is taken into account. The thin dashed curves on the right panel represent the approximate analytic expression eq. (E.5) given in the appendix which is not valid above the maximum of the bulk viscosity and therefore not shown for the large amplitude results.

The dot-dashed curves in the neutron star plot on the left panel of fig. 5.1 show the damping time if the crust is assumed to start already at the higher density $n_0/2$ instead of $n_0/4$ so that only the contribution from the correspondingly smaller core is taken into account[1]. Although the damping times are larger, as expected, the amplitude at which the viscous damping can saturate the mode is not drastically changed, so that our results given below remain qualitatively unchanged in this case. Actually, when the damping from the crust would be properly taken into account this should rather enhance the damping and decrease the r-mode amplitude compared to those obtained in this work. In the case of the strange star on the right panel of fig. 5.1 the dashed curves also show the analytic approximation discussed in appendix E, where the star is assumed to be homogeneous. As can be seen, the corresponding expression eq. (E.5) gives an approximate estimate for the damping time at all temperatures and for amplitudes up to the maximum of the viscosity, and only fails at higher amplitudes, where the bulk viscosity cannot saturate the r-mode anymore and where it is thereby not physically relevant. The deviations compared to the numeric result stem mainly from the fact that the density in the strange star is not entirely constant (fig.4.1 in chapter 4).

Previous neutron star analyses [79, 80] have employed an r-mode profile that does not feature the stronger additional radial dependence due to the low density enhancement of the inverse squared speed of sound A, shown in fig. 4.3, for a realistic equation of state. E.g. the r-mode profile given in eq. (6.6) of [53] features roughly a generic r^3-dependence. The strong r-dependence in our present treatment, however, strongly amplifies the damping in the outer regions of the star. Therefore, the contribution of the crust to the viscous damping should be relevant and would further decrease the saturation amplitude. The current restriction of our analysis to the core presents

[1]The range $n_0/4$ to $n_0/2$ should provide an estimate for the uncertainty of this boundary. For instance in [130] an intermediate value of $n_0/3$ is given.

therefore an upper bound for the saturation amplitude obtained when the damping of the whole star is considered. The second order effects in contrast increase the small amplitude instability region [43] and can correspondingly be expected to likewise increase the saturation amplitude. A more thorough treatment of all these effects in the future is clearly desirable.

5.3 Saturation amplitudes

Because of the strong decrease of the viscous damping time due to the suprathermal enhancement the damping can dominate at sufficiently large amplitudes. In this case the definition of the instability regions have to be extended. The latter are standardly defined in the subthermal regime and are independent of the amplitude. One could extend this concept by the definition of amplitude dependent instability regions which would shrink with increasing amplitude. However, since the amplitude can neither be inferred from observation nor is it a parameter that can be dialed, but is rather determined dynamically, we refrain from this possibility and rather introduce the concept of a *static saturation amplitude*. The latter is defined by the amplitude at which the r-mode would saturate at fixed temperature and frequency and is given by the solution of the equation

$$\frac{1}{\tau_G(\Omega)} + \sum_l \left(\frac{1}{\tau_S^{(l)}(T)} + \frac{1}{\tau_B^{(l)}(T, \Omega, \alpha_{sat})} \right) = 0 \tag{5.8}$$

where l runs over the contributions from the different shells of the star. The boundaries of the above mentioned amplitude dependent instability regions are by definition simply the contour lines $\alpha_{sat}(T, \Omega)$=const. and the boundary of the classic instability region, in particular, corresponds to $\alpha_{sat} = 0$. In case several solutions of eq. (5.8) exist, only the smallest one is physical and if no solution exists then viscous damping

alone cannot saturate the r-mode according to this definition. Actually, at the same time the r-mode grows, the star generally also cools or reheats and spins down respectively up so that the above amplitudes do not have to be reached. In particular the star could leave the parameter regions where a saturation according to the above criterion is not possible before the r-mode can actually explode.

5.3.1 Analytic approximation

Similar to the analytic expression for the boundary of the instability region [15] an analytic expression for the static saturation amplitude can be obtained. The analytic linear approximation $\tau_B^{\sim}$ applies as long as the r-mode amplitude is small enough so that the bulk viscosity is sufficiently below its maximum. When the r-mode amplitude is at the same time large enough that the highest power in eq. (5.6) dominates, the damping time becomes temperature independent. Both conditions are met sufficiently far inside the instability region so that the damping time simplifies to

$$\frac{1}{\tau_B^{\sim}} \xrightarrow[j=N=\delta/2]{} \frac{2^{4+N} m^N \left((2m+1)!!\right)^{N+1} \left((2N+1)!!\right)^2 \left(m\left(N+1\right)\right)! \chi_N \tilde{V}_{m,N}}{\pi^N \left(m+1\right)^{5(N+1)} \left(m!\right)^N \left(m-1\right)! \left(N+1\right)! \left(2\left(m+1\right)\left(N+1\right)+1\right)!! \kappa^{2N+2} \tilde{J}_m} \cdot \frac{\Lambda_{\mathrm{QCD}}^9 R^{5+4N} \alpha^{2N} \Omega^{4N+2}}{\Lambda_{EW}^4 M}$$

At saturation this has to match the gravitational time scale $1/\tau_B + 1/\tau_G = 0$ which yields the general result

$$\alpha_{sat} = \left(\frac{\pi^{1+\delta/2} (m-1)^{2m} (m+1)^{3+5\delta/2-2m} (m+2)^{2+2m} ((m-1)!)^{1+\delta/2} \left(\frac{\delta}{2}+1\right)!}{2^{\delta/2-1} ((2m+1)!!)^{3+\frac{\delta}{2}} ((\delta+1)!!)^{2} (m\left(\frac{\delta}{2}+1\right))! \chi_{\frac{\delta}{2}}} \right)^{1/\delta}$$
$$\cdot \frac{\left(\left(2(m+1)\left(\frac{\delta}{2}+1\right)+1\right)!!\kappa^{\delta+2}\right)^{1/\delta} \tilde{J}_m^{2/\delta} \Lambda_{EW}^{4/\delta} G^{1/\delta} M^{2/\delta}}{\tilde{V}_{m,\frac{\delta}{2}}^{1/\delta} \Lambda_{QCD}^{9/\delta} R^{2+(5-2m)/\delta} \Omega^{2-2m/\delta}} \tag{5.9}$$

where κ is defined by eq. (4.2). In the cases of strange stars with non-leptonic processes $\delta = 2$ and hadronic matter with modified Urca processes $\delta = 6$ this gives for the $m = 2$ r-mode

$$\alpha_{sat}^{(SS)} \approx 5.56 \cdot 10^{-5} \frac{\tilde{J}}{\tilde{V}_1^{1/2}} \frac{M_{1.4}}{R_{10}^{5/2}} \approx 1.61 \frac{(1-c)^2 M_{1.4}}{m_{150}^4 \mu_{300}^{1/2} R_{10}^{5/2}} \tag{5.10}$$
$$\alpha_{sat}^{(NS)} \approx 10.8 \frac{\tilde{J}^{1/3}}{\tilde{V}_3^{1/6}} \frac{M_{1.4}^{1/3}}{R_{10}^{13/6} \Omega_{ms}^{4/3}}$$

where $\tilde{J} \equiv \tilde{J}_2$ and $\tilde{V}_i \equiv \tilde{V}_{2,i}$ are given for the normalization scales used in table 5.1. Here m_{150}, μ_{300}, $M_{1.4}$, R_{10} and Ω_{ms} are the effective strange quark mass in units of 150 MeV, the quark chemical potential in units of 300 MeV, the stars mass in units of $1.4\,M_\odot$, the radius in units of 10 km and the angular velocity in units of 2π kHz corresponding to a millisecond pulsar, respectively. For strange stars the above expression for the intermediate amplitude bulk viscosity damping time has the same frequency dependence as the gravitational time scale eq. (4.17), so α_{sat} is basically constant throughout the instability region. However, it rises with decreasing frequency for neutron stars where the frequency dependence of the bulk viscosity is weaker. In contrast to the analytic expressions for the extrema of the instability region given in [15], which are very insensitive to the microscopic transport parameters, the saturation amplitude is more sensitive to the suprathermal bulk viscosity parameter

$\tilde{V}$. Whereas the saturation amplitude of neutron stars still depends on $\tilde{V}$ rather mildly due to the power 1/6, the saturation amplitude for strange stars obtained from the generic equation of state eq. (4.1) decreases with the "interaction parameter" c and even more strongly with the effective strange quark mass m_s.

5.3.2 Numeric solution

Let us now discuss the numerical solution for the saturation amplitude. In the following plots figs. 5.2 to 5.6 the static saturation amplitude is shown as a function of temperature and amplitude and they feature generally 3 distinct regions. The light (blue) surface shows the saturation amplitude where the r-mode growth is stopped by suprathermal damping. Due to the characteristic behavior of the bulk viscosity [81] which does not feature an amplitude enhancement for temperatures above the temperature T_{max} eq. (4.35), the r-mode is not damped at all by viscous effects in the high temperature regime as denoted by the dark (red) area on the right hand side. In the flat (green) region surrounding the instability region the r-mode is entirely stable and already damped by the shear or the subthermal bulk viscosity so that $\alpha_{sat}=0$.

The left panel of fig. 5.2 shows the static saturation amplitude for the $m = 2$ r-mode of a $1.4\,M_\odot$ neutron star. Although this might be hard to see in certain regions of the plot, the saturation amplitude rises steeply, within a narrow interval, from zero at the boundary of the instability region towards its interior. At large frequencies it reaches a plateau value that is nearly independent of the temperature as predicted by the analytic expression eq. (5.9). As described by the latter expression, inside the instability region the saturation amplitude rises strongly with decreasing frequency and since the instability region shrinks in width and eventually ends at low frequencies where the amplitude vanishes and the mode is damped, it features a peak-like structure. The maximum static saturation amplitude reached at the peak

is in this case unphysically large whereas the plateau value at the Kepler frequency is still roughly 3.5. The suprathermal bulk viscosity can therefore in principle saturate r-modes within the lower part of the instability region. However, in the present case, where only the damping of the core is taken into account, the static saturation amplitudes are at the limit where a standard r-mode analysis is valid. Moreover these amplitudes are so far larger than those of alternative saturation mechanisms [108, 127, 106, 107].

It is interesting to mention once more, though, that the extreme radial dependence of the r-mode profile eq. (4.7) strongly weights the outer regions of the star due to power law dependences of the inverse bulk viscosity damping time eq. (5.1) with exponents $O(30)$ for neutron and hybrid stars which is further enhanced by the density dependence of the inverse speed of sound. The contribution of the crust could thereby be decisive to obtain a realistic estimate of the impact of the non-linear viscosity. In this context it is also important that a similar enhancement of the bulk viscosity has been found for superfluid matter [131]. As noted in [15] there is a second instability region at high temperatures above 10^{11} K and as argued above the suprathermal bulk viscosity cannot saturate the r-mode in this high temperature regime. It is an interesting question if the r-mode can become large during this initial part of a star's evolution, and if so whether the r-mode is saturated at sufficiently small values by other non-linear mechanism or if the r-mode growth is not stopped before it reaches the regime where the structural stability of the star is at stake. In the latter case this instability phase might extend the violent supernova stage and actively shape the remnant by additional mass shedding and thereby determine its initial size and angular momentum. We will discuss these points further in the conclusion.

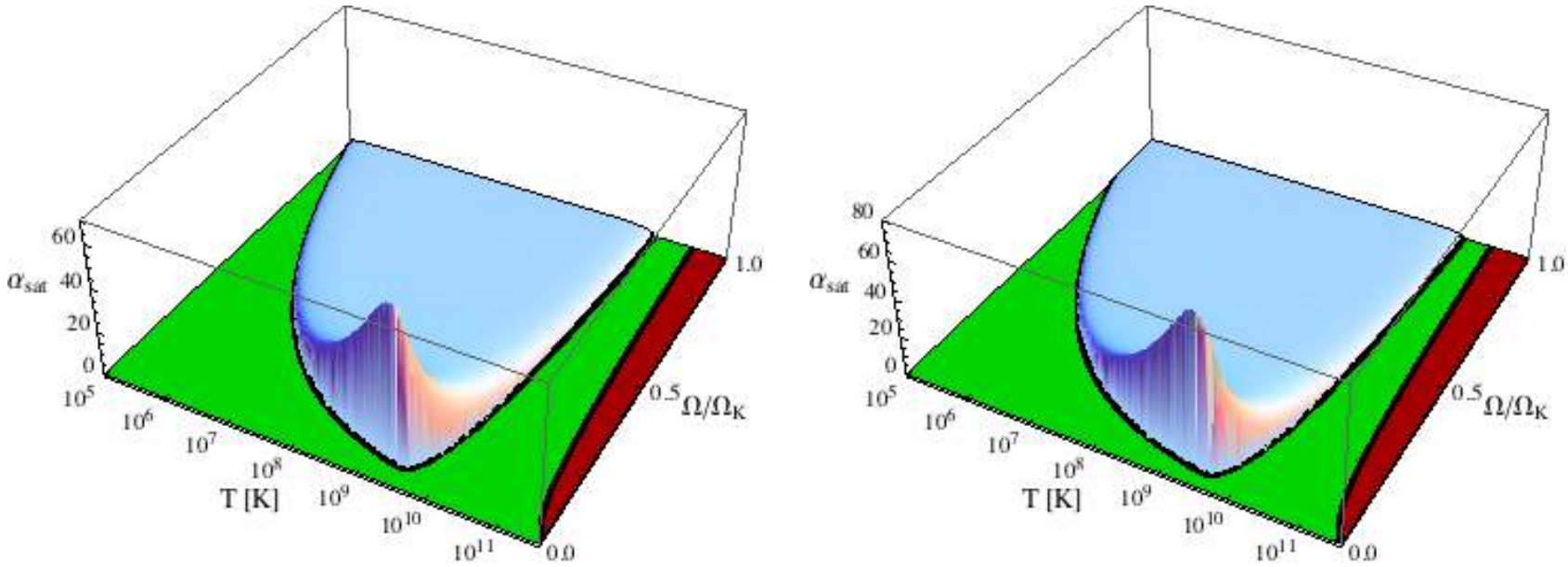

Figure 5.2: The static saturation amplitude, at which the r-mode growth is stopped by suprathermal viscous damping for the APR neutron stars. *Left panel:* $1.4\,M_\odot$. *Right panel:* $2.0\,M_\odot$. The light (green) shaded area denotes the stable region where the r-mode is damped away. At large frequencies a plateau with amplitudes $O(1)$ is reached. In the dark (red) region at high temperatures the r-mode is entirely unstable and cannot be saturated by viscous effects.

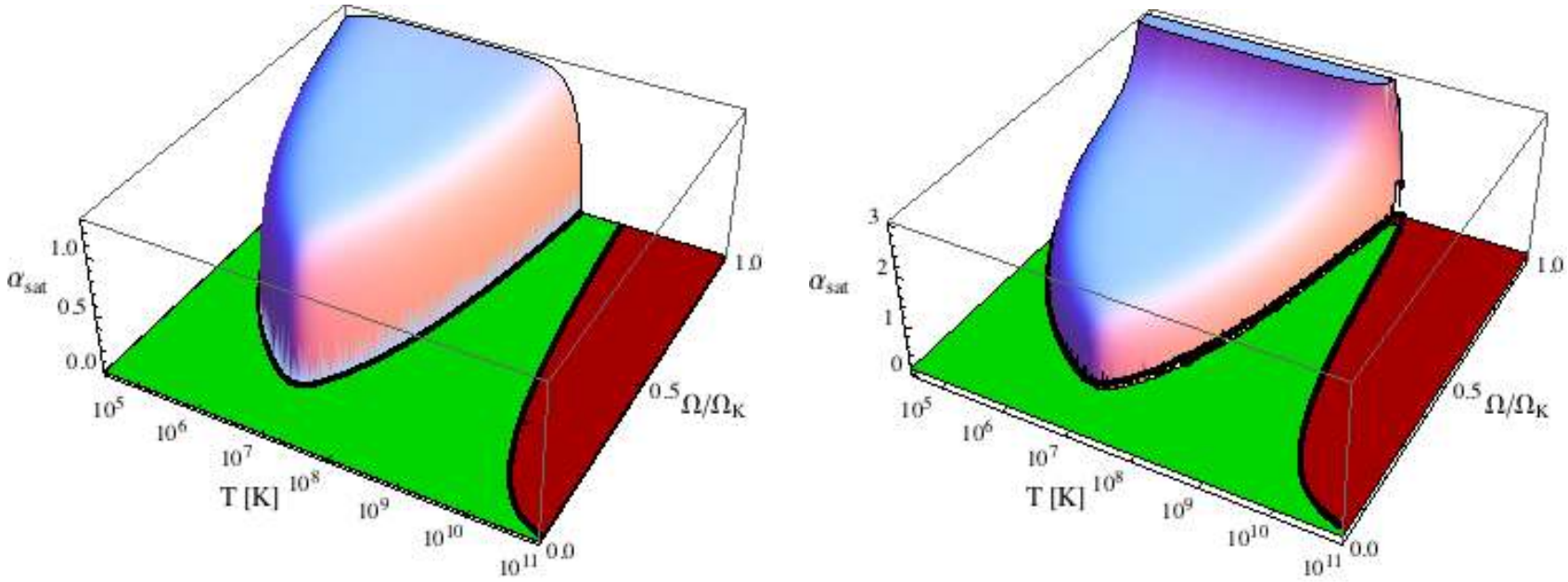

Figure 5.3: The saturation amplitude for the considered strange stars. *Left panel:* $1.4\,M_\odot$. *Right panel:* $2.0\,M_\odot$. In the latter case the suprathermal viscosity cannot stop the r-mode instability at frequencies larger than the maximum frequency of the stability window (where the saturation amplitude diverges) - for the considered star slightly below the Kepler frequency - as well as in the high temperature part of the instability region. The saturation amplitudes of the plateau in the lower part of the instability region are of the same order as in the hadronic case shown in fig. 5.2.

The saturation amplitude for the $1.4\,M_\odot$ strange star is shown on the left panel of fig. 5.3. Since the maximum of the stability window is above the Kepler frequency there are in this plot two separate parts of the instability region. As predicted by eq. (5.9) the plateau value of the saturation amplitude in the lower part is approximately temperature and frequency independent. Strikingly it is of similar size as the saturation amplitude for the $1.4\,M_\odot$ neutron star at its Kepler frequency. The high temperature part of the instability region where the viscosity again cannot saturate the r-mode extends in this case down to lower temperatures than for neutron stars.

The left panel of fig. 5.4 shows the corresponding plot for the $1.4\,M_\odot$ hybrid star. As found previously in [15] the instability region has here three parts that are separated by two stability windows arising from the resonant behavior of the bulk viscosities in the different shells. Due to their parametrically different temperature dependence the bulk viscosity of the quark shell dominates at low temperature, whereas the bulk viscosity of the hadronic shell dominates at high temperatures. Correspondingly the saturation amplitude in the low temperature part of the instability region shows the qualitative behavior found for strange matter whereas the intermediate temperature part shows the qualitative behavior found for hadronic matter. Since the region where the peak in fig. 5.2 is located is "cut out" by the stability window, the remaining peak of the hadronic intermediate part of the instability region in fig. 5.4 reaches only a much lower amplitude.

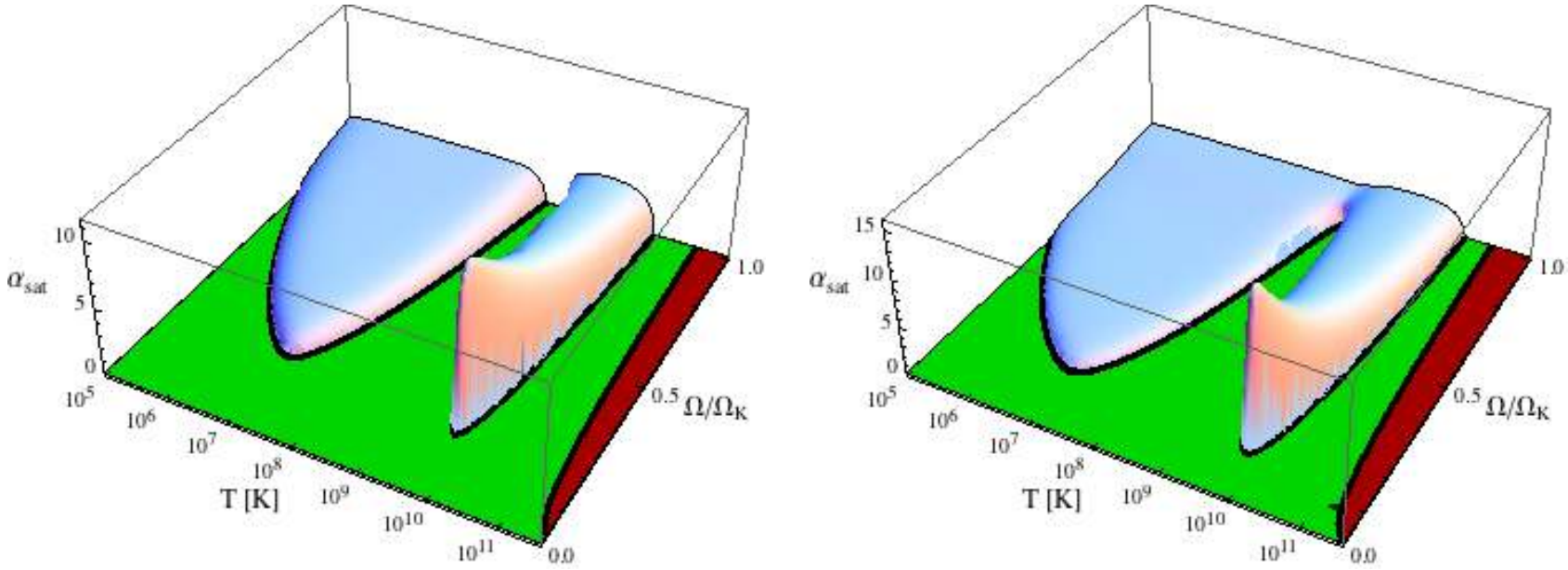

Figure 5.4: The saturation amplitude for the considered hybrid stars. *Left panel:* $1.4\,M_\odot$. *Right panel:* $2.0\,M_\odot$. The saturation in the low temperature part of the instability region is mostly established by the bulk viscosity of the quark core, whereas the saturation in the mid temperature part comes mainly from the hadronic shell.

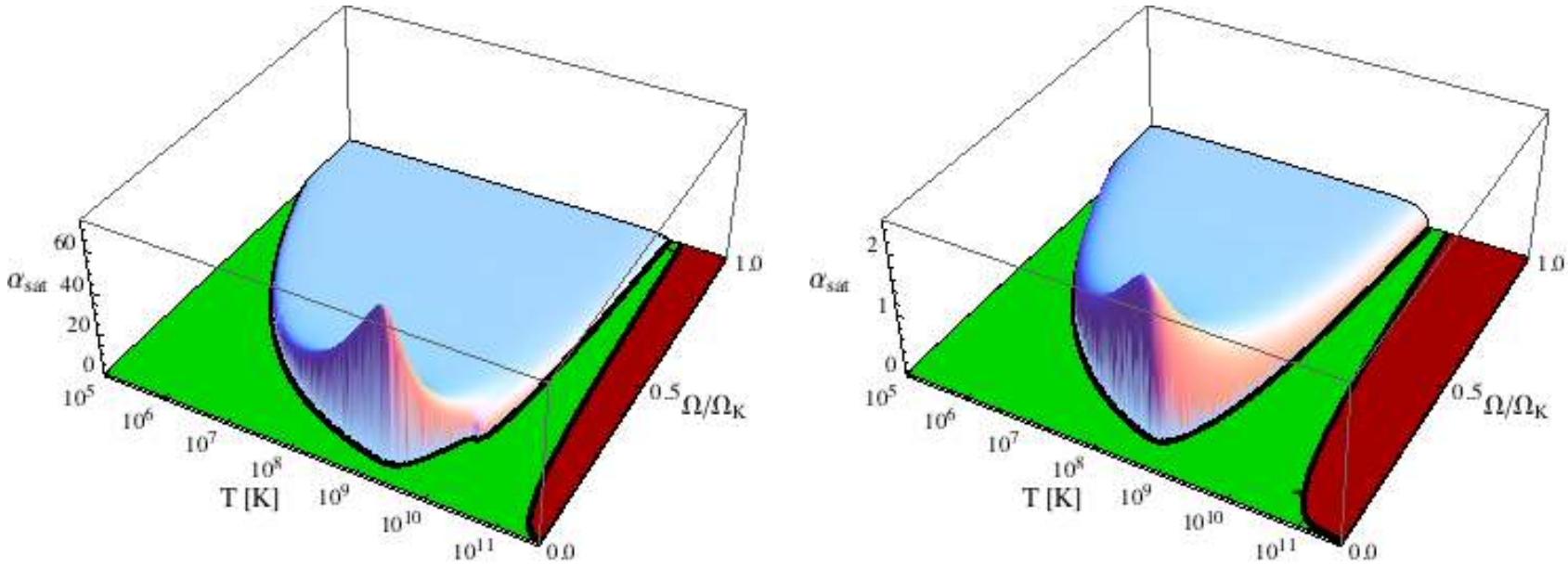

Figure 5.5: The static saturation amplitude, at which the r-mode growth is stopped by suprathermal viscous damping for the APR neutron stars at the maximum mass 2.21 $M_\odot$, where direct Urca processes become allowed. *Left panel:* direct Urca is only allowed in a small inner core region, see Table 4.1. *Right panel:* the same model when direct Urca is artificially turned on in the entire core.

The result for the heavy $2.0\,M_\odot$ neutron star is given on the right panel of fig. 5.2. As had been found previously in [15] the instability region is larger for such heavy stars. The figure shows in addition that saturation occurs at a somewhat higher amplitude. The $2.0\,M_\odot$ strange star is given on the right panel of fig. 5.3. In this case the maximum of the stability window is below the Kepler frequency. Similar to the high temperature behavior discussed before, the r-mode cannot be damped by viscous effects above this maximum. It is interesting to recall from [15] that in the case of quark matter an approximate analytic expression for the location of the maximum of the stability window exists

$$\Omega_{max}^{(SS)} \approx \frac{0.434 m_s^{4/3} R^{1/3}}{(1-c)^{1/3} G^{1/3} M^{2/3}} \tag{5.11}$$

$$T_{max}^{(SS)} \approx \frac{0.210\,(1-c)^{1/3}\, m_s^{2/3} R^{1/6}}{\hat{\Gamma}^{1/2} G^{1/6} \mu_q^{3/2} M^{1/3}} \tag{5.12}$$

where $\hat{\Gamma} \equiv \tilde{\Gamma}/\mu_q^5$. This shows that in addition to a large star mass, a small effective strange quark mass in the quark matter equation of state eq. (4.1) increases the total instability region both at high frequency and high temperature. In contrast, for the heavy $2.0\,M_\odot$ hybrid star shown on the right panel of fig. 5.4 such a total instability region does not arise since although the quark core cannot saturate the r-mode, the hadronic shell alone still provides sufficient damping to do so. In summary r-modes in massive stars are more unstable than in light stars since both their small amplitude instability regions are larger and they are less efficiently saturated by the large amplitude enhancement of the bulk viscosity.

The left panel of fig. 5.5 shows the static saturation amplitude for a neutron star with $2.21\,M_\odot$ which is the maximum mass allowed by the APR equation of state. In this case direct Urca reactions are possible in a small inner core region of mass

$0.85\,M_\odot$. As had already been observed in [15], direct Urca reactions only slightly alter the instability boundary by a small notch at its right hand side. Since suprathermal damping from outer layers dominates due to the strong radial dependence of the r-mode the static saturation amplitude is likewise only slightly reduced by the small direct Urca core. However, because the size of the inner direct Urca core depends strongly on the equation of state and there are equations of state where the direct Urca core is considerably larger, we show on the right panel of fig. 5.5 for comparison the (unphysical) case that the direct Urca reactions are artificially switched on in the entire core. This represents an upper limit for the possible effect of direct Urca reactions and shows that in this extreme case the static saturation amplitude at large frequency is reduced and the increase towards lower frequencies is considerably weakened according to the $1/\Omega$-behavior predicted by eq. (5.9).

In contrast to the previous results that evaluated the damping time eq. (5.1) numerically the top, left panel of fig. 5.6 employs the approximate analytic expression eq. (5.6) for the $m = 2$ mode of the $1.4\,M_\odot$ neutron star. Comparing it to the numerical result in fig. 5.2 shows that the corrections are very small and because the maximum of the bulk viscosity of hadronic matter with modified Urca reactions is reached only for large amplitudes, eq. (5.6) provides a very good approximation in this case. In contrast, the use of the linear approximation which neglects the large amplitude decrease of the bulk viscosity, strongly overestimates the damping for the case of strange stars and misses the previously discussed total instability region at high frequency in fig. 5.3.

Fig. 5.6 also shows the saturation amplitudes of different multipole r-modes, given for the first four multipoles $m = 2$ to 5 of the $1.4\,M_\odot$ neutron star . The higher multipoles saturate at lower amplitudes than the $m = 2$ and therefore the use of the linear approximate is well justified in this case. Interestingly, although the right

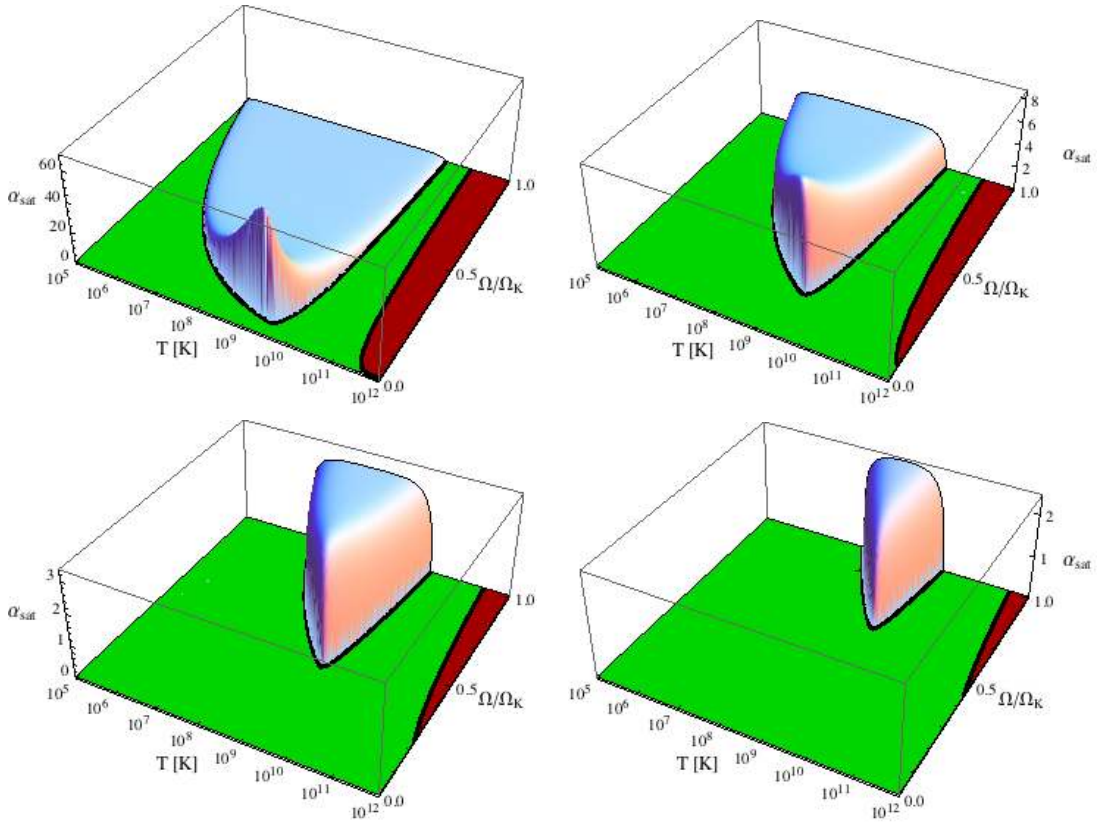

Figure 5.6: Saturation amplitudes for the first four multipole r-modes of the $1.4\,M_\odot$ neutron star (top, left: $m = 2$; top, right: $m = 3$; bottom, left: $m = 4$; bottom right: $m = 5$). The results are obtained in the linear approximation eq. (5.6).

segments of the lower part of the instability boundary of these higher order r-modes had been shown to be very similar to that of the fundamental $m = 2$ mode (see chapter 4), fig. 5.6 shows that although the peak value of the saturation amplitude of these modes decreases, the value at the Kepler frequency stays nearly constant. Therefore, these higher multipoles could be relevant for the spin-down evolution since the spin-down torque due to gravitational wave emission depends strongly on the amplitude [50]; for sufficiently small amplitude modes this dependence is quadratic. So if the suprathermal damping is responsible for the r-mode saturation, the restriction to the lowest order mode, that had been employed in all present analyses, should present only a first approximation. The saturation amplitudes of the different $1.4\,M_\odot$

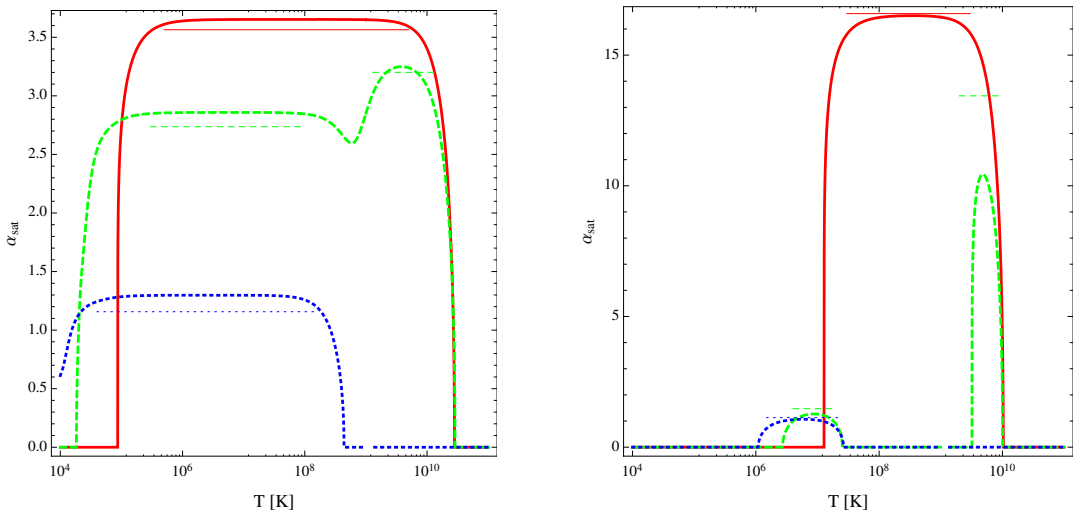

Figure 5.7: Comparison of the saturation amplitudes for the different $1.4\,M_\odot$ stars. *Left panel:* Stars spinning with a period of 1 ms. *Right panel:* Same for stars rotating with a period of 4 ms. Shown are the considered neutron star (solid), the hybrid star (dashed) and the strange star (dotted). The thick curves present the numerical results and the thin horizontal segments denote the analytic values obtained from eq. (5.9).

stars are finally compared with each other and the analytic approximation eq. (5.6) in fig. 5.7. Surprisingly, all stars feature saturation amplitudes of the same order of magnitude for millisecond pulsars, despite their very different microscopic and structural aspects. As noted before, for larger oscillation periods hadronic stars and to some extent also hybrid stars feature considerably larger saturation amplitudes than strange stars due to the parametrically different frequency dependence, see eq. (5.9). The analytic approximation yields in most cases a reasonable approximation to the full results with errors below the 10% level. In general the analytic result overestimates the actual amplitude since it only describes the result far away from the boundaries and boundary effects play a role. In contrast at large frequencies the analytic approximation underestimates the saturation amplitude since the considered frequencies are already close to the critical values, where the saturation amplitude diverges, see fig. (5.3). Nevertheless, the analytic approximation provides an important

and reliable estimate for the order of magnitude of the static saturation amplitude which, as will be discussed in more detail below, provides an upper limit for saturation amplitudes taken in dynamical star evolutions.

5.4 Conclusions

Using the general results for the bulk viscosity that include its non-linear behavior at large amplitudes we have derived expressions for the r-mode damping time that show that in the regime below the resonant temperature of the bulk viscosity, large amplitude r-modes are damped on considerably shorter time scales than low amplitude oscillations. In contrast, the universal maximum of the bulk viscosity found in chapter 3 implies that at very high temperatures and frequencies r-modes cannot be damped at all by viscous effects since there is no enhancement in the suprathermal limit. We find that for most stars considered in this work the corresponding critical frequency is above the Kepler frequency. On the other hand the r-modes of all considered stars are unstable at temperatures that are expected to be present when a proto-neutron star is created. At lower temperatures our results lead to an extension of the concept of the instability region of an r-mode since the latter is only initially unstable at small amplitudes but the suprathermal viscous damping can saturate the r-mode growth at finite amplitudes. We find that well within the instability region the static saturation amplitude α_{sat} defined in the text is temperature independent and takes values $O(1)$ at milli-second frequencies for all considered stars. This is incidentally the order of magnitude that had been assumed in early r-mode analyses [50]. Yet, the static values obtained here represent only an upper limit for the actual amplitude reached in the dynamic evolution. Our numeric results are confirmed by approximate analytic expressions which reveal the dependence of these results on the

various underlying parameters. We also studied higher multipoles and find that although the first few multipoles have instability regions that are sizable, they feature similar saturation amplitudes as the fundamental $m=2$ mode for millisecond pulsars and could thereby be relevant.

It is interesting to compare our saturation mechanism and the obtained results for the saturation amplitudes with previously proposed mechanisms. In general when there are different competing saturation mechanisms, the one with the smallest saturation amplitude should dominate and effectively saturate the mode. Explicit numerical analyses of the general relativistic hydrodynamical equations [105, 106, 107] would present the ideal way to study the saturation and star evolution. Whereas some of these studies find saturation only at large amplitudes, in others the r-mode can be completely destroyed by the decay into daughter modes once it exceeds amplitudes $O\left(10^{-2}\right)$ [107], see also [132]. However, the numerical complexity limits these analyses so far to unphysically large values of the radiation reaction force that are orders of magnitude above the physical value and it is not clear to what extent the obtained results can be extrapolated to the physical case. Another proposed saturation mechanism relies on the non-linear coupling of different oscillation modes [127, 108, 133, 132]. These analyses find that this mechanism could saturate r-modes at amplitudes as low as $O\left(10^{-5}\right)$. Due to the considerable difficulties of a complete description of such a mode coupling mechanism, these analyses use systems of coupled oscillators which represent a simplification of the complicated coupling of collective star oscillations. In summary, within the present approximation to neglect the neutron star crust, competing mechanisms will very likely dominate and saturate the r-mode at lower values than the suprathermal enhancement of the viscosity. However, these mechanisms still involve simplifications and uncertainties. Our novel saturation mechanism, in contrast, relies on standard viscous effects and microscopic physics that is quantitatively

well understood.

Let us now discuss the implications of our results for the spin-down of compact stars. In the supernova formation process where a much larger star contracts to a very compact object that takes over the angular momentum it seems plausible that fast rotating proto-neutron stars could be formed which spin with frequencies close to the Kepler limit. According to our results r-mode oscillations are unstable in this initial hot stage $T \gtrsim 10^{10} K$ and cannot be saturated by viscous effects for all considered forms of dense matter. Generically, the cooling is very fast in this regime so that the evolution could leave this instability region before large amplitude r-modes develop or spin down the star. The star will then cool until it reaches the lower instability zone and the r-mode develops. According to fig. 5.7 in this regime the r-mode can be saturated by viscous damping. For strange stars such a saturation does not seem to be required at all since the instability region is in this case located at comparably low temperatures [134] where the cooling becomes slow and the star either quickly spins down [135], or when reheating effects are considered it reheats again [136], and leaves the instability region before the amplitude becomes large. In this case the evolution wiggles around the instability line thereby spinning down the star, but this can take billions of years due to the strong reheating.

In contrast in the case of neutron and hybrid stars without strangeness, the instability region is reached at large temperatures where cooling is still fast and reheating effects are moderate, so that the evolution quickly penetrates the instability region and a saturation mechanism is indeed required to stop the r-mode growth [50]. Since the static saturation amplitude increases continuously at the boundary of the instability region the discussed *static* value does not have to be reached but a *dynamic* equilibrium could be established at a lower saturation amplitude that is reached once the r-mode is sufficiently large that the spindown becomes efficient. Due to this the

viscous saturation could dominate competing saturation mechanisms. Once the r-mode is saturated, the question is which one of two competing processes, cooling or spin-down, is faster. Since the cooling is slowing down at lower temperatures it is likely that the spin-down wins and the evolution leaves the instability region near its lower boundary. In this case no young compact stars with frequencies larger than a tenth of the Kepler frequency would be possible which is in good agreement with observations. An answer to the above questions requires a detailed study of the combined spin-down and cooling evolution of the star.

Strikingly our results suggest even another possibility for the spindown of young stars that would be even faster and more violent. The core bounce during the supernova process should excite rather large amplitude oscillation modes in the forming compact core. Since r-modes are unstable in this regime (see chapter 4) these will grow further. Because of the initial high temperatures, neutrinos are trapped inside the proto-neutron stars for roughly a minute [137]. Since a neutron star crust that could provide an efficient damping mechanism [123] is not formed at this point, and as our results show viscous effects cannot stop the r-mode growth, the amplitude could indeed become large if other non-linear saturation mechanisms likewise cannot operate efficiently in this turbulent environment. In this case the loss of angular momentum could proceed not by gravitational wave emission but by actual mass shedding and thereby effectively as an extension of the supernova explosion that is driven by r-modes. Since such a violent spindown should be fast the star could end up at the lower boundary of the high temperature instability region before the star becomes transparent to neutrinos and the cooling process starts. Clearly, in this initial stage, which cannot rigorously be separated from the aftermath of the supernova explosion, the dynamics is highly non-linear and our simple r-mode analysis might not directly apply. Whether such a mechanism is feasible will therefore require fur-

ther study, but this mechanism would naturally explain the observed absence of fast, young pulsars independent of their internal composition and it is striking that the frequencies of the high temperature instability boundary also seem to agree well with fastest pulsars that are young enough that they cannot be spun up by accretion [1].

Finally, r-modes should also be relevant for old accreting stars in binary systems that are spun up and could enter the instability region at low temperatures from below [125]. As discussed in chapter 4, strange and hybrid stars feature stability windows at low temperatures where the r-mode is absent, so that such stars could accelerate to frequencies close to the Kepler frequency. In contrast for neutron stars there is no stability window at low temperatures so that an accreting star would enter the unstable regime already at low frequencies. Recall that the saturation amplitude of neutron stars due to bulk viscosity has a characteristic form with a pronounced peak close to the minimum of the instability region. In case the r-mode is saturated by suprathermal bulk viscosity, the steep rise of the amplitude close to the maximum should spin down the star quickly and so that it cannot penetrate deep into the instability region. This means that such stars should cluster close to the boundary which might be a signature once more observational data for the temperature of compact stars becomes available.

Appendices

Appendix A

Scattering mean free path

The scattering mean free path is determined by the 2-body interaction cross section [66]. The relevant scattering amplitude is the sum of four Feynman diagrams, the contact term and the s, t, and u-channel diagrams, see Fig. 2.1. In the s, t, and u-channels there is a virtual particle that can go on-shell, which means that its self-energy must be included to avoid an unphysical divergence. (The fact that the virtual particle can go on-shell means that the $2 \to 2$ collision rate already includes the contribution from $1 \to 2$ splitting process, so these need not be calculated separately [138, 139]. We have performed this separate calculation and verified that the result has the same parametric dependence as the one we obtain below.) The rate (per unit volume) for the $2 \to 2$ scattering process is

$$\Gamma_{2\to 2} = \tfrac{1}{2} \int_{p,k,p',k'} (2\,\pi)^4 \delta^4(P + K - P' - K') |\mathcal{M}|^2\, f_p\, f_k\, (1 + f_{p'})\, (1 + f_{k'}), \qquad \text{(A.1)}$$

where

$$\int_p = \int \frac{d^3p}{2\,\epsilon_p\,(2\,\pi)^3} \qquad\qquad f_p = \frac{1}{e^{E_p/T} - 1} \qquad \text{(A.2)}$$

and

$$|\mathcal{M}|^2 = |\mathcal{M}_{\rm s}|^2 + |\mathcal{M}_{\rm t}|^2 + |\mathcal{M}_{\rm u}|^2 + I \qquad \text{(A.3)}$$

where I represents the contact and interference terms, and the matrix elements are given in Eq. (2.53). The dominant contribution in the scattering matrix $|\mathcal{M}|^2$ comes from $|\mathcal{M}_{\rm s}|^2 + |\mathcal{M}_{\rm t}|^2 + |\mathcal{M}_{\rm u}|^2$, since these each have a large enhancement when the virtual particle is close to being on-shell. The contact term and interference terms have no such enhancement, and so make a much smaller contribution to the rate. Note that to avoid the collinear singularities in our calculations, we include the one-loop self energy in the calculation of kaon propagator and $|\mathcal{M}|^2$.

We now give a detailed explanation of the evaluation of $|\mathcal{M}_{\rm s}|^2$; the others can be obtained by similar methods. We first define the virtual particle momentum $Q = (E_q, \mathbf{q})$ and shift the integral over $\mathbf{k}$ to an integral over $\mathbf{q}$. We can then still use the momentum-conserving delta-function to do the integral over $\mathbf{k}'$. We then choose the direction of $\mathbf{q}$ as the z-axis, so the angular part of the $\mathbf{q}$ integral gives a factor of $4\,\pi$ and the remaining integrand is azimuthally symmetric, so the 2 remaining azimuthal integrals give a factor of 2π. This leaves three integrals over the magnitudes of $\mathbf{p}$, $\mathbf{k}'$ and $\mathbf{q}$ as well as over two polar angles, between $\mathbf{q}$ and $\mathbf{p}$ and between $\mathbf{q}$ and $\mathbf{k}'$. We then introduce the auxiliary variable ω via the identity

$$\delta(E_p + E_k - E_{p'} - E_{k'}) = \int_{-\infty}^{\infty} d\omega \delta(\omega - E_p + E_{p'})\, \delta(\omega + E_k - E_{k'}). \tag{A.4}$$

The integral over the two polar angles can then be done using these two delta-functions, leaving behind four integrals over p, k', ω and q,

$$\Gamma_s = A \int_0^{\infty} dq \int_{\nu\, q}^{\infty} d\omega \int_{(\omega - \nu\, q)/2\nu}^{(\omega+\nu\, q)/2\nu} dp \int_{(\omega-\nu\, q)/2\nu}^{(\omega+\nu\, q)/2\nu} dk'\, |\mathcal{M}_s|^2\, f_{\nu p}\, f_{\omega-\nu p}\, (1+f_{\omega-\nu k'})\, (1+f_{\nu k'}) \tag{A.5}$$

To make the temperature dependence explicit we introduce a new set of variables

$(x, y, w,$ and $z)$. For the s-channel these are

$$x = \frac{\nu p}{T} \qquad y = \frac{\nu k'}{T} \qquad w = \frac{\omega}{T} \qquad z = \frac{\nu q}{T} \ , \tag{A.6}$$

and the Mandelstam variable is $s = w^2 - z^2$. This leads to the full expression for the s-channel rate,

$$\Gamma_s = \frac{g^4 T^{12}}{16\nu^{17}(2\pi)^5 f_\pi^8} \int_0^\infty dz \int_z^\infty dw \int_{(w-z)/2}^{(w+z)/2} dx \int_{(w-z)/2}^{(w+z)/2} dy \, F(x,y,w) \frac{G(x,w,s)G(y,w,s)}{s^2 + (\Pi^+/T^2)^2} \tag{A.7}$$

where Π^+ is related to the imaginary part of the self energy (see below) and

$$F(x,y,w) = f_x \, f_{w-x}(1+f_y)(1+f_{w-y}) \qquad G(x,w,s) = w^2 \left(3x(1-\nu^2)(w-x) - s\right)^2 \tag{A.8}$$

The self-energy term has both a real and an imaginary part, however the real part is much smaller [66]. We will therefore only consider the imaginary part Im $\Pi(\omega, q)$, obtained in Refs. [76, 77, 66],

$$\begin{aligned} \text{Im } \Pi(w,z) &= \Pi^+ \Theta(w^2 - z^2) + \Pi^- \Theta(z^2 - w^2) \\ \Pi^+ &= \frac{g^2 \, T^6}{16\pi\nu^7 f_\pi^4} \frac{1}{z f_w} \int_{\frac{w-z}{2}}^{\frac{w+z}{2}} dy \; G(y,w,s) \, f_y \, f_{w-y} \\ \Pi^- &= \frac{g^2 \, T^6}{8\pi\nu^7 f_\pi^4} \frac{1}{z f_w} \int_{\frac{w+z}{2}}^{\infty} dy \; G(y,w,t) \, f_y \, [1 + f_{y-w}] \end{aligned}$$

where Π^+ is relevant for the s-channel where $w > z$, and Π^- is relevant for the t- and u-channels where $w < z$. We have neglected the tadpole contribution to the self-energy: it only corrects the kaon velocity by term proportional to λT^4 [66].

In the remaining 4-dimensional integral (A.7) we can now use a simple approximation to greatly simplify the integral. In the expression for Γ_s the integral over w is sharply peaked at the limit of integration where $w = z$, i.e. $\omega = \pm\nu q$ $(s = 0)$. The

integral takes the form

$$\int_z^\infty dw \frac{I(w,z)}{(w^2-z^2)^2+(\Pi^+(w,z)/T^2)^2} \approx \frac{\pi T^2}{4\,\Pi^+(z,z)\,z} I(z,z)\ , \tag{A.9}$$

This expression is valid when $I(w,z)$ is slowly varying near the singular point $w = z$ and when $\Pi^+/T^2 \ll 1$ because $\Pi \sim g^2T^6$ and $T \ll f_\pi, \Delta, \mu_K$. Applying this approximation to the s-channel contribution, we find

$$\Gamma_s = \frac{g^4T^{14}}{16\nu^{17}(2\pi)^5 f_\pi^8}\frac{\pi}{4}\int_0^\infty dz \int_0^z dx \int_0^z dy f_x f_{z-x}(1+f_y)(1+f_{z-y})\frac{G(x,z,0)G(y,z,0)}{\Pi^+(z,z)z}. \tag{A.10}$$

where

$$\Pi^+(z,z) = \frac{g^2T^6}{16\pi\nu^7 f_\pi^4}\frac{1}{zf_z}\int_0^z dx\ f_x\, f_{z-x}\, G(x,z,0)\ . \tag{A.11}$$

We can then see that the integral over x in Eq. (A.10) partially cancels the integral contained in Π^+ leaving behind only a double integral. Using $G(y,z,0)$ from Eq. (A.8), we have

$$\Gamma_s = \frac{g^2T^8(1-\nu^2)^2}{\nu^{10}f_\pi^4}J\ , \tag{A.12}$$

where J is a pure number given by

$$\begin{aligned} J &= \frac{9}{128\pi^3}\int_0^\infty dz\ \int_0^z dy\ y^2\,z^2\,(z-y)^2\,f_z\,(1+f_y)\,(1+f_{z-y}) \\ &\approx 0.466\ . \end{aligned} \tag{A.13}$$

Applying the same method to the t- and u-channel integrals, we find that they all give the same rate, so the total rate is

$$\Gamma_{\rm total} = 1.40\,\frac{g^2\,T^8\,(1-\nu^2)^2}{\nu^{10}f_\pi^4}\ . \tag{A.14}$$

The scattering mean free path is defined as

$$l_K^{\rm scat} = \frac{\nu n}{\Gamma} \ , \tag{A.15}$$

where n is the particle density (2.19). So the scattering mean free path of the Goldstone kaons is

$$l_K^{\rm scat} = 0.0881 \frac{\nu^8}{(1-\nu^2)^2} \frac{f_\pi^4}{g^2 T^5} = 3.44 \times 10^{-4} \frac{\nu^8}{(1-\nu^2)^2} \frac{f_\pi^2 \, \Delta^4}{C^2 \, \mu_K^2 \, \sin^2 \varphi} T^{-5} \ , \tag{A.16}$$

For comparison, the scattering mean free path of the phonon is [66]

$$l_H^{\rm scat} = 0.181 \, \frac{v^8}{(1-v^2)^2} \frac{\mu_q^4}{T^5} = 5.02 \times 10^{-3} \frac{\mu_q^4}{T^5} \tag{A.17}$$

so the ratio of the two is

$$\frac{l_K^{\rm scat}}{l_H^{\rm scat}} = 17.546 \frac{\nu^8}{(1-\nu^2)^2} \frac{f_\pi^4}{g^2 \mu_q^4} \approx 2.14 \times 10^{-4} \frac{f_\pi^2 \Delta^4 |\delta m|^3}{C^2 m_K^5 \mu_q^4} \ . \tag{A.18}$$

Since μ_q is much larger than any of the other energy scales, this implies that the scattering mean free path of the kaon, like the shear mean free path, is generally much shorter than that of the phonon, giving the Goldstone kaon a much wider range of temperatures where it can be treated hydrodynamically.

We have noted in Sec. 2.3 that we expect the shear mean free path to be a better indicator of the range of validity of hydrodynamics, but for the sake of completeness we now estimate the temperature at which $l_K^{\rm scat}$ will become greater than 1 km, in the case of very unfavorable parameter choices that lead to a long mean free path. We will use the values used at the end of Sec. 2.5.2 to illustrate how high the shear viscosity can be, namely $f_\pi = 150$ MeV, $\Delta = 150$ MeV, $\delta m = -1.0$ MeV, $m_K = 4.0$ MeV and $C = 0.2$. In this case the scattering mean free path is shorter than 1 km for

$T \gtrsim 0.006$ MeV. For more favorable choices of the couplings this critical temperature will be much lower. In comparison, from (A.17) the scattering mean free path for phonons is shorter than 1 km for $T > 0.04$ MeV.

We have used a linear dispersion for the kaon in calculating the mean free path, which is a requirement for getting a co-linear enhancement. However, there are sources of non-linearities in the dispersion. One comes directly from our expansion of the full kaon dispersion in (2.11). If we had kept higher order terms, we would get a contribution that behaves as

$$E = \nu p(1 + \gamma p^2) \tag{A.19}$$

where $\gamma > 0$. This positive curvature would still allow for the co-linear splitting and joining processes. Therefore, keeping this term would provide a subleading contribution to the calculation presented here.

However, we ignored how the higher order derivative interactions themselves could change the kaon dispersion. Something similar has been calculated for the superfluid phonons, [140], where γ was found to be negative and therefore the $1 \leftrightarrow 2$ processes are kinematically forbidden. If the corresponding non-linearity for the kaons were positive, then as above, the calculation presented here would remain the same. However, if the curvature were negative as for the phonons, then the mean free path would be altered at leading order. This is basically because the non-linearity itself would act to regulate the on-shell propagator and the scattering rate would go like $1/\gamma$ instead of $1/\Pi$ (where Π is the self-energy). The appropriate scales to compare are γT^2 and Π/T^2 and in the case of the phonons, $\gamma T^2 \gg \Pi/T^2$, such that this correction would make the mean free path even larger and affect the validity of hydrodynamics. See [141] for a calculation involving the non-linear phonon dispersion and its affect on regulating the phonon propagator in a calculation of the thermal conductivity. However, it should be noted that including the non-linearity would only provide a subleading

correction to the shear viscosity for either sign of γ because the shear viscosity is insensitive to that region of phase space.

Appendix B

Power counting sharply peaked integrals

Here we discuss in more detail the evaluation of integrals of the type (A.9), having a slowly-varying component I multiplied by a function with a sharp Lorentzian peak at the edge of the range of integration. In appendix A we assumed that I was non-zero at the edge of the range and we kept only the leading contribution. Here we include higher-order corrections by Taylor-expanding the numerator,

$$\int_0^z dw \frac{I(w,z)}{(w^2-z^2)^2+\epsilon^2} \sim \int_0^z \frac{I(z,z)+(w-z)I'(z,z)+\frac{1}{2}(w-z)^2 I''(z,z)+\ldots}{(w^2-z^2)^2+\epsilon^2} \,, \tag{B.1}$$

where $I'(z,z)$ is the first derivative of I with respect to w, evaluated at $w=z$. We then find

$$\begin{aligned} J_1 \equiv \int_0^z dw \frac{1}{(w^2-z^2)^2+\epsilon^2} &\sim \frac{\pi}{4z\epsilon} \\ J_2 \equiv \int_0^z dw \frac{z-w}{(w^2-z^2)^2+\epsilon^2} &\sim -\frac{\ln\epsilon}{4z^2} \\ J_3 \equiv \int_0^z dw \frac{(z-w)^2}{(w^2-z^2)^2+\epsilon^2} &\sim \frac{1}{8z} \end{aligned} \tag{B.2}$$

This gives us a scheme for power counting any integrals of the form given by (B.1). The relevant property is the dependence on ϵ, since the collision integrals for transport properties take the form (B.1) with $\epsilon = \Pi/T^2 \propto g^2 T^4 \ll 1$.

We can now justify the statement made in Sec. 2.4 that when we calculate the shear viscosity using a polynomial expansion of the function $g(p)$ (2.43), the dominant contribution comes from $g(p) = 1/p$, i.e. choosing the minimum-exponent parameter n to be -1.

Calculations of the mean free path and the shear viscosity both involve a rate calculation which contains collision integrals. In the mean free path collision integral (A.7) there is a sharp peak in the integrand at $w = z$ corresponding to a co-linear divergence, where two kaons have parallel momenta, and exchange a kaon whose momentum lies in the same direction. In the mean free path calculation this near-divergence is regulated by the self-energy, so the result depends on the self-energy ($\sim 1/\epsilon$).

In the case of the shear viscosity, we expect the integral not to have a co-linear divergence, since shear viscosity measures momentum transfer, so processes that do not change the momentum direction of the particles make no contribution. We therefore expect that the collision integrand in the shear viscosity should go to zero at $w = z$ in such a way that the result does not depend on the self-energy. The true physical $g(p)$ function will give an integrand that has this property. However, if we make a bad guess at $g(p)$ (by using inappropriate basis polynomials in the expansion (2.43)) then each individual term will have a co-linear divergence, which will only cancel out when we add up the contributions from many terms. The best guesses for $g(p)$ are therefore ones which yield a collision integrand with no co-linear divergence, i.e no dependence on the self-energy.

In both the mean free path and the shear viscosity calculations the collision in-

Min-exponent parameter n	Behavior of Δ^0_{ij} near $w = z$	ϵ-dependence of collision integral
$n = -1$	$(z-w)^2$	independent
$n = -2$	$(z-w)$	$-\ln\epsilon$
$n \neq -2, -1$	$(z-w)^0$	$1/\epsilon$

Table B.1: Table of behavior of Δ_{ij} (part of the collision integrand) near the co-linear singularity, and the collision integral; ϵ represents the self-energy. Only the $n = -1$ case has the proper physical suppression of co-linear contributions to the shear viscosity.

tegral takes the form (B.1). The difference between them lies in behavior of the numerator $I(w, z)$ in the co-linear regime $w \to z$. In the mean free path calculation (appendix A), the numerator stays finite in this regime, so the collision integral is of the form J_1 (B.2) and is strongly dependent on the self-energy. In the shear viscosity calculation, the numerator contains an additional factor $\Delta^s_{ij}\Delta^t_{ij}$ (see Eq. (2.48)), which we'll call the transport term. The behavior of the transport term in the co-linear regime is therefore crucial in suppressing the self-energy dependence.

Using expansions of $g(p)$ with only one term ($N = 0$) we calculate Δ^0_{ij} and the shear-viscosity collision integral for different choices of n. We summarize the results in Table B.1. We see that the choice $n = -1$ fully suppresses the co-linear singularity and gives a collision integral that is independent of the self-energy. The choice $n = -2$ partially suppresses co-linear scattering and gives the collision integral a very weak dependence on the self-energy. Other values of n do not suppress the co-linear scattering at all and are akin to the calculation of the mean free path. This explains our finding in Sec. 2.4, Table 2.2 that $n = -1$ is the the optimal choice for fast convergence of the polynomial approximation for $g(p)$ in the shear viscosity, that $n = -2$ is the next best choice, and other values of n have very poor convergence.

Appendix C

Approximate evaluation of the collision integral

Here we describe how the collision integral is reduced to a five-dimensional numerical integral, in which we have factored out the temperature dependence and part of the dependence on the kaon speed ν. We begin with the matrix M (2.48) that enters in to the calculation of the shear viscosity. As described in Sec. 2.4 and appendices A and B, we get a good estimate of the shear viscosity by assuming $g(p) = 1/p$, i.e. we set $N = 0$ and $n = -1$. Then, as described after Eq. (2.54), we can eliminate seven of these integrals by using the δ-function and spherical symmetry. We rescale the momenta with temperature, and find

$$M_{00} = \frac{1}{10 \cdot 2^8 \, \pi^6 \, \nu^6} \left(\frac{T}{\nu}\right)^{13} \int d\Gamma \; f_x \, f_y \, (1 + f_z) \, (1 + f_w) |\overline{\mathcal{M}}(\nu, g, \lambda)|^2 \, \bar{\Delta}^0_{ij} \, \bar{\Delta}^0_{ij} \quad \text{(C.1)}$$

where $f_x \equiv 1/(e^x - 1)$, and

$$\int d\Gamma = \int_0^\infty dx \int_0^\infty dy \int_{-1}^1 d\alpha \int_{-1}^1 d\beta \int_0^\pi d\phi \; \frac{z^2}{1 - \alpha} \; , \quad \text{(C.2)}$$

$$x = \frac{\nu p}{T} \qquad y = \frac{\nu k}{T} \qquad z = \frac{\nu k'}{T} = \frac{x\,y\,(1-\alpha)}{x(1-\beta)+y(1-\gamma)} \qquad w = \frac{\nu p'}{T} = x + y - z \ , \tag{C.3}$$

$$\alpha = \hat{\mathbf{p}} \cdot \hat{\mathbf{k}} \qquad \beta = \hat{\mathbf{p}} \cdot \hat{\mathbf{k}}' \qquad \gamma = \hat{\mathbf{k}} \cdot \hat{\mathbf{k}}' = \alpha\beta + \sqrt{(1-\alpha^2)(1-\beta^2)}\cos(\phi) \tag{C.4}$$

From (2.53), $\overline{\mathcal{M}} \equiv (\nu/T)^8 \mathcal{M}$ depends on the speed ν and the couplings g and λ as well as the rescaled momenta x, y, z. From (2.49), $\bar{\Delta}^0_{ij} \equiv (\nu/T)\,\Delta^0_{ij}$ depends only on the rescaled momenta. The expression for z comes from solving the energy-conserving δ-function, and ϕ is the difference in azimuthal angles between the vectors $\mathbf{p}, \mathbf{k}$ and $\mathbf{p}, \mathbf{k}'$.

We have scaled out all the temperature dependence of the integrand, but there is still some dependence on ν and the couplings g and λ which comes in via $\mathcal{M}$. The integral can be evaluated numerically using (2.49) and (2.53) for given values of ν, g, λ.

We now show how to obtain the approximate analytic forms for η given in (2.59), which are valid in the regime $g^2/\lambda \ll 1$ and $g^2/\lambda \gg 1$.

Using (C.1) in (2.51) and evaluating A_0^{-1} from (2.44), we find that

$$\eta = \frac{\text{const}}{\nu^8\, M_{00}(\nu)} \tag{C.5}$$

where const represents a function independent of ν. We can obtain the function $h_1(\nu)$ in (2.59) by going to large λ in which case $\mathcal{M} = \mathcal{M}_c$, and then calculating the shear viscosity with all the dimensionful parameters in the coupling constant λ set equal to unity. To calculate $h_2(\nu)$, we go to large g where $\mathcal{M} = \mathcal{M}_s + \mathcal{M}_t + \mathcal{M}_u$ and do the same thing. In both cases we find

$$h_{1,2} = \frac{A_{1,2}\,\nu^{11}}{\int d\Gamma\, f(\Gamma) |\mathcal{M}_{1,2}(\nu)|^2} \tag{C.6}$$

where $A_{1,2}$ is a pure number and $f(\Gamma)$ represents the parts of the integrand of (C.1) that are independent of ν. From (2.48) we find that

$$\mathcal{M}_{1,2} \sim c_{1,2}^{(0)} + c_{1,2}^{(1)}\nu^2 + c_{1,2}^{(2)}\nu^4 \tag{C.7}$$

Therefore, we expect

$$h_{1,2}(\nu) = C_{1,2}\frac{\nu^{11}}{\sum_{i=0}^{4} a_{1,2}^{(i)}\nu^{2i}} \ , \tag{C.8}$$

justifying our statement in the paragraph below Eq. (2.59) and the resulting scaling in Fig. 2.4.

Finally, we can explain why h_1 and h_2 are so small (see Fig.2.4). This is a direct result of M_{00} being large. Because the all interactions of the Goldstone kaons are derivative interactions, the collision integral involves high powers of momenta. Schematically, it has the form

$$\int_0^\infty dx\ x^d f_x \sim (d+1)! \tag{C.9}$$

where $d = 12$ in our case. Since $1/13! \approx 1.6 \times 10^{-10}$ it is not surprising that h_1 and h_2 are of that order.

Appendix D

R-mode and amplitude conventions

In this appendix we review a few standard expressions for r-modes and discuss different conventions used in the literature. The form of the r-mode oscillation is most conveniently derived [142] from the underlying equations that determine the fluctuation of the potential $\delta U = \delta h + \delta\Phi$, where h is the enthalpy and Φ the gravitational potential, since then the hydrodynamic Euler equation for the harmonic, cylindrically symmetric perturbation reduces from a differential to an ordinary linear equation and can be solved analytically by matrix inversion. The expression for δU reads to leading order in a slow rotation expansion

$$\delta U \approx \sqrt{\frac{m}{\pi\left(m+1\right)^{3}\left(2m+1\right)!}}\alpha R^{2}\Omega^{2}\left(\frac{r}{R}\right)^{m+1}P_{m+1}^{m}\left(\cos\theta\right)\mathrm{e}^{im\phi} \tag{D.1}$$

The velocity fluctuation is obtained from δU by application of a differential operator [142] and yields to leading order in a slow rotation expansion [45]

$$\delta\vec{v} = \alpha R\Omega\left(\frac{r}{R}\right)^{m}\vec{Y}_{mm}^{B}\mathrm{e}^{i\omega t}$$

This expression provides the definition of α within the convention used here. In spherical coordinates this expression yields the explicit form

$$\delta\vec{v} = \frac{(-1)^m}{2^m m!}\sqrt{\frac{m\,(2m+1)\,(2m)!}{4\pi\,(m+1)}}\alpha R\Omega \cdot \left(\frac{r}{R}\right)^m (\sin\theta)^{m-1}\,\mathrm{e}^{i(m\phi+\omega t)}\left(-i\hat{\theta}+\cos\theta\hat{\phi}\right)$$

where $\hat{\theta}$ and $\hat{\phi}$ are unit vectors in polar and azimuthal direction. With this definition and for $\alpha = 1$ the maximum value, taken at the equator and in direction of $\hat{\theta}$, is roughly $\delta\vec{v}/\vec{v} \approx 0.3$, so that the approximation breaks down for $\alpha \gg 1$ since mass shedding will occur for fast spinning stars. The corresponding maximum density fluctuation $\delta n/\bar{n}$ obtained from eq. (4.7) is more than an order of magnitude smaller.

In contrast in [43] an alternative convention α' of the amplitude was introduced that is related to the above α by

$$\alpha = \sqrt{\frac{\pi\,(m+1)^3\,(2m+1)!}{m}}\alpha'$$

i.e. defined by eq. (D.1) without the algebraic prefactor.

Appendix E

Approximate result for the viscous damping of the strange quark matter

Whereas the bulk viscosity of semi-leptonic processes in hadronic and quark matter require in general a numeric solution, for the dominant contribution from non-leptonic processes in strange quark matter an approximate solution valid in both subthermal and suprathermal regimes is possible. The approximate analytic result for the bulk viscosity in the suprathermal regime obtained from a Fourier analysis, is given by (see chapter 3)

$$\zeta^{>} \approx \frac{2}{3\sqrt{3}} \frac{C^2}{B\omega} h\left(\frac{9\sqrt{3}\chi}{8} \frac{\tilde{\Gamma} B C^2 T^{\delta-2}}{\omega} \left(\frac{\Delta n_*}{\bar{n}_*}^2 \right) \right) \tag{E.1}$$

where $\chi \equiv \chi_1$ and

$$h(z) = \frac{9}{4z} \left(\left(\sqrt{z^2+1} - z \right)^{\frac{2}{3}} + \left(\sqrt{z^2+1} + z \right)^{\frac{2}{3}} - 2 \right) \tag{E.2}$$

A very good parameterization valid in both the sub- and suprathermal regime is given by [81]

$$\zeta_{par} \approx \zeta^{<} + \theta(T_{max} - T)\frac{\zeta_{max} - \zeta^{<}}{\zeta_{max}}\zeta^{>} \tag{E.3}$$

Since the functional form of the suprathermal viscosity eq. (E.2) is still complicated and does not allow to perform the necessary subsequent integrations to obtain the r-mode damping time in an analytic form, we give an approximate analytic result that is valid up to the maximum of the bulk viscosity. To this end we perform a global polynomial interpolation to the function $h(z)$ in the interval $[0, z_{max}]$. In order to appropriately describe the low amplitude behavior and the qualitative form below the maximum requires at least a quartic polynomial which is then uniquely determined as

$$h_{pol}(z) = z - \frac{1}{2\sqrt{3}}z^2 + \frac{1}{27}z^3 - \frac{1}{324\sqrt{3}}z^4 \tag{E.4}$$

The leading linear term in eq. (E.4) reproduces the approximate intermediate linear result given by Madsen [78], whereas the other terms ensure the proper large amplitude saturation. The analytic form and the polynomial approximation agree in the relevant region below the maximum point-wise on the 5% level and the corresponding integrals required for the damping time to even better accuracy.

The density in a strange star is nearly constant and so the density dependent quantities can be approximated by their value at the radius of the star, denoted by the suffix R. Performing the integration over the r-mode profile eq. (4.7), we find the approximate analytic result for the viscous damping time

$$\begin{aligned}\frac{1}{\tau_B^{>}} \approx \frac{16}{5103}\frac{A_R^2 C_R^2 \Omega^3 R^5}{B_R M \tilde{J}} \Bigg(& \frac{\frac{3}{2}\Omega\tilde{\Gamma}_R B_R T^{\delta}}{\Omega^2 + \frac{9}{4}\tilde{\Gamma}_R^2 B_R^2 T^{2\delta}} \\ & + \frac{2430}{143}\theta\big(T_{max} - T\big)\frac{(\Omega - \frac{3}{2}\tilde{\Gamma}_R B_R T^{\delta})^2}{\Omega^2 + \frac{9}{4}\tilde{\Gamma}_R^2 B_R^2 T^{2\delta}} g\big(\chi\tilde{\Gamma}_R A_R^2 B_R C_R^2 R^4 \Omega^3 T^{\delta-2}\alpha^2\big)\Bigg)\end{aligned} \tag{E.5}$$

where g is the polynomial

$$g(x) = x - \frac{151875}{9044}x^2 + \frac{1063125}{7429}x^3 - \frac{290631796875}{587723048}x^4$$

Bibliography

[1] R. N. Manchester, G. B. Hobbs, A. Teoh, and M. Hobbs, *The ATNF Pulsar Catalogue*, Astron. J. **129** (2005) 1993, [astro-ph/0412641].

[2] M. G. Alford, A. Schmitt, K. Rajagopal, and T. Schafer, *Color superconductivity in dense quark matter*, Rev. Mod. Phys. **80** (2008) 1455–1515, [arXiv:0709.4635].

[3] D. Page and S. Reddy, *Dense Matter in Compact Stars: Theoretical Developments and Observational Constraints*, Ann.Rev.Nucl.Part.Sci. **56** (2006) 327–374, [astro-ph/0608360].

[4] P. Demorest, T. Pennucci, S. Ransom, M. Roberts, and J. Hessels, *Shapiro Delay Measurement of A Two Solar Mass Neutron Star*, Nature **467** (2010) 1081–1083, [arXiv:1010.5788].

[5] B. A. Jacoby, A. Hotan, M. Bailes, S. Ord, and S. Kulkarni, *The Mass of a millisecond pulsar*, Astrophys.J. **629** (2005) L113–L116, [astro-ph/0507420].

[6] J. M. Lattimer and M. Prakash, *Neutron Star Observations: Prognosis for Equation of State Constraints*, Phys.Rept. **442** (2007) 109–165, [astro-ph/0612440].

[7] R. F. Sawyer, *Bulk viscosity of hot neutron–star matter and the maximum rotation rates of neutron stars*, Phys. Rev. **D39** (1989) 3804–3806.

[8] C. Cutler, L. Lindblom, and R. J. Splinter, *Damping times for neutron star oscillations*, **363** (Nov., 1990) 603–611.

[9] P. Jaikumar, G. Rupak, and A. W. Steiner, *Viscous damping of r-mode oscillations in compact stars with quark matter*, Phys. Rev. **D78** (2008) 123007, [arXiv:0806.1005].

[10] E. Flowers and N. Itoh, *Transport properties of dense matter*, **206** (May, 1976) 218–242.

[11] A. Akmal, V. R. Pandharipande, and D. G. Ravenhall, *The equation of state for nucleon matter and neutron star structure*, Phys. Rev. **C58** (1998) 1804–1828, [nucl-th/9804027].

[12] G. Baym, C. Pethick, and P. Sutherland, *The Ground state of matter at high densities: Equation of state and stellar models*, Astrophys. J. **170** (1971) 299–317.

[13] J. W. Negele and D. Vautherin, *Neutron star matter at subnuclear densities*, Nucl. Phys. **A207** (1973) 298–320.

[14] M. Alford, M. Braby, M. W. Paris, and S. Reddy, *Hybrid stars that masquerade as neutron stars*, Astrophys. J. **629** (2005) 969–978, [nucl-th/0411016].

[15] M. Alford, S. Mahmoodifar, and K. Schwenzer, *Viscous damping of r-modes: Small amplitude instability*, Phys. Rev. **D85** (2012) 024007, [arXiv:1012.4883].

[16] B. C. Barrois, *Superconducting Quark Matter*, Nucl.Phys. **B129** (1977) 390.

[17] D. Bailin and A. Love, *SUPERFLUID QUARK MATTER*, J.Phys.A **A12** (1979) L283.

[18] D. Bailin and A. Love, *Superfluidity and Superconductivity in Relativistic Fermion Systems*, Phys.Rept. **107** (1984) 325.

[19] M. G. Alford, K. Rajagopal, and F. Wilczek, *QCD at finite baryon density: Nucleon droplets and color superconductivity*, Phys.Lett. **B422** (1998) 247–256, [hep-ph/9711395].

[20] R. Rapp, T. Schafer, E. V. Shuryak, and M. Velkovsky, *Diquark Bose condensates in high density matter and instantons*, Phys.Rev.Lett. **81** (1998) 53–56, [hep-ph/9711396].

[21] N. Itoh, *Hydrostatic Equilibrium of Hypothetical Quark Stars*, Prog. Theor. Phys. **44** (1970) 291.

[22] A. R. Bodmer, *Collapsed nuclei*, Phys. Rev. **D4** (1971) 1601–1606.

[23] E. Witten, *Cosmic Separation of Phases*, Phys. Rev. **D30** (1984) 272–285.

[24] N. Andersson, *A New class of unstable modes of rotating relativistic stars*, Astrophys.J. **502** (1998) 708–713, [gr-qc/9706075].

[25] P. F. Bedaque and T. Schafer, *High density quark matter under stress*, Nucl.Phys. **A697** (2002) 802–822, [hep-ph/0105150].

[26] H. D. Politzer, *Reliable Perturbative Results for Strong Interactions?*, Phys.Rev.Lett. **30** (1973) 1346–1349.

[27] D. Gross and F. Wilczek, *Ultraviolet Behavior of Nonabelian Gauge Theories*, Phys.Rev.Lett. **30** (1973) 1343–1346.

[28] T. Schafer, *Kaon condensation in high density quark matter*, Phys.Rev.Lett. **85** (2000) 5531–5534, [nucl-th/0007021].

[29] M. G. Alford, J. A. Bowers, and K. Rajagopal, *Crystalline color superconductivity*, Phys.Rev. **D63** (2001) 074016, [hep-ph/0008208].

[30] M. Alford, C. Kouvaris, and K. Rajagopal, *Gapless color flavor locked quark matter*, Phys.Rev.Lett. **92** (2004) 222001, [hep-ph/0311286].

[31] T. Schafer, *Quark hadron continuity in QCD with one flavor*, Phys.Rev. **D62** (2000) 094007, [hep-ph/0006034].

[32] D. Aguilera, *Spin-one color superconductivity in compact stars?: An Analysis within NJL-type models*, Astrophys.Space Sci. **308** (2007) 443–450, [hep-ph/0608041].

[33] T. Schafer, *Meson supercurrent state in high density QCD*, Phys.Rev.Lett. **96** (2006) 012305, [hep-ph/0508190].

[34] N. Glendenning, *Neutron Stars Are Giant Hypernuclei?*, Astrophys.J. **293** (1985) 470–493.

[35] D. Kaplan and A. Nelson, *Strange Goings on in Dense Nucleonic Matter*, Phys.Lett. **B175** (1986) 57–63.

[36] J. C. Collins and M. Perry, *Superdense Matter: Neutrons Or Asymptotically Free Quarks?*, Phys.Rev.Lett. **34** (1975) 1353.

[37] D. Yakovlev, K. Levenfish, and Y. Shibanov, *Cooling neutron stars and superfluidity in their interiors*, Phys.Usp. **42** (1999) 737–778, [astro-ph/9906456].

[38] R. C. Tolman, *Static solutions of Einstein's field equations for spheres of fluid*, Phys. Rev. **55** (1939) 364–373.

[39] J. R. Oppenheimer and G. M. Volkoff, *On Massive neutron cores*, Phys. Rev. **55** (1939) 374–381.

[40] J. M. Lattimer and M. Prakash, *Neutron Star Structure and the Equation of State*, Astrophys. J. **550** (2001) 426, [astro-ph/0002232].

[41] J. Papaloizou and J. E. Pringle, *Non-radial oscillations of rotating stars and their relevance to the short-period oscillations of cataclysmic variables*, **182** (Feb., 1978) 423–442.

[42] J. L. Friedman and S. M. Morsink, *Axial instability of rotating relativistic stars*, Astrophys. J. **502** (1998) 714–720, [gr-qc/9706073].

[43] L. Lindblom, G. Mendell, and B. J. Owen, *Second-order rotational effects on the r-modes of neutron stars*, Phys. Rev. **D60** (1999) 064006, [gr-qc/9902052].

[44] J. Madsen, *Probing strange stars and color superconductivity by r- mode instabilities in millisecond pulsars*, Phys. Rev. Lett. **85** (2000) 10–13, [astro-ph/9912418].

[45] L. Lindblom, B. J. Owen, and S. M. Morsink, *Gravitational radiation instability in hot young neutron stars*, Phys.Rev.Lett. **80** (1998) 4843–4846, [gr-qc/9803053].

[46] J. Provost, G. Berthomieu, and A. Rocca, *Low Frequency Oscillations of a Slowly Rotating Star - Quasi Toroidal Modes*, **94** (Jan., 1981) 126.

[47] J. Papaloizou and J. Pringle, *Non-radial oscillations of rotating stars and their relevance to the short-period oscillations of cataclysmic variables*, Mon.Not.Roy.Astron.Soc. **182** (1978) 423–442.

[48] S. Chandrasekhar, *Solutions of two problems in the theory of gravitational radiation*, Phys. Rev. Lett. **24** (1970) 611–615.

[49] J. L. Friedman and B. F. Schutz, *Secular instability of rotating Newtonian stars*, Astrophys. J. **222** (1978) 281.

[50] B. J. Owen *et. al.*, *Gravitational waves from hot young rapidly rotating neutron stars*, Phys. Rev. **D58** (1998) 084020, [gr-qc/9804044].

[51] N. Andersson, K. D. Kokkotas, and B. F. Schutz, *Gravitational radiation limit on the spin of young neutron stars*, Astrophys. J. **510** (1999) 846, [astro-ph/9805225].

[52] C. D. Ott, A. Burrows, T. A. Thompson, E. Livne, and R. Walder, *The Spin Periods and Rotational Profiles of Neutron Stars at Birth*, Astrophys. J. Suppl. **164** (2006) 130–155, [astro-ph/0508462].

[53] L. Lindblom and B. J. Owen, *Effect of hyperon bulk viscosity on neutron-star r- modes*, Phys. Rev. **D65** (2002) 063006, [astro-ph/0110558].

[54] F. Ozel, D. Psaltis, S. Ransom, P. Demorest, and M. Alford, *The Massive Pulsar PSR J1614-2230: Linking Quantum Chromodynamics, Gamma-ray Bursts, and Gravitational Wave Astronomy*, arXiv:1010.5790.

[55] B. J. Owen, *How to adapt broad-band gravitational-wave searches for r-modes*, Phys.Rev. **D82** (2010) 104002, [arXiv:1006.1994].

[56] **LIGO Scientific Collaboration** Collaboration, B. Abbott *et. al.*, *Setting upper limits on the strength of periodic gravitational waves using the first science data from the GEO 600 and LIGO detectors*, Phys.Rev. **D69** (2004) 082004, [gr-qc/0308050].

[57] **LIGO Scientific Collaboration** Collaboration, B. Abbott *et. al.*, *First all-sky upper limits from LIGO on the strength of periodic gravitational waves using the Hough transform*, Phys.Rev. **D72** (2005) 102004, [gr-qc/0508065].

[58] **The Virgo Collaboration** Collaboration, T. L. S. Collaboration *et. al.*, *Searches for gravitational waves from known pulsars with S5 LIGO data*, Astrophys.J. **713** (2010) 671–685, [arXiv:0909.3583].

[59] **LIGO Scientific Collaboration** Collaboration, J. Abadie *et. al.*, *First search for gravitational waves from the youngest known neutron star*, Astrophys.J. **722** (2010) 1504–1513, [arXiv:1006.2535].

[60] M. G. Alford, M. Braby, and S. Mahmoodifar, *Shear viscosity due to kaon condensation in color-flavor locked quark matter*, Phys.Rev. **C81** (2010) 025202, [arXiv:0910.2180].

[61] R. Casalbuoni and R. Gatto, *Effective theory for color flavor locking in high density QCD*, Phys.Lett. **B464** (1999) 111–116, [hep-ph/9908227].

[62] D. B. Kaplan and S. Reddy, *Novel phases and transitions in quark matter*, Phys. Rev. **D65** (2002) 054042, [hep-ph/0107265].

[63] D. T. Son, *Light Goldstone boson and domain walls in the K0-condensed phase of high density quark matter*, hep-ph/0108260.

[64] M. G. Alford, M. Braby, and A. Schmitt, *Critical temperature for kaon condensation in color-flavor locked quark matter*, J. Phys. **G35** (2008) 025002, [arXiv:0707.2389].

[65] C. Manuel and F. J. Llanes-Estrada, *Bulk viscosity in a cold CFL superfluid*, JCAP **0708** (2007) 001, [arXiv:0705.3909].

[66] C. Manuel, A. Dobado, and F. J. Llanes-Estrada, *Shear viscosity in a CFL quark star*, JHEP **09** (2005) 076, [hep-ph/0406058].

[67] D. T. Son and M. A. Stephanov, *Inverse meson mass ordering in color-flavor-locking phase of high density QCD*, Phys. Rev. **D61** (2000) 074012, [hep-ph/9910491].

[68] D. T. Son and M. A. Stephanov, *Inverse meson mass ordering in color-flavor-locking phase of high density QCD: Erratum*, Phys. Rev. **D62** (2000) 059902, [hep-ph/0004095].

[69] V. Kleinhaus, M. Buballa, D. Nickel, and M. Oertel, *Pseudoscalar Goldstone bosons in the color-flavor locked phase at moderate densities*, Phys. Rev. **D76** (2007) 074024, [arXiv:0707.0632].

[70] S. Reddy, M. Sadzikowski, and M. Tachibana, *Neutrino processes in the K0 condensed phase of color flavor locked quark matter*, Phys. Rev. **D68** (2003) 053010, [nucl-th/0306015].

[71] G. Rupak and T. Schafer, *Shear viscosity of a superfluid Fermi gas in the unitarity limit*, Phys. Rev. **A76** (2007) 053607, [arXiv:0707.1520].

[72] E. Lifshitz and L. Pitaevskii, *Physical kinetics*, Butterworth-Heinemann (1981).

[73] J.-W. Chen and E. Nakano, *Shear Viscosity to Entropy Density Ratio of QCD below the Deconfinement Temperature*, Phys. Lett. **B647** (2007) 371–375, [hep-ph/0604138].

[74] A. Dobado and S. N. Santalla, *Pion gas viscosity at low temperature and density*, Phys. Rev. **D65** (2002) 096011, [hep-ph/0112299].

[75] M. L. Bellac, *Thermal field theory*, Cambridge Univ. Press (1996).

[76] M. G. Alford, M. Braby, S. Reddy, and T. Schafer, *Bulk viscosity due to kaons in color-flavor-locked quark matter*, Phys. Rev. **C75** (2007) 055209, [nucl-th/0701067].

[77] M. G. Alford, M. Braby, and A. Schmitt, *Bulk viscosity in kaon-condensed color-flavor locked quark matter*, J. Phys. **G35** (2008) 115007, [arXiv:0806.0285].

[78] J. Madsen, *Bulk viscosity of strange dark matter, damping of quark star vibration, and the maximum rotation rate of pulsars*, Phys. Rev. **D46** (1992) 3290–3295.

[79] A. Reisenegger and A. A. Bonacic, *Bulk viscosity, r-modes, and the early evolution of neutron stars*, astro-ph/0303454.

[80] A. A. Bonacic, *Gravitational radiation and bulk viscosity in neutron stars*, Master thesis, Universidad Catolica de Chile (2003).

[81] M. G. Alford, S. Mahmoodifar, and K. Schwenzer, *Large amplitude behavior of the bulk viscosity of dense matter*, J.Phys.G **G37** (2010) 125202, [arXiv:1005.3769].

[82] M. Alford, S. Mahmoodifar, and K. Schwenzer, *Suprathermal viscosity of dense matter*, AIP Conf.Proc. **1317** (2011) 380–387, [arXiv:1009.4182].

[83] B. Betz, D. Henkel, and D. H. Rischke, *Complete second-order dissipative fluid dynamics*, J. Phys. **G36** (2009) 064029.

[84] M. G. Alford and A. Schmitt, *Bulk viscosity in 2SC quark matter*, J. Phys. **G34** (2007) 67–102, [nucl-th/0608019].

[85] B. A. Sa'd, I. A. Shovkovy, and D. H. Rischke, *Bulk viscosity of spin-one color superconductors with two quark flavors*, Phys. Rev. **D75** (2007) 065016, [astro-ph/0607643].

[86] M. G. Alford and A. Schmitt, *Bulk viscosity in 2SC and CFL quark matter*, AIP Conf. Proc. **964** (2007) 256–263, [arXiv:0709.4251].

[87] B. A. Sa'd, I. A. Shovkovy, and D. H. Rischke, *Bulk viscosity of strange quark matter: Urca versus non- leptonic processes*, Phys. Rev. **D75** (2007) 125004, [astro-ph/0703016].

[88] H. Dong, N. Su, and Q. Wang, *Bulk viscosity in nuclear and quark matter: A short review*, J. Phys. **G34** (2007) S643–6476, [astro-ph/0702181].

[89] M. Mannarelli and C. Manuel, *Bulk viscosities of a cold relativistic superfluid: color- flavor locked quark matter*, arXiv:0909.4486.

[90] X.-G. Huang, M. Huang, D. H. Rischke, and A. Sedrakian, *Anisotropic Hydrodynamics, Bulk Viscosities and R-Modes of Strange Quark Stars with Strong Magnetic Fields*, arXiv:0910.3633.

[91] H. Heiselberg, *The Weak conversion rate in quark matter*, Phys. Scripta **46** (1992) 485–488.

[92] P. Haensel, K. P. Levenfish, and D. G. Yakovlev, *Bulk viscosity in superfluid neutron star cores. I. Direct Urca processes in npeμ matter*, Astron. Astrophys. **357** (2000) 1157–1169, [astro-ph/0004183].

[93] P. Haensel, K. P. Levenfish, and D. G. Yakovlev, *Bulk viscosity in superfluid neutron star cores. II. Modified Urca processes in npeμ matter*, Astron. Astrophys. **327** (2001) 130–137, [astro-ph/0103290].

[94] D. Chatterjee and D. Bandyopadhyay, *Bulk viscosity in kaon condensed matter*, Phys. Rev. **D75** (2007) 123006, [astro-ph/0702259].

[95] M. E. Gusakov, *Bulk viscosity of superfluid neutron stars*, Phys. Rev. **D76** (2007) 083001, [arXiv:0704.1071].

[96] D. Chatterjee and D. Bandyopadhyay, *Role of antikaon condensation in r-mode instability*, arXiv:0712.4347.

[97] M. G. Alford and G. Good, *Leptonic contribution to the bulk viscosity of nuclear matter*, arXiv:1003.1093.

[98] P. B. Jones, *Bulk viscosity of neutron-star matter*, Phys. Rev. **D64** (2001) 084003.

[99] P. Haensel, K. P. Levenfish, and D. G. Yakovlev, *Bulk viscosity in superfluid neutron star cores. III. Effects of Σ^- hyperons*, Astron. Astrophys. **381** (2002) 1080–1089, [astro-ph/0110575].

[100] D. Chatterjee and D. Bandyopadhyay, *Hyperon Bulk Viscosity in the Presence of Antikaon Condensate*, **680** (June, 2008) 686–694, [arXiv:0712.3171].

[101] A. Reisenegger, *Deviations from chemical equilibrium due to spindown as an internal heat source in neutron stars*, Astrophys. J. **442** (1995) 749, [astro-ph/9410035].

[102] B. L. Friman and O. V. Maxwell, *Neutron Star Neutrino Emissivities*, Astrophys. J. **232** (1979) 541.

[103] P. Haensel and R. Schaeffer, *Bulk viscosity of hot-neutron-star matter from direct URCA processes*, Phys. Rev. **D45** (1992) 4708–4712.

[104] J. M. Lattimer, M. Prakash, C. J. Pethick, and P. Haensel, *Direct URCA process in neutron stars*, Phys. Rev. Lett. **66** (1991) 2701–2704.

[105] L. Lindblom, J. E. Tohline, and M. Vallisneri, *Non-Linear Evolution of the r-Modes in Neutron Stars*, Phys. Rev. Lett. **86** (2001) 1152–1155, [astro-ph/0010653].

[106] P. Gressman, L.-M. Lin, W.-M. Suen, N. Stergioulas, and J. L. Friedman, *Nonlinear r-modes in neutron stars: Instability of an unstable mode*, Phys. Rev. **D66** (2002) 041303.

[107] L.-M. Lin and W.-M. Suen, *Nonlinear r-modes in neutron stars: A hydrodynamical limitation on r-mode amplitudes*, Mon. Not. Roy. Astron. Soc. **370** (2006) 1295–1302, [gr-qc/0409037].

[108] R. Bondarescu, S. A. Teukolsky, and I. Wasserman, *Spin Evolution of Accreting Neutron Stars: Nonlinear Development of the R-mode Instability*, Phys. Rev. **D76** (2007) 064019, [arXiv:0704.0799].

[109] A. Kurkela, P. Romatschke, and A. Vuorinen, *Cold Quark Matter*, arXiv:0912.1856.

[110] T. Schafer and K. Schwenzer, *Neutrino emission from ungapped quark matter*, Phys. Rev. **D70** (2004) 114037, [astro-ph/0410395].

[111] A. W. Steiner, *The Neutron Star Crust: Nuclear Physics Input*, Phys. Rev. **C77** (2008) 035805, [arXiv:0711.1812].

[112] K. D. Kokkotas and B. G. Schmidt, *Quasi-normal modes of stars and black holes*, Living Rev. Rel. **2** (1999) 2, [gr-qc/9909058].

[113] M. Gabler, U. Sperhake, and N. Andersson, *Non-linear radial oscillations of neutron stars*, Phys. Rev. **D80** (2009) 064012, [arXiv:0906.3088].

[114] B. Haskell, N. Andersson, and A. Passamonti, *r-modes and mutual friction in rapidly rotating superfluid neutron stars*, arXiv:0902.1149.

[115] E. S. Fraga, R. D. Pisarski, and J. Schaffner-Bielich, *Small, dense quark stars from perturbative QCD*, Phys. Rev. **D63** (2001) 121702, [hep-ph/0101143].

[116] E. S. Fraga and P. Romatschke, *The role of quark mass in cold and dense perturbative QCD*, Phys. Rev. **D71** (2005) 105014, [hep-ph/0412298].

[117] N. Andersson and K. D. Kokkotas, *The R-mode instability in rotating neutron stars*, Int. J. Mod. Phys. **D10** (2001) 381–442, [gr-qc/0010102].

[118] K. H. Lockitch, N. Andersson, and J. L. Friedman, *The Rotational modes of relativistic stars. 1. Analytic results*, Phys.Rev. **D63** (2001) 024019, [gr-qc/0008019].

[119] K. H. Lockitch, J. L. Friedman, and N. Andersson, *The Rotational modes of relativistic stars: Numerical results*, Phys.Rev. **D68** (2003) 124010, [gr-qc/0210102].

[120] J. Ruoff and K. D. Kokkotas, *On the r mode spectrum of relativistic stars: Inclusion of the radiation reaction*, Mon.Not.Roy.Astron.Soc. **330** (2002) 1027, [gr-qc/0106073].

[121] P. S. Shternin and D. G. Yakovlev, *Shear viscosity in neutron star cores*, Phys. Rev. **D78** (2008) 063006, [arXiv:0808.2018].

[122] H. Heiselberg and C. J. Pethick, *Transport and relaxation in degenerate quark plasmas*, Phys. Rev. **D48** (1993) 2916–2928.

[123] L. Bildsten and G. Ushomirsky, *Viscous Boundary-Layer Damping of R-Modes in Neutron Stars*, Astrophys. J. Lett. **529** (Jan., 2000) L33–L36, [astro-ph/].

[124] N. K. Glendenning, ed., *Compact stars : nuclear physics, particle physics, and general relativity*, 2000.

[125] A. Reisenegger and A. A. Bonacic, *Millisecond pulsars with r-modes as steady gravitational radiators*, Phys.Rev.Lett. **91** (2003) 201103, [astro-ph/0303375].

[126] E. F. Brown, L. Bildsten, and P. Chang, *Variability in the Thermal Emission from Accreting Neutron Star Transients*, astro-ph/0204102.

[127] P. Arras, E. E. Flanagan, S. M. Morsink, A. K. Schenk, S. A. Teukolsky, *et. al.*, *Saturation of the R mode instability*, Astrophys.J. **591** (2003) 1129–1151, [astro-ph/0202345].

[128] M. G. Alford, S. Mahmoodifar, and K. Schwenzer, *Viscous damping of r-modes: Large amplitude saturation*, Phys.Rev. **D85** (2012) 044051, [arXiv:1103.3521].

[129] I. A. Shovkovy and X. Wang, *Bulk viscosity in the nonlinear and anharmonic regime of strange quark matter*, New J.Phys. **13** (2011) 045018, [arXiv:1012.0354].

[130] N. Chamel and P. Haensel, *Physics of Neutron Star Crusts*, Living Rev.Rel. **11** (2008) 10, [arXiv:0812.3955].

[131] M. G. Alford, S. Reddy, and K. Schwenzer, *Bridging the gap by shaking superfluid matter*, Phys. Rev. Lett. **108** (2012) 111102, [arXiv:1110.6213].

[132] J. Brink, S. A. Teukolsky, and I. Wasserman, *Nonlinear couplings of R-modes: Energy transfer and saturation amplitudes at realistic timescales*, Phys.Rev. **D70** (2004) 121501, [gr-qc/0406085].

[133] R. Bondarescu, S. A. Teukolsky, and I. Wasserman, *Spinning down newborn neutron stars: nonlinear development of the r-mode instability*, Phys. Rev. **D79** (2009) 104003, [arXiv:0809.3448].

[134] J. Madsen, *How to identify a strange star*, Phys. Rev. Lett. **81** (1998) 3311–3314, [astro-ph/9806032].

[135] N. Andersson, D. Jones, and K. Kokkotas, *Strange stars as persistent sources of gravitational waves*, Mon.Not.Roy.Astron.Soc. **337** (2002) 1224, [astro-ph/0111582].

[136] A. Drago, G. Pagliara, and I. Parenti, *A Compact star rotating at 1122 Hz and the r-mode instability*, Astrophys.J. **678** (2008) L117–L120, [arXiv:0704.1510].

[137] M. Prakash, I. Bombaci, M. Prakash, P. J. Ellis, J. M. Lattimer, *et. al.*, *Composition and structure of protoneutron stars*, Phys.Rept. **280** (1997) 1–77, [nucl-th/9603042].

[138] P. Arnold, G. D. Moore, and L. G. Yaffe, *Transport coefficients in high temperature gauge theories: (I) Leading-log results*, JHEP **11** (2000) 001, [hep-ph/0010177].

[139] P. Arnold, G. D. Moore, and L. G. Yaffe, *Transport coefficients in high temperature gauge theories. II: Beyond leading log*, JHEP **05** (2003) 051, [hep-ph/0302165].

[140] K. Zarembo, *Dispersion laws for Goldstone bosons in a color superconductor*, Phys. Rev. **D62** (2000) 054003, [hep-ph/0002123].

[141] M. Braby, J. Chao, and T. Schaefer, *Thermal conductivity of color-flavor locked quark matter*, arXiv:0909.4236.

[142] J. R. Ipser and L. Lindblom, *Oscillations and stability of rapidly rotating neutron stars*, Phys.Rev.Lett. **62** (1989) 2777–2780.